DOI: 10.1070/RCR4839

Self-assembled semiconducting monolayers in organic electronics

Alexey S. Sizov, Elena V. Agina, Sergey A. Ponomarenko

Enikolopov Institute of Synthetic Polymeric Materials, Russian Academy of Sciences
ul. Profsoyuznaya 70, 117393 Moscow, Russian Federation

The results of studies dealing with the self-assembly of semiconducting monolayers of conjugated oligomers are integrated and analyzed. General information about the design of organic field effect transistors is given and the details of calculation of their key parameters are described. The main classes of conjugated oligomers used as semiconductors in organic field effect transistors are considered. The modern achievements in the fabrication of microelectronic devices based on self-assembled monolayer semiconductors are demonstrated and the results of the most successful use of such systems are presented. The bibliography includes 102 references.

Contents

1. Introduction 1226
2. Overview of organic field effect transistors 1227
3. Calculation of the key parameters of organic field effect transistors 1228
4. Selection of materials for organic field effect transistors 1231
5. Organic field-effect transistors based on self-assembled semiconducting monolayers 1239

1. Introduction

Self-assembly is a spontaneous formation of ordered structures from components that takes place without external stimuli and is controlled *via* appropriate design of the components.[1] This notion has quite a number of definitions and, in the general case, covers a broad range of phenomena.[2] One should distinguish between self-assembly and self-organization, which means the spontaneous formation, under certain conditions, of supramolecular structures with a higher hierarchical level of organization than present in the initial system. The supramolecular structures are formed either spontaneously or as a result of electrostatic or donor-acceptor interactions, hydrogen bonds or medium effects (solvophobic interactions).[3] Thus, self-organization is a special case of self-assembly. As examples of self-assembly, consider the formation of atoms from subatomic particles, the formation of a lipid bilayer in water, and galaxy formation from stars. Examples of self-organization are the formation of molecular crystals and spontaneous folding of a polypeptide chain to generate the tertiary protein structure.

In the beginning of the 1960s, it was shown that organic crystals, which represent a classic example of self-organization, can behave as semiconductors upon injection of charge carriers from electrodes or upon photoexcitation.[4, 5] It is worth noting that these compounds are dielectrics in the traditional view, because they possess rather wide band gaps, usually 2.4 – 4 eV. Nevertheless, the term organic semiconductor is widely used in the literature to mean an organic compound able to behave as a semiconductor.

Further studies of the optoelectronic properties of organic crystals gave rise to a new interdisciplinary research area at the boundary between chemistry, physics and materials science — organic electronics. The use of materials based on organic compounds opens up prospects for the design of innovative optoelectronic devices, which are distinguished by low cost, low weight, flexibility and trans-

A.S.Sizov. Candidate of Chemical Sciences, Junior Researcher at the ISPM RAS.
Telephone: +7(495)332 – 5847, e-mail: sizov@ispm.ru
Current research interests: design of innovative organic microelectronic devices based on conjugated oligomers, including organic field effect transistors, organic integrated circuits, gas sensors; search for procedures for forming thin films with specified optoelectronic properties based on organic compounds; characterization of functional organic electronic layers by various methods.
E.V.Agina. Candidate of Chemical Sciences, Leading Researcher at the ISPM RAS.
Telephone: +7(495)332 – 5847, e-mail: agina@ispm.ru
Current research interests: molecular and supramolecular self-assembly in bulk and in thin films of linear and branched carbosilane-siloxanes with various functional, including mesogenic and semiconducting, groups; search for efficient techniques for fabrication of highly ordered, including two-dimensional, nanomaterials with specified structures and properties, based on carbosilane-siloxanes.
S.A.Ponomarenko. Corresponding Member of the RAS, Doctor of Chemical Sciences, Director of the ISPM RAS.
Telephone: +7(495)332 – 5858, e-mail: ponomarenko@ispm.ru
Current research interests: molecular design and synthesis of novel conjugated organic and organosilicon structures, first of all, based on thiophene and silicon chemistry, possessing high charge carrier mobility, efficient luminescence, good processability from solutions, oxidative and thermal stabilities and other properties required for high-performance materials and technologies for organic electronics, optoelectronics and photonics.

Received 31 May 2018
Translation: Z.P.Svitanko

© 2018 Uspekhi Khimii, Russian Academy of Sciences and Turpion Ltd.

parency. In organic electronics, self-assembly processes are widely used to fabricate functional layers for different types of devices. This is due to the fact that energy consuming manufacturing processes traditional for electronic industry such as plasma treatment, ion sputtering or chemical vapour deposition are hardly applicable to organic electronics. First, the use of these methods implies surface treatment by chemically or physically active components, which adversely affects the structure and properties of the underlying organic layers. Second, high energy consumption of particular manufacturing stages increases the overall cost of the device. A challenging issue of organic electronics is the search for new materials and processing techniques that would produce, in combination, new-generation electronic devices *via* exclusively solution processing.

Key devices of organic electronics are an organic field effect transistors (OFET). The charge transport in OFETs occurs in a thin semiconducting film and the current values can vary within orders of magnitude as a result of external voltage application to the gate electrode. It was shown experimentally that the charge-transporting layer in OFETs is 3 – 5 nm thick; this corresponds to 1 or 2 oligomer monolayers.[6,7] The key role is played by the lower monolayer adjacent to the dielectric, while the next layer is auxiliary and promotes charge transfer at the defective sites of the lower monolayer. Thus, mono- and bilayer OFETs are of particular interest,[8,9] as they considerably reduce the consumption of the semiconductor material without the loss of electrical properties. Furthermore, a monolayer semiconductor is highly sensitive to the environmental conditions and composition of the environment due to the direct contact of atmospheric gases with the charge-transporting layer, which makes monolayer OFETs promising for the design of highly sensitive chemical sensors.

There are several recent reviews with the subject closely related to or partially overlaping with that of the present review.[8–11] The review of Kagan[9] published in 2011 covers the achievements of that time in the design of self-assembled monolayer semiconductors in organic electronics. However, this research area has considerably progressed during the past years, with the record-high electrical characteristics increasing by more than two orders of magnitude. Therefore, it is pertinent to survey the state-of-the-art research. The review of Borshchev and Ponomarenko[8] presents an analysis of the dependence of electrical properties of semiconducting monolayers on the chemical structure of the initial compound, whereas the present review is focused on monolayer fabrication procedures and how they affect the semiconducting properties. In the review of Casalini *et al.*,[10] semiconducting monolayers are discussed only briefly in the context of broader subject matter. The review of Yang *et al.*[11] devoted to the prospective practical applications of two-dimensional organic crystals based on non-functional compounds also deserves mention.

The present review consists of four parts. The first part gives an overview of OFETs, because the self-assembled semiconducting monolayers are mainly used in this type of devices. The second part analyzes the distinctive features of OFETs manifested in calculation of their key parameters such as charge carrier mobility and threshold voltage. In the third part, we consider some promising classes of organic semiconductors. The final, fourth part describes the most successful examples of the design of self-assembled semiconducting monolayers and devices based on them.

The following abbreviations are used in the review:
AFM — atomic force microscopy,
BP3T — α,α′-bis(biphenyl-4-yl)terthiophene,
BTBT — [1]benzothieno[3,2-b][1]benzothiophene,
DB — doctor blade,
DH6T — α,ω-dihexylsexithiophene,
DIC microscopy— differential interference contrast microscopy,
DPBT — diphenyl-bithiophene,
HOMO — highest occupied molecular orbital,
LB — Langmuir – Blodgett,
LS — Langmuir – Schaefer,
LQY — luminescence quantum yield,
MISFET — metal – insulator – semiconductor field-effect transistor,
ODMS — octyldimethylchlorosilane,
OFET — organic field effect transistor,
OLED — organic light emitting diode,
OLET — organic light emitting transistor,
PEN — poly(ethylene naphthalate),
PMMA — poly(methyl methacrylate),
RFID — radio frequency identification,
SAM — self-assembled monolayer,
SAMFET — self-assembled monolayer field effect transistor,
SASM — self-assembled semiconducting monolayers,
SC — spin coating,
SLD — scattering length density,
TFT — thin film transistor.
Designations of physical quantities:
C — electric capacitance per unit area,
d_s — semiconductor layer thickness,
E_{SAM} —SAM-generated electric field,
F — deposition rate,
f — frequency,
g — transconductance,
$I_{on/off}$ — on/off current ratio,
I_{sd} — source-to-drain current,
L — length of the conducting channel,
μ —charge carrier mobility,
n_0 — charge carrier density without applied voltage,
R_s — contact resistance,
Θ — coverage,
V_0 — zero voltage,
V_d — drain voltage,
V_{dd} — supply voltage,
V_{fa} — flat band potential,
V_g — gate voltage,
V_{in} — input voltage,
V_{out} — output voltage,
V_s — source voltage,
V_{sd} — source-to-drain voltage,
V_t — threshold voltage,
VAC — volt-ampere curve,
W — width of the conducting channel.

2. Overview of organic field effect transistors

Organic field effect transistor is an electronic device comprising electrodes that are called ‘drain’, ‘source’ and ‘gate’, gate dielectric and organic semiconductor (Fig. 1). The OFET architecture is similar to the architecture of a thin-film transistor, which was first proposed in 1962.[12] Currently, devices of this geometry are widely used in digital

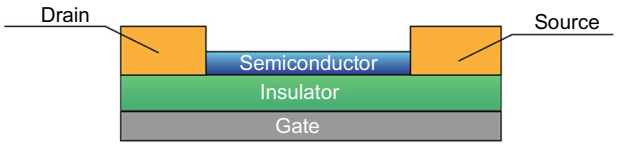


Figure 1. Schematic diagram of an organic field effect transistor.

optoelectronic devices of relatively large size such as liquid crystal displays with amorphous silicon-based control transistors. The architecture of TFT is optimized for operation with semiconducting materials with low conductivity, because the drain and the source are directly connected to a semiconductor through an ohmic contact. Unlike the other two frequent architectures of field effect transistors, that is, the MISFET and Schottky barrier field effect transistors, thin film transistors are devoid of a charge carrier-depleted area separating the device from the other part of the substrate. The low currents in the transistor off-state are ensured only by the low conductivity of the semiconducting layer. One more important feature of TFTs is that they operate in the saturation regime rather than inversion regime.

At the end of the 1990s, it was found that the operation theory developed for inorganic MISFET (metal–insulator–semiconductor field-effect transistor) can also be applied to OFETs.[13] The volt-ampere curves of the transistors are described by the following equations:

in the linear regime

$$I_{sd} = \frac{W}{L}\mu C(V_g - V_t)V_{sd} \quad (1)$$

in the saturation regime

$$I_{sd} = \frac{W}{2L}\mu C(V_g - V_t)^2 \quad (2)$$

where I_{sd} and V_{sd} are the source-to-drain current and voltage, respectively; V_g is the gate voltage; V_t is the threshold voltage at which the current starts to increase; C is the dielectric capacitance per unit area; and W and L are the width and the length of the conducting channel, respectively.

In organic field effect transistors, charges migrate within a thin (not more than several nanometres thick) layer on the surface between the organic semiconductor and the dielectric.[6,7,14] The key parameters derived from the electrical characteristics of OFETs is the mobility of charge carriers (μ), the on/off current ratio ($I_{on/off}$), the threshold voltage (V_t) and the subthreshold slope ($\partial V_g/\partial I_{ds}$). The mobility is defined as the drift velocity acquired by the elementary electric charge in a 1 V m^{-1} electric field. The on/off current ratio (the difference between the transistor source and drain currents in the on and off states) is determined by a number of factors: the maximum on-state current depending on the charge carrier mobility, the size of the device and the operating voltage. Low off-state currents ($< 10^{-11}$ A) are ensured, first of all, by the high chemical purity of the organic semiconductor as well as its stability under ambient conditions.[15] The threshold voltage is the voltage at which the transistor switches from the off to on state. The

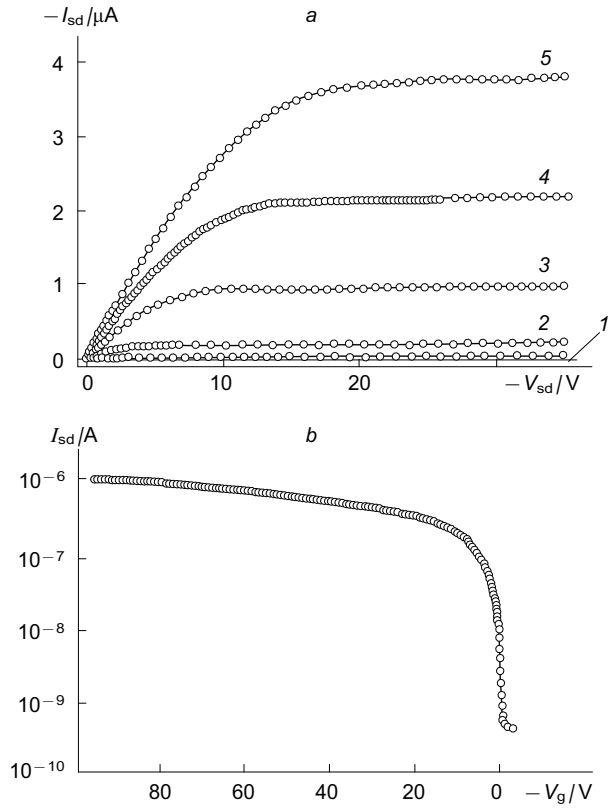


Figure 2. Typical output (*a*) and transfer (*b*) characteristics of an OFET based on single-crystal rubrene.[16]
(*a*) $-V_g$ = 0 (*1*), 5 (*2*), 10 (*3*), 15 (*4*), 20 V (*5*);
b: $\mu = 1 \pm 0.1$ cm^2 V^{-1} s^{-1}, T = 300 K, V_{sd} = 1 V.

subthreshold slope is usually measured in volts per decade; this parameter shows by how many volts the gate voltage of the OFET must be changed for the current to change 10-fold.

The key OFET parameters are evaluated by plotting the current *vs.* drain voltage (output characteristics) and current *vs.* gate voltage (transfer characteristics) dependences. Typical volt–ampere characteristics of a p-type transistor, that is, a transistor in which holes are the main charge carriers in the semiconducting layer, are shown in Fig. 2. The linear operation regime of the transistor at which the current exhibits a linear dependence on the voltage V_{sd} is clearly seen in the $V_{sd} < V_g - V_t$ region of the series of output curves (see Fig. 2 *a*). At a certain current value, the current *vs.* voltage curve is saturated, which corresponds to switching to the saturation regime $V_{sd} > V_g - V_t$. A typical transfer characteristics of the OFET in which the above-mentioned operation regimes of the transistor can also be distinguished in the indicated operating voltage ranges is depicted in Fig. 2 *b*. The OFET linear operation is observed at high values of V_g. Podzorov *et al.*[16] noted that the most reliable carrier mobility values are obtained exactly in this regime.

3. Calculation of the key parameters of organic field effect transistors

Expressions (1) and (2) are widely used to calculate the key characteristics of OFETs — the carrier mobility and the

threshold voltage. Nevertheless, it is noteworthy that these expressions have been derived for the MISFET architecture and their transfer to the TFT structure with an organic semiconductor implies several additional assumptions, which are not always fulfilled for OFETs. For this reason, a highly significant issue is an appropriate choice of conditions for OFET testing and for calculation of the key parameters.

The threshold voltage for MISFETs is the gate voltage at which transition to the inversion mode takes place and a conducting channel between the source and drain is formed.[13] In terms of solid-state physics, the threshold voltage means the gate voltage at which the Fermi level of the semiconductor/dielectric interface is located in the middle of the semiconductor band gap. In thin film transistors (including organic transistors), the drain and source have an ohmic contact with the semiconductor and the gate voltage stimulates the current to flow along the channel; hence, the number of charge carriers in the channel increases. In view of these considerations, there should be no threshold voltage in the OFETs.[17] However, a non-zero threshold voltage is observed in experiments. This phenomenon is well-known for TFT based on amorphous silicon. It was attributed to the carrier mobility being dependent on the gate voltage. Since the band gap of amorphous silicon has a high density of localized states, when the gate voltage is low, the charge transport occurs *via* hopping between these states and is characterized by low mobility of charge carriers. As the gate voltage increases, these states are filled and the subsequent transport is characterized by band conduction with high carrier mobility. In this case, the threshold voltage corresponds to transition from hopping to band conduction. A more complex situation occurs in organic transistors. First, the mobility of charge carriers may depend on the electric field strength, which is related to the transport mechanism in organic semiconductors. Second, the non-zero threshold voltage measured in experiments is caused by the presence of free charge carriers in the transistor channel under ambient conditions. Therefore, relations (1) and (2) are not always applicable for calculation of the carrier mobility and interpretation of experimental threshold voltage values.[13]

Horowitz *et al.*[18] devised a model of an OFET operating in the carrier saturation regime. The authors introduced a zero voltage defined *via* charge carrier density in the absence of applied voltage

$$V_0 = \pm \frac{q\, n_0\, d_s}{C} + V_{fa} \tag{3}$$

where q is the elementary charge; n_0 is the carrier density without applied voltage; d_s is the semiconducting layer thickness; V_{fa} is the so-called flat band voltage taking account of the work-function difference between the semiconductor and the gate. In practice, the last term is often neglected. The sign of V_0 is determined by the type of major charge carriers in the semiconductor: plus corresponds to holes and minus corresponds to electrons. Using this model and assuming a weak dependence of the carrier mobility on the electric field and equality between the density of free and localized carriers in the organic semiconductor, the authors derived the following theoretical dependences for the volt – ampere curves of OFETs:

in the linear regime

$$I_{sd} = \frac{W}{L} \mu\, C \left[(V_g - V_0) V_{sd} - \frac{V_d^2}{2} \right] \tag{4}$$

in the saturation regime

$$I_{sd} = \frac{W}{2L} \mu\, C (V_g - V_0)^2 \tag{5}$$

Relations (4) and (5) resemble relations (1) and (2) in the form; however, in the case of OFETs, the V_t value is replaced by V_0, *i.e.*, by a value with a different physical meaning. Nevertheless, in most publications that consider OFETs, the designation V_t is used.

The developed model was illustrated[18] by the results of investigation of transistors based on α,ω-dihexylsexithiophene thermally deposited on the PMMA layer used as the gate dielectric. They compared the electrical properties of organic transistors under ambient conditions and their analogues that had been stored *in vacuo*. The variation of the square root of the current as a function of the gate voltage under ambient conditions is plotted in Fig. 3 *a*. It can be seen that the dependence is linear, as predicted by relation (5). This was used to calculate the charge carrier mobility $\mu = 0.056$ cm^2 V^{-1} s^{-1} and the $V_0 = 5.9$ V. It can be seen that the sign of V_0 corresponds to the major type of charge carriers in α,ω-dihexylsexithiophene, that is, holes. The conductivity calculated for $V_g = 0$ was 0.001 S cm^{-1}. A similar dependence obtained for the device *in vacuo* is depicted in Fig. 3 *b*. This dependence is not linear. For a

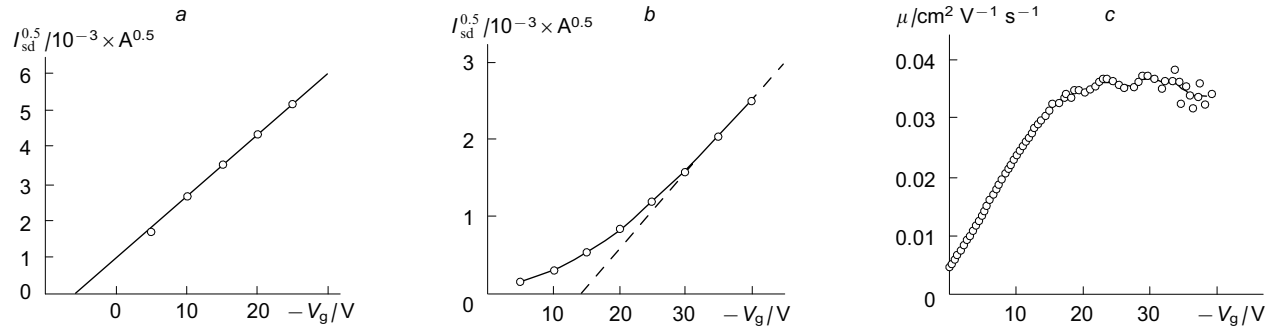


Figure 3. Current *vs.* gate voltage plot for an OFET based on α,ω-dihexylsexithiophene kept in air (*a*) and in vacuum (*b*) and a charge carrier mobility *vs* gate voltage plot (*c*).[18]

straight line plotted through three points at the highest gate voltage, the OFET parameters were $\mu = 0.034$ cm^2 V^{-1} s^{-1} and $V_0 = -13.9$ V, and the conductivity was very low, amounting to 10^{-6} S cm^{-1}. The voltage V_0 thus obtained does not correspond to relation (3) in the sign and does not correlate with low conductivity in the magnitude. It was noted that most of the real OFETs behave as the latter type of devices, *i.e.*, they show a non-linear dependence of the square root of the current on the gate voltage, which makes the calculation of key OFET parameters ambiguous. For solving this problem, the dependence of carrier mobility on the gate voltage was plotted (see Fig. 3 *c*). This plot shows a linear increase at low voltage and saturation at high voltage. The researchers [18] concluded that the measured threshold voltage for the OFETs is determined by the dependence of carrier mobility on the electric field strength rather than by the carrier density in the absence of applied voltage (V_0). A probable physical reason behind this dependence is the hopping mechanism of charge transport in organic semiconductors.

Horowitz *et al.*[19] investigated the dependence of the carrier mobility on the gate voltage for the OFETs based on linear oligothiophenes with different lengths of conjugation (4, 6 or 8 thiophene rings). Similar dependences were obtained for all of the studied compounds. For correct estimation of the carrier mobilities, the authors proposed numerical differentiation of relation (4). In practice, they measured the transfer characteristics of the device at low drain voltage (in the linear regime) for the calculation of key parameters. This approach provided the most uniform distribution of the carrier density in the transistor channel.

Apart from the charge carrier mobility, the authors [19] studied the effect of OFET contact resistances arising at the semiconductor/electrode interface on the measured electrical characteristics of the device. The contact effects can be taken into account by introducing an additional term into relation (4)

$$I_{sd} = \frac{W}{L}\mu C\,(V_g - V_0)(V_{sd} - I_{sd}R_s) \qquad (6)$$

where $I_{sd}R_s$ is the voltage drop across the contact resistance. It was noted that the nature of contact effects cannot be determined unambiguously and additional investigations are required. Two possible reasons were hypothesized: either a difference between the Fermi level of the electrode material and the HOMO level of the organic semiconductor, giving rise to an injection barrier, or diffusion of gold atoms into the semiconducting layer during the electrode deposition. For estimation of the electrical properties of OFETs, it is necessary to include the contribution of contact effects, because this gives rise to a considerable correction to the measured value of carrier mobility. The calculated values of the total contact resistance at different gate voltages and $V_0 = 0$ and 4.25 V (in this case, the parameter V_0 was selected empirically) are presented in Fig. 4 *a*. These dependences show a saturation pattern and increasing contact resistance with increasing gate voltage. The maximum R_s values were equal for different V_0 , which was in line with the theoretical dependence for the contact resistance

$$R_s = \frac{1}{g} - \frac{L}{W\mu C(V_g - V_0)} \qquad (7)$$

where $g = I_{sd}/V_{sd}$ is the drain conductance.

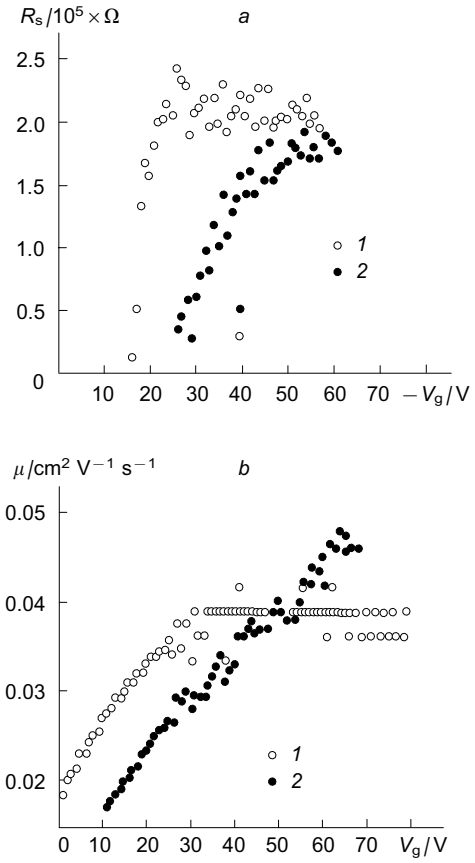


Figure 4. Contact resistance of an OFET based on octithiophene (8T) *vs.* gate voltage at $V_0 = -4.5$ (*1*) and 0 V (*2*) (*a*) and charge carrier mobility *vs.* gate voltage without (*1*) and with (*2*) allowance for contact effects (*b*).[19]

The dependences of carrier mobility on the gate voltage with and without the contact resistance correction are reflected in Fig. 4 *b*. The effect of contact resistance is pronounced at high voltage where the uncorrected dependence shows saturation of the measured carrier mobility. Meanwhile, if the correction is applied, the mobility has a linear dependence on the gate voltage. This effect was observed previously for oligothiophenes [20] and pentacene;[21] however, Horowitz *et al.*[19] showed for the first time that saturation of the measured mobility is caused by contact effects. It is noteworthy that the effect of contact resistances on the properties of OFETs is described in quite a few publications. Of interest is the review of Natali and Caironi [22] devoted to minimization of contact resistances and to efficient injection of charge carriers into OFETs.

It is worth noting that relations (1) and (2), which were initially derived for MISFETs, are not always applicable. Nevertheless, by analysis of published data, it is possible to formulate the following algorithm for adequate evaluation of the electrical properties of OFETs using expressions (1) and (2):[23]

— manufacturing of several devices based on similar semiconducting films with different channel lengths;

— measuring the transfer characteristics at low gate voltage (in the linear regime) for each device;

— plotting the dependence of the total resistance (channel resistance + contact resistance) on the channel length at

different gate voltages and approximating the results by theoretical dependence (7);

— calculating the true conductivity of the OFET channel from the slope of the curves;

— calculating the mobility of charge carriers and the threshold voltage.

This approach implies that the semiconductor is homogeneous and isotropic; it does not take into account the effect of domain boundaries of the semiconducting film. When the film has a domain structure, the procedure for derivation of the key characteristics can become much more complicated. This analysis has been carried out[24] for a special case of disk-shaped domains and in the absence of contact resistance between the domains and at the domain/electrode interface and is considered in detail below.

It is worth noting that numerous publications with insufficiently substantiated evaluation of the carrier mobility have appeared in recent years, first of all, in chemical and materials science journals; this is especially true for publications that present $\mu > 1$ cm^2 V^{-1} s^{-1}. The incorrect evaluation can be attributed to various reasons, including the effect of contact resistance, gate leakage and other factors. Critical analysis of numerical data is beyond the scope of the present review; however, we refer to a paper of Choi *et al.*,[25] which gives a detailed consideration of the problems of correct evaluation of organic semiconducting properties.

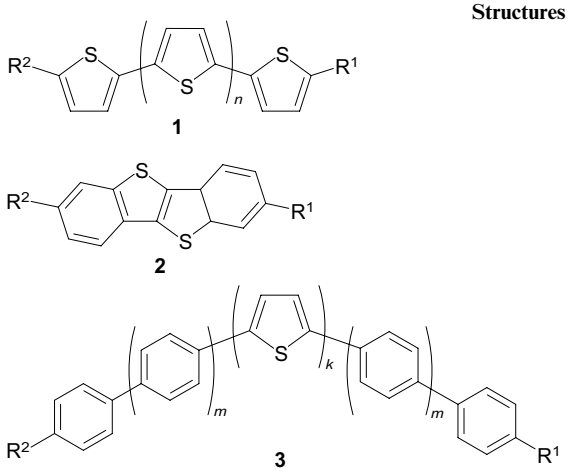
4. Selection of materials for organic field effect transistors

Two key types of organic semiconducting materials are known: conjugated oligomers and polymers. Polymers are polydisperse systems, the self-organization of which to highly ordered monolayers is an intricate and poorly reproducible process, because it depends not only on the molecular mass and molecular mass distribution, but also on the content and nature of terminal groups. The conjugated oligomers used in organic electronics are, most often, individual organic compounds that can be isolated highly purified and their self-organization to monolayers is due, most of all, to crystallization or formation of mesomorphic phases. The self-organization processes compete with interaction with the substrate, follow general trends and are well reproduced. In view of the above, in the vast majority of works, conjugated oligomers have been used to manufacture SAM-based devices.

The chemical nature of conjugated oligomers can be varied over broad limits. Conjugated oligoacetylenes, oligo(*p*-phenylenes), oligo(phenylene vinylenes), oligopyrroles, oligothiophenes and other compounds are known. Unfortunately, most of compounds of the mentioned classes are either easily oxidized in the presence of air oxygen [oligoacetylenes, oligo(phenylene vinylenes), oligopyrroles] and, therefore, organic devices based on them are non-durable and need to be encapsulated, which increases the manufacturing cost, or poorly soluble in organic solvents [oligo(*p*-phenylenes)] and can be deposited only by vacuum sublimation, which extremely complicates the monolayer fabrication. Exceptions are provided by various oligothiophene derivatives, which simultaneously possess high thermal and thermooxidative stabilities and good solubility; this allows the manufacture of highly reproducible devices with long lifetimes by solution processing. In view of the foregoing, it is not surprising that most of publications on SAMFETs with outstanding characteristics were carried out using thiophene derivatives.

The classes of compounds used most widely for OFET manufacture include oligothiophenes, benzothienobenzothiophenes and oligo(thiophene phenylenes) (structures **1** – **3**).

Structures 1 – 3



R^1, R^2 = Alk, H; n = 1 – 5; m = 0, 1; k = 1 – 3

4.1. Oligothiophenes

Oligothiophenes **1** are a promising class of compounds used as organic semiconductors in OFETs owing to high mobility of charge carriers, good thermal and thermooxidative stability and reproducibility of electrical characteristics. Halik *et al.*[26] described transistors based on dialkyl-substituted α,α′-oligothiophenes with different lengths of conjugation in the bottom-gate top-contact (Fig. 5 *a*) and bottom-gate bottom-contact (see Fig. 5 *b*) configurations. The didecylquatro-, -quinque- and -sexithiophene films were deposited by thermal evaporation on a pretreated structured substrate. The best electrical characteristics for all of the compounds were found for bottom-contact devices. The authors attributed this result to high resistance at the semiconductor/electrode interface arising upon electrode deposition over the semiconductor. A typical transfer characteristics of the OFET based on sexithiophene derivative **7** corresponds to p-type OFETs (see Fig. 5 *c*). For this compound, the highest carrier mobility of 0.5 cm^2 V^{-1} s^{-1}, the subthreshold slope of 3.1 V per decade and on/off current ratio of 10^5 were attained. The higher carrier mobilities exceeding the known values for oligothiophenes were attributed to highly smooth surface of the dielectric used [poly(4-vinylphenol)], with the surface roughness being ~7 Å. Successful operation was demonstrated for simple OFET-based integrated circuits, an inverter and a five-stage ring oscillator with a short signal propagation delay of 30 μs per stage.

Another study of the same research team[27] addresses the relationship between the molecular structure of the organic semiconductor and the electrical properties of the corresponding OFETs for several α,α′-oligothiophenes with different lengths of conjugated cores and symmetrical organic substituents (structures **4** – **9**). The transistor configurations correspond to those described in the above study.[26] It was

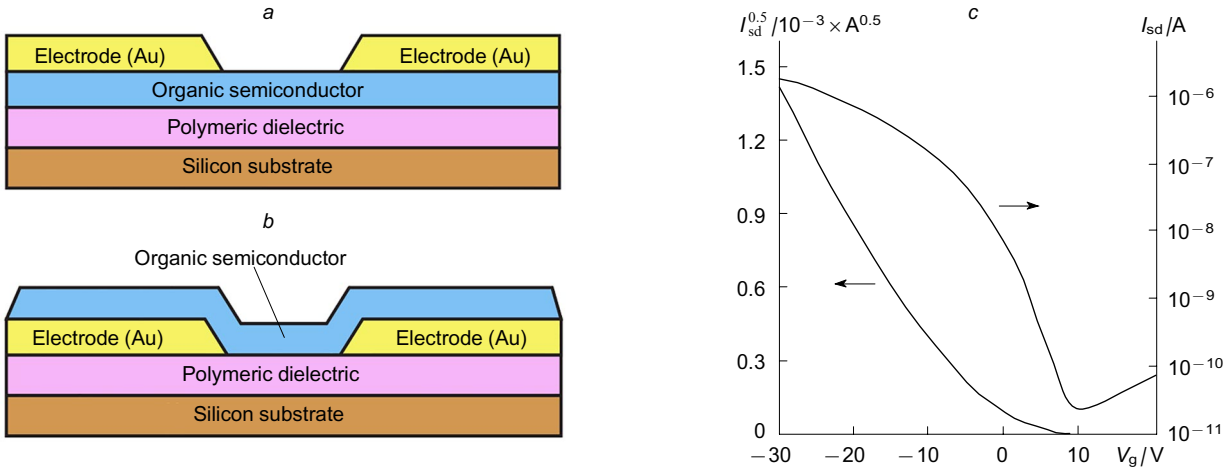


Figure 5. Schematic diagrams of OFETs in the bottom-gate top-contact (*a*) and bottom-gate bottom-contact (*b*) geometries and typical transfer characteristics of an OFET based on dihexylsexithiophene for $V_d = -20$ V (*c*).[26]

found that in the top-contact topology, the length of the conjugated moiety affects relatively slightly the electrical properties of the OFETs, whereas the length of the alkyl groups is a crucial factor for effective operation. The authors attributed this finding to the fact that long alkyl chains create a barrier for charge carrier injection and decrease the measured mobility. In the bottom-contact topology, neither the length of the conjugated moiety nor the length of alkyl substituents has a noticeable effect on electrical properties. The highest mobility of charge carriers equal to 1.1 $cm^2\ V^{-1}\ s^{-1}$ was found for devices based on short alkyl chain compounds (Fig. 6). At the time of publication, this was the record-high value for OFETs based on semiconductors other than pentacene. In the case of both configurations, unsubstituted sexithiophene **9** demonstrated a minimum mobility of charge carriers, which was attributed to an important role of alkyl substituents for the optimal molecular packing of the semiconductor to be formed in the layer and for efficient π–π interaction to occur.

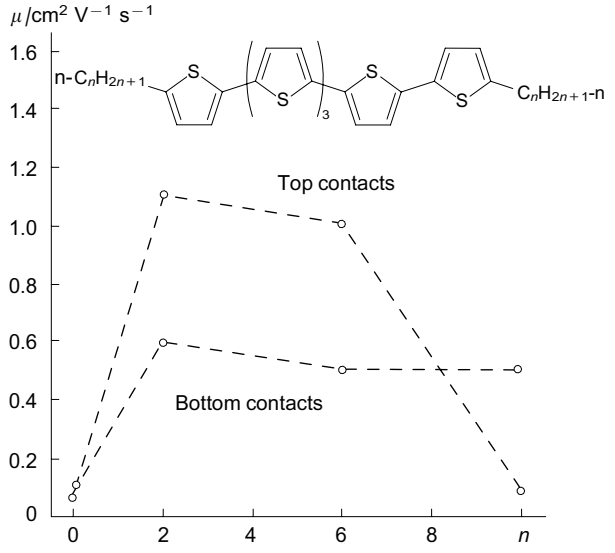
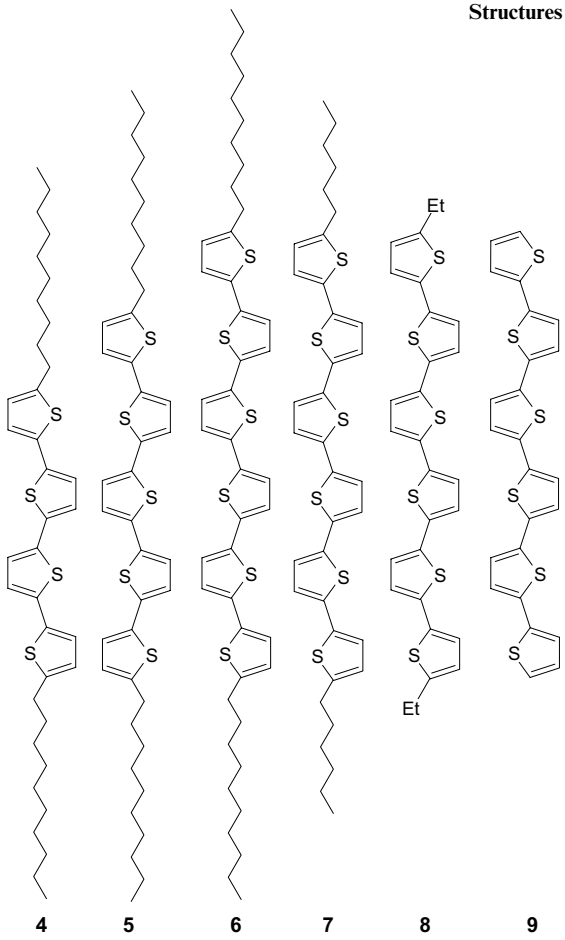


Figure 6. Charge carrier mobility *vs.* the length of symmetrical alkyl substituents in oligothiophenes **6**–**9**.[27]

Xia *et al.*[28] investigated the morphology of thin films composed of α,α′-sexithiophenes with aliphatic substituents containing 0 to 10 carbon atoms as a function of substrate

Structures 4–9



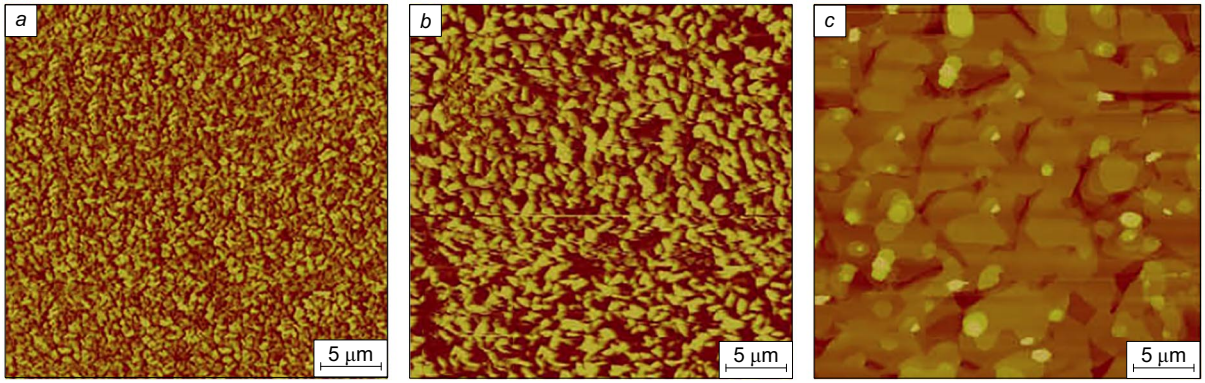


Figure 7. AFM images of α,ω-didecylsexithiophene **6** films thermally deposited on a silicon substrate at a temperature of 20 (*a*), 80 (*b*) and 120 °C (*c*).[28]

temperature during thermal deposition. Figure 7 shows the variation of the organic layer morphology with increasing temperature of the substrate during deposition of didecylsexithiophene **6** as a typical case. It was found that a layer with a domain morphology is formed at any temperature. The characteristic size of the domain increases with increasing substrate temperature. This trend was established for all of the compounds. Note that the substrate temperature for didecylsexithiophene is 120 °C, which is higher than the melting point (108 °C). At this temperature, the maximum domain size was ~1 μm. The authors attributed this result to the fact that the phase transition may serve as an additional factor significantly increasing the size of the domain during film growth.

It is of interest that, despite considerable differences in the morphology, carrier mobility did not depend on the substrate temperature during thermal deposition for any of the films. This was explained in the following way: the initial stages of film growth are described as the Frank – van der Merwe layer-by-layer growth over the whole temperature range; subsequently, at greater film thickness, the growth follows the layer-by-layer mechanism and the Stransky – Krystanov island growth mechanism determining the layer morphology, which can be observed by AFM. It was suggested that the film surface morphology makes an insignificant contribution to the electrical properties of OFETs, because only 1 or 2 lower layers of the semiconducting films are current-carrying. To confirm this assumption, monolayer films of dihexylsexithiophene **7** were studied. The substrate coverage was varied from 50% (half-monolayer) to 150% (complete monolayer and incompletely covered second layer). The devices with 50% coverage of the monolayer did not exhibit electrical properties; this was attributed to the absence of a common conducting channel in the transistor. When the substrate coverage was close to 100%, the carrier mobility in the OFETs was 0.05 $cm^2\ V^{-1}\ s^{-1}$, which is ~1 order of magnitude lower than that for thick polycrystalline films of the same compound (0.67 $cm^2\ V^{-1}\ s^{-1}$). It is of interest that the carrier mobilities at 150% coverage of the substrate by a monolayer proved to be close to the values measured for a polycrystalline film (0.25 $cm^2\ V^{-1}\ s^{-1}$). This fact illustrates the important role of the second layer for the charge transport and confirms the assumption that the charge transport in the oligothiophene films occurs predominantly in a thin layer at the dielectric/semiconductor interface.

Xia *et al.*[28] investigated stability of the electrical characteristics of OFETs based on sexithiophene derivatives and the change in the key transistor parameters during operation at elevated temperatures. All of the studied oligomers were stable in air during at least 8 days. A lower stability was found for unsubstituted sexithiophene **9**, which may be due to its susceptibility to oxidation at the α-position. The substituted oligothiophenes were highly stable, withstanding up to 100 days in air. It was also found that with temperature rise from 25 to 80 °C, the carrier mobility decreases from 0.7 to 0.1 $cm^2\ V^{-1}\ s^{-1}$ and the threshold voltage shifts to positive values by 12 V. It is important that upon storage of devices for 20 h at room temperature, the initial electrical characteristics are fully restored. The authors concluded that the factors affecting the electrical properties cannot be unambiguously determined on the basis of the available data; however, they noted high stability of the devices and their ability to restore characteristics after the heat treatment.

4.2. Benzothienobenzothiophenes

In 2007, Japanese researchers[29] proposed for the first time a new class of compounds — benzothienobenzothiophenes (structure **2**) — to be used as semiconductors for OFETs.[29] A number of symmetrical BTBT derivatives with different aliphatic substituent lengths (5 to 14 carbon atoms in the chain) were synthesized and studied. Irrespective of the substituent length, the BTBT derivatives were found to form uniform films deposited by spin coating on the silicon dioxide surface. The charge carrier mobility considerably depended on the aliphatic substituent length, with the best electrical characteristics being found for the 13-carbon aliphatic chain (the mobility was in the range of 1.20 – 2.75 $cm^2\ V^{-1}\ s^{-1}$). Apart from the high mobility of charge carriers, BTBT-based compounds had a good solubility (up to 90 g $litre^{-1}$ for the 9-carbon substituent), which made them promising materials for solution processing. However, devices based on new materials exhibited a considerable drawback, namely, high threshold voltage in OFETs (about −20 V with drain and source electrodes made of gold); this was a consequence of low HOMO level (−5.5 eV) inherent in benzothienobenzothiophenes.[30]

Amin *et al.*[31] studied dialkyl-substituted BTBT derivatives with 12- and 13-carbon aliphatic spacers. The authors set ourselves the task to decrease the operating voltages of BTBT-based transistors by exploiting the following two factors. First, it was proposed to use ultrathin gate dielectrics based on nanometre-thick AlO_x. Second, it was proposed to cover the surface of the dielectric by self-assembled interfacial monolayers of tetradecylphosphonic (C_{14}-PA) and 12,12,13,13,14,14,15,15,16,16,17,17,18,18,18*H*-pentadecylfluorooctadecylphosphonic ($F_{15}C_{18}$-PA) acids. The molecules of these compounds have a dipole moment directed along the molecular axis. Surface modification of the dielectric in the OFETs with this self-assembled interfacial layer generates an electrostatic field in the transistor active layer, which may change the threshold voltage of the transistor.[32] Thus, by combination of two above factors, the operating voltage of the device can be decreased.

The transfer characteristics of OFETs based on 2,7-bis-(tridecyl)[1]benzothieno[3,2-*b*][1]benzothiophene (C_{13}-BTBT-C_{13}) with the ultrathin (3.6 nm) AlO_x dielectric and the hybrid AlO_x + self-assembled monolayer dielectric are depicted in Fig. 8. In the former case, the operating voltages of the transistor were decreased to $V_g = -3$ V and $V_{sd} = -2$ V. Like in the case of 'thick' dielectrics, these devices demonstrated relatively high μ values (up to 2 $cm^2\ V^{-1}\ s^{-1}$), but the on/off current ratio decreased from 10^8 to 10^3-10^5, mainly due to increasing gate leakage current as a result of using the ultrathin dielectric. As to transistors based on the hybrid dielectric, the additional self-assembled monolayer decreased the gate leakage current; as a result, the ratio $I_{on/off}$ increased. The use of C_{14}-PA-based SAM virtually did not change the threshold voltage of the OFET, whereas with the $F_{15}C_{18}$-PA-based SAM, the threshold voltage decreased in magnitude from -1.8 to -0.8 V. The authors attributed this result to the effect of the electrostatic field of the SAM dipole layer, which boosted saturation of the conducting channel with holes and gave rise to a current at a lower applied voltage.

One more promising BTBT derivative has been reported by Amin *et al.*[33] The authors proposed using 2-tridecyl[1]benzothieno[3,2b][1]benzothiophene (C_{13}-BTBT) as the organic semiconductor for OFETs. Like the paper cited above,[31] this study addressed transistors with bottom-gate top-contact topology. Upon thermal deposition of C_{13}-BTBT films on the thin (3.6 nm) AlO_x dielectric surface, the carrier mobility was close to that found for disubstituted analogue, namely to 1.2 ± 0.3 $cm^2\ V^{-1}\ s^{-1}$ (Ref. 31). However, in the case of semiconductor deposition on the dielectric treated with the self-assembled C_{14}-PA monolayer, the carrier mobility increased by more than an order of magnitude, up to 14.2 ± 2.6 $cm^2\ V^{-1}\ s^{-1}$.

In order to interpret the considerable increase in the carrier mobility resulting from treatment of the dielectric with the interfacial layer, the authors investigated the

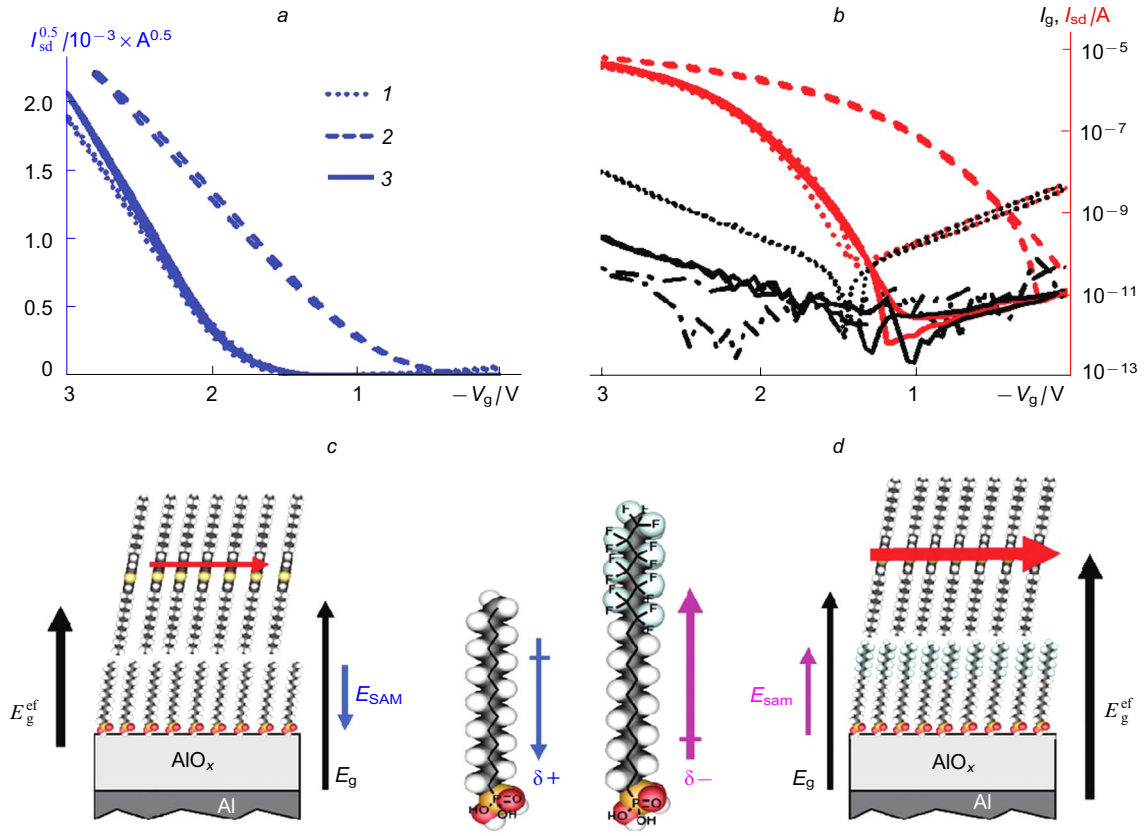


Figure 8. Transfer characteristics of OFETs based on C_{13}-BTBT-C_{13} with the ultrathin (3.6 nm) AlO_x dielectric (*a*) and hybrid AlO_x + SAM dielectric at $V_{sd} = -2$ V (*b*) and schematic images of SAMs on the aluminium oxide surface modified by C_{14}-PA (additional electric field is directed downward) (*c*) and by $F_{15}C_{18}$-PA (additional electric field is directed upward) (*d*).[31]
(*a*, *b*) (*1*) AlO_x, (*2*) $F_{15}C_{18}$-PA, (*3*) C_{14}-PA; (*c*, *d*) red arrows point to the charge transport area.

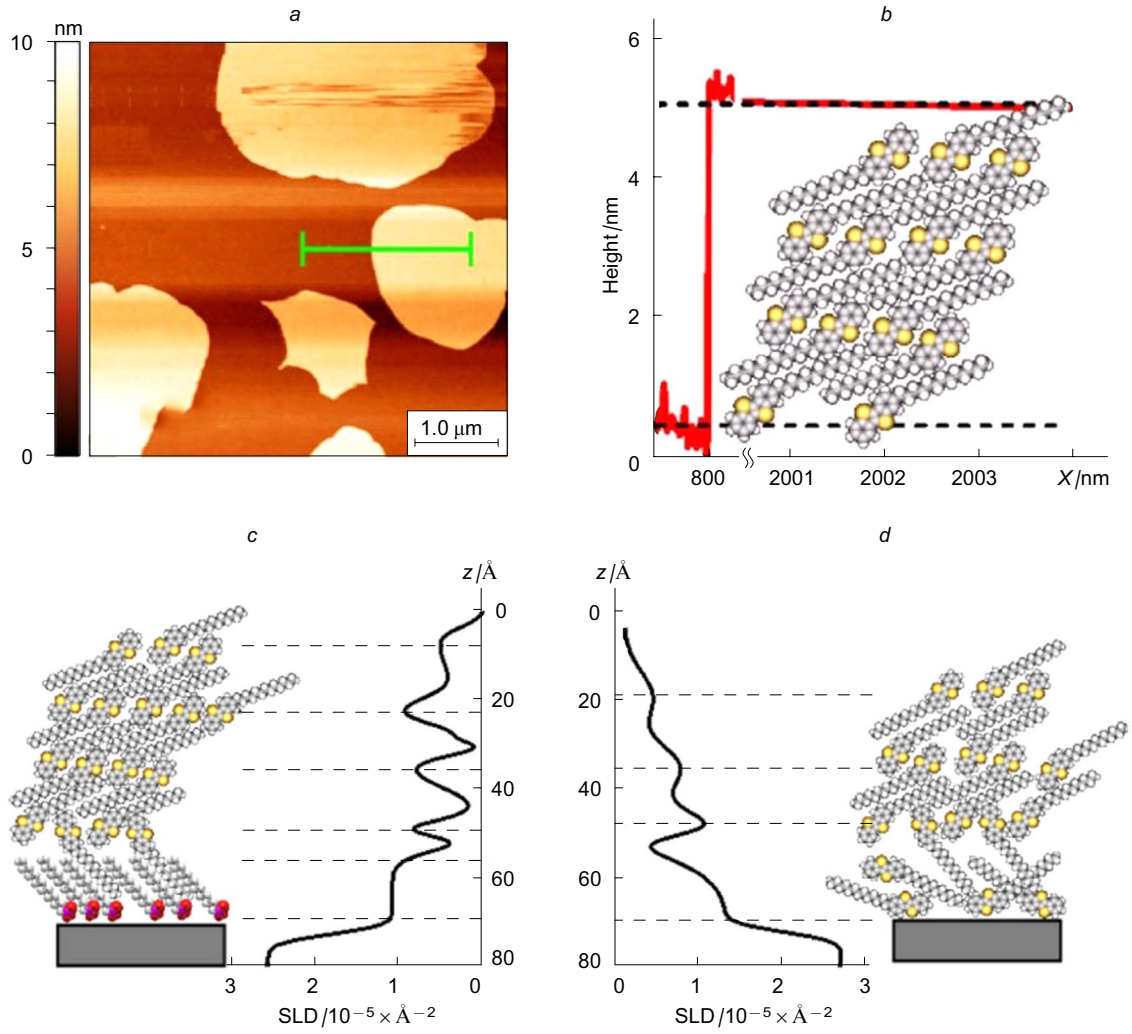


Figure 9. AFM morphology of the C_{13}-BTBT films in the initial growth stage (*a*), AFM surface cross-section and assumed molecular packing (*b*) and grazing incidence X-ray diffraction data (SLD model) for thin C_{13}-BTBT films on the hybrid AlO_x/C_{14}-PA dielectric (*c*) and aluminium oxide (*d*).[33]
(*a*) Green colour marks the area used to take the surface cross-section (see Fig. *d*).

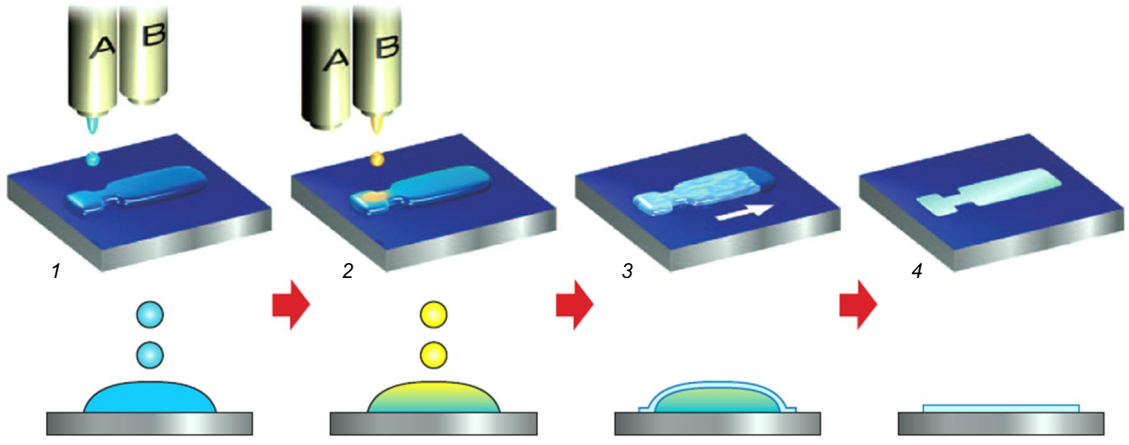


Figure 10. Chart for inkjet printing of C_8-BTBT-C_8 single crystals;[34] (*1* – *4*) numbers of stages, see text.

morphology of the C_{13}-BTBT film in the initial growth stage by AFM. The separate smooth disk-like islands of the layer were 5.1 nm high (Fig. 9 *a*), which exceeded not only the calculated length of the molecule, but also the height of the possible bilayer in the case of vertical arrangement of the molecules. This suggested a molecular packing for monosubstituted BTBT derivatives crucially different from the packing of their disubstituted analogues with strong π–π interaction and overlap of the alkyl groups of molecules located in different layers (see Fig. 9 *b*). In order to understand the difference between the C_{13}-BTBT molecular packings with and without SAM, the authors used grazing incidence X-ray diffraction and the SLD model. The presence of a repetition period of 13–14 Å in the resulting electron density distributions attested to repeating fragments with strong π–π interaction (BTBT) occurring in the layer. However, the electron density at the interface with a dielectric was lower without SAM than with SAM. The authors attributed this to low ordering (see Fig. 9 *c*,*d*) of the lower part of the semiconductor responsible for the electrical transport in OFET in the case where this layer was deposited directly on the dielectric and a considerably better ordering in the case of deposition over the SAM. For this reason, transistors with an additional interfacial layer demonstrated more than an order of magnitude higher mobilities of charge carriers.

Especially interesting is the study of Japanese researchers[34] who developed an approach for growing single crystals of a disubstituted BTBT derivative, 2,7-dioctyl[1]-benzothieno[3,2-*b*][1]benzothiophene (C_8-BTBT-C_8), using inkjet printing, which is distinguished by high rate and convenience of handling. An important specific feature of the obtained crystals is the exceptionally high carrier mobility (on average, 16.4 $cm^2\ V^{-1}\ s^{-1}$). According to the procedure proposed by the authors, the film was supposed to grow from a mixture of the solvent and antisolvent; this gave organic semiconductor single crystals. These films were formed using silicon substrates with a thermally grown 100 nm-thick oxide layer. Prior to inkjet printing, isolated areas (patterns) of a specified shape with highly hydrophilic surface were formed on the substrate. The patterns were generated by UV or ozone treatment and subsequent growth of the self-assembled hexamethyldisilazane layer on the substrate followed by deposition of the photoresist onto the layer. The chart of single crystal growth is shown in Fig. 10. First (stage *1*), a drop of the antisolvent (DMF) was applied on the structured substrate by inkjet printing. Next (stage *2*), several drops of semiconductor ink, a solution of C_8-BTBT-C_8 in dichlorobenzene, were printed over the antisolvent drop. The drops printed in this way were intermixed in a substrate area predefined by the pattern. During evaporation of the solvent mixture, nucleation centres were formed on the drop surface. The positions of these centres were randomly distributed within the pattern; however, it was found that the position of the start of nucleation can be controlled *via* design of the shape of the initial pattern. Thus, in areas where drops had high surface-to-volume ratio, the probability of nucleation proved to be high and the single crystal growth occurred *via* slow movement of the single crystallization front (stage *3*) to give a single crystal (stage *4*).

The morphology and the structure of the resulting films were studied by atomic force and polarizing optical microscopy, X-ray diffraction and polarized light absorption spectroscopy. The films were found to be single crystalline with a high optical anisotropy. The molecular packing of the crystals had a herringbone structure, like packings of the single crystals of other conjugated oligomers such as anthracene[35] and pentacene.[36]

The semiconducting properties of the printed C_8-BTBT-C_8 single crystals were tested in the top-gate top-contact OFETs. Gold contacts were used as the source and drain and parylene C served as the gate dielectric. The electrical properties were measured under argon at a temperature of 300 K. Figure 11 *a* shows the transfer characteristics of the obtained OFET. In the saturation regime, the carrier mobility was on average 16.4 $cm^2\ V^{-1}\ s^{-1}$, while the maximum value was 31.3 $cm^2\ V^{-1}\ s^{-1}$. The on/off current ratio was 10^5– 10^7, the subthreshold slope was −2 V per decade, and the threshold voltage was about −10 V. The authors also noted the absence of apparent hysteresis in the device VAC. It is important that the electrical characteristics of the obtained transistors were retained during 8 months under ambient conditions (the decrease in the carrier mobility was <10%). The relatively high non-linearity of the output curves (see Fig. 11 *b*) in the region of low V_{sd} attested to the presence of contact resistance at the electrode/semiconductor interface. Furthermore, the output characteristics did not show saturation at high V_{sd} values, which may be attributable to the presence of rather high parasitic currents in the OFET. The calculation of OFETs in the

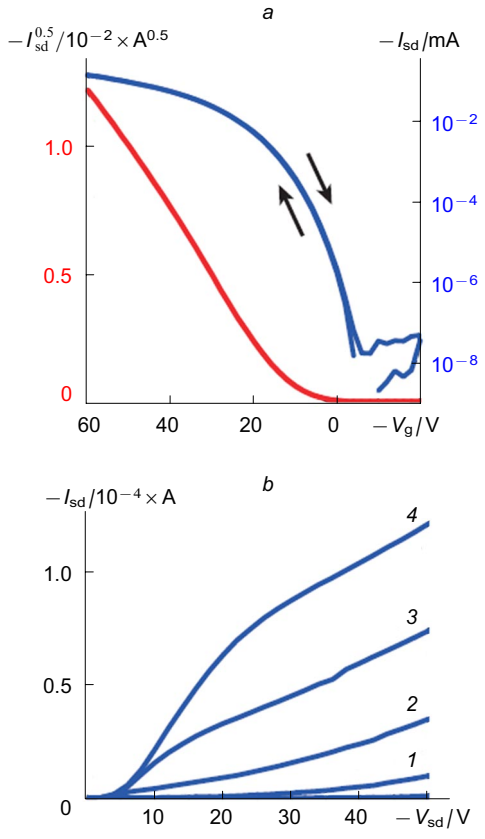


Figure 11. Volt-ampere curves for OFETs based on inkjet printed single crystals of C_8-BTBT-C_8: transfer characteristics (*a*), series of output characteristics of OFETs at different gate voltages (*b*).[34] (*a*) $V_{sd} = -60$ V; *b*: $-V_g = 30$ (*1*), 40 (*2*), 50 (*3*), 60 V (*4*).

saturation regime from the VACs of transistors with these specific features can lead to overestimated mobility values.[22] Nevertheless, high semiconducting properties of the formed single crystals are beyond doubt and the developed printing approach is versatile and applicable to the preparation of a broad range of organic semiconductors.

4.3. Oligothiophenephenylenes

A promising application of OFETs is the manufacturing of light emitting devices, so-called organic light emitting transistors.[37] Although organic light emitting diodes have been used in electronics for a rather long time, the number of scientific publications devoted to OLETs is increasing. The interest in the OLETs is related, on the one hand, to their planar architecture, which allows direct investigation of charge carrier recombination and exciton formation,[38] and, on the other hand, to potentially high quantum efficiency compared to that of OLEDs.[39]

The efficiency of OLETs is attained due to key factors such as high exciton density in the light emitting transistor channel, which is ensured by high mobility of two types of charge carriers and high luminescence efficiency. However, currently, both properties can be combined in one organic semiconductor material only in exceptional cases.[40] This is explained by the fact that, first, high mobility of charge carriers may be due to dense molecular packing of the material and, second, the dense packing gives rise to non-radiative channels of exciton relaxation, which reduces the quantum efficiency.[41] Oligothiophenephenylenes (structure

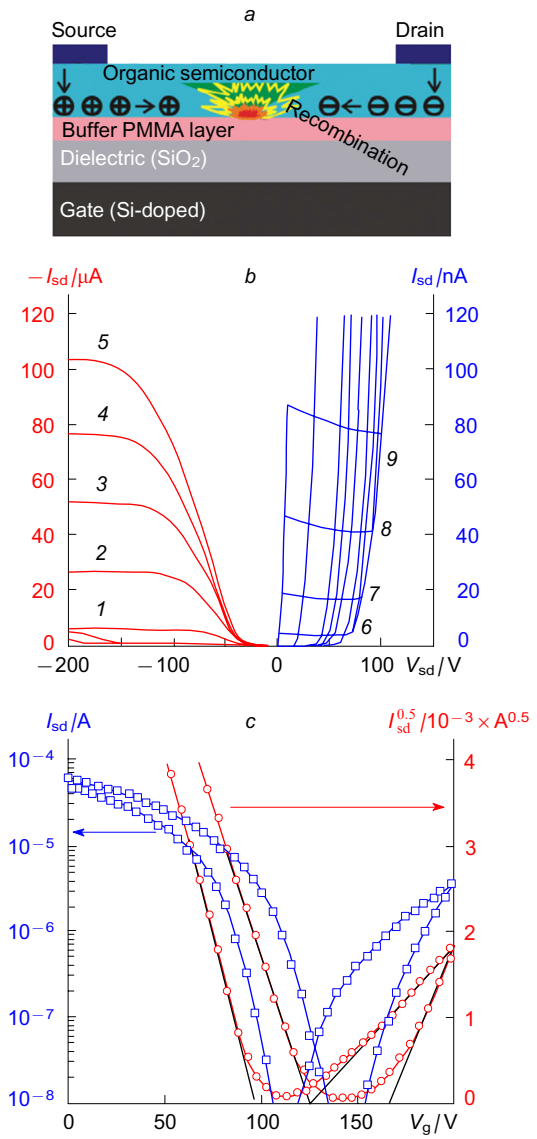


Figure 12. Schematic diagram of an OLET based on the BP3T single crystal (*a*), OLET output characteristics in the hole saturation regime (red-coloured lines) and electron saturation regime (blue-coloured lines) (*b*) and transfer characteristics of an OLET with n-type channel at V_{sd} = 80 V (*c*).[42]
(*b*) V_g = −100 (*1*), −120 (*2*), −140 (*3*), −160 (*4*), −180 (*5*), 120 (*6*), 140 (*7*), 160 (*8*), 180 V (*9*); (*c*) one transfer characteristics is given (forward and backward sweeps) on two scales corresponding to two ordinate axes, μ_e = 0.03–0.17 cm^2 V^{-1} s^{-1}, μ_h = 1.42–1.64 cm^2 V^{-1} s^{-1}.

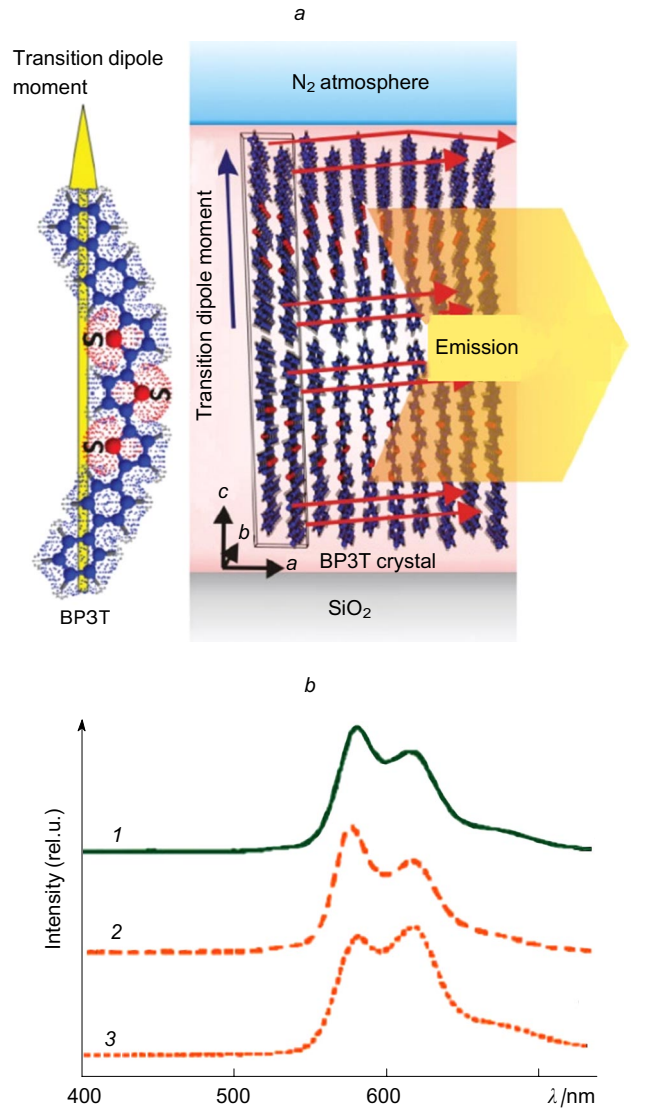


Figure 13. Illustration of the wave guide effect for the BP3T single crystal (*a*), photoluminescence spectrum of the crystal (*1*) and electroluminescence spectra (*2*, *3*) of two OLETs based on this crystal (*b*).[42]

3) represent a class of conjugated oligomers that combine a moderate carrier mobility and high luminescence efficiency.

Bisri *et al.*[42] have grown single crystals of α,α′-bis(biphenyl-4-yl)terthiophene, which demonstrated both high luminescence efficiency (80%) and ambipolar conductivity. The diagram of the OLET based on a BP3T single crystal is presented in Fig. 12 *a*. The BP3T single crystals were grown by vapour deposition and then electrostatically laminated onto a silicon substrate with thermally grown SiO_2 coated with a thin (4–6 nm) PMMA layer. The transistor source and drain were deposited by the thermal method through a shadow mask. For efficient injection of electrons and holes in the device, asymmetrical gold and calcium electrodes were used.

The volt–ampere (output) curves of the device are presented in Fig. 12 *b*. The obtained OLETs demonstrate the ambipolar semiconducting properties. The non-linearity of transistor operation in the hole saturation region at low voltages is indicative of large contact resistances at the electrode/semiconductor interface. The mobility of charge carriers was calculated for the saturation regime from transfer characteristics (see Fig. 12 *c*). The average carrier mobilities were 1.64 and 0.17 $cm^2\ V^{-1}\ s^{-1}$ for holes and electrons, respectively. In the authors' opinion, the high mobility was provided by the PMMA buffer layer, by matching between the electron levels of the electrode materials and the semiconducting layer and by growth of single crystals in the absence of water or oxygen traces.

Unlike OLETs considered in earlier publications,[38,43] devices based on BP3T showed the maximum luminescence in the plane parallel to the plane of the crystal (Fig. 13 *a*). For this reason, single crystal faces showed the most intense luminescence. Thus, the single crystal itself served as the wave guide, and the optical loss resulting from light transmission through crystal surfaces was minimized. The photoluminescence spectra of the BP3T single crystal and electroluminescence spectra of two analogous OLETs based on this compound are shown in Fig. 13 *b*. Note the mutual correlation of positions of the photo- and electroluminescence peaks (578 and 616 nm), which is well-correlated with the data published previously for other light emitting compounds.[44] The relative intensity of the electroluminescence peaks varied for different devices fabricated by the same procedure, in particular, it depended on the crystal size.

Yet another interesting study is devoted to OLETs based on 2,5-bis(biphenyl-4-yl)thiophene (BP1T) single crystals and operated by alternating-current voltage.[45] Unlike most of the studies on this subject, in this work, the authors investigated the optoelectronic properties of the oligothiophenephenylene single crystals upon application of alternating-current gate voltage. The electrical circuit for device operation is shown in Fig. 14 *a*: the frequency *f* varied from 2 Hz to 20 kHz, the gate voltage amplitude ranged from 40 to 100 V, the absolute magnitude of the direct current voltage on drain and source electrodes was in the range from 30 to 100 V, and the voltage sign corresponded to the

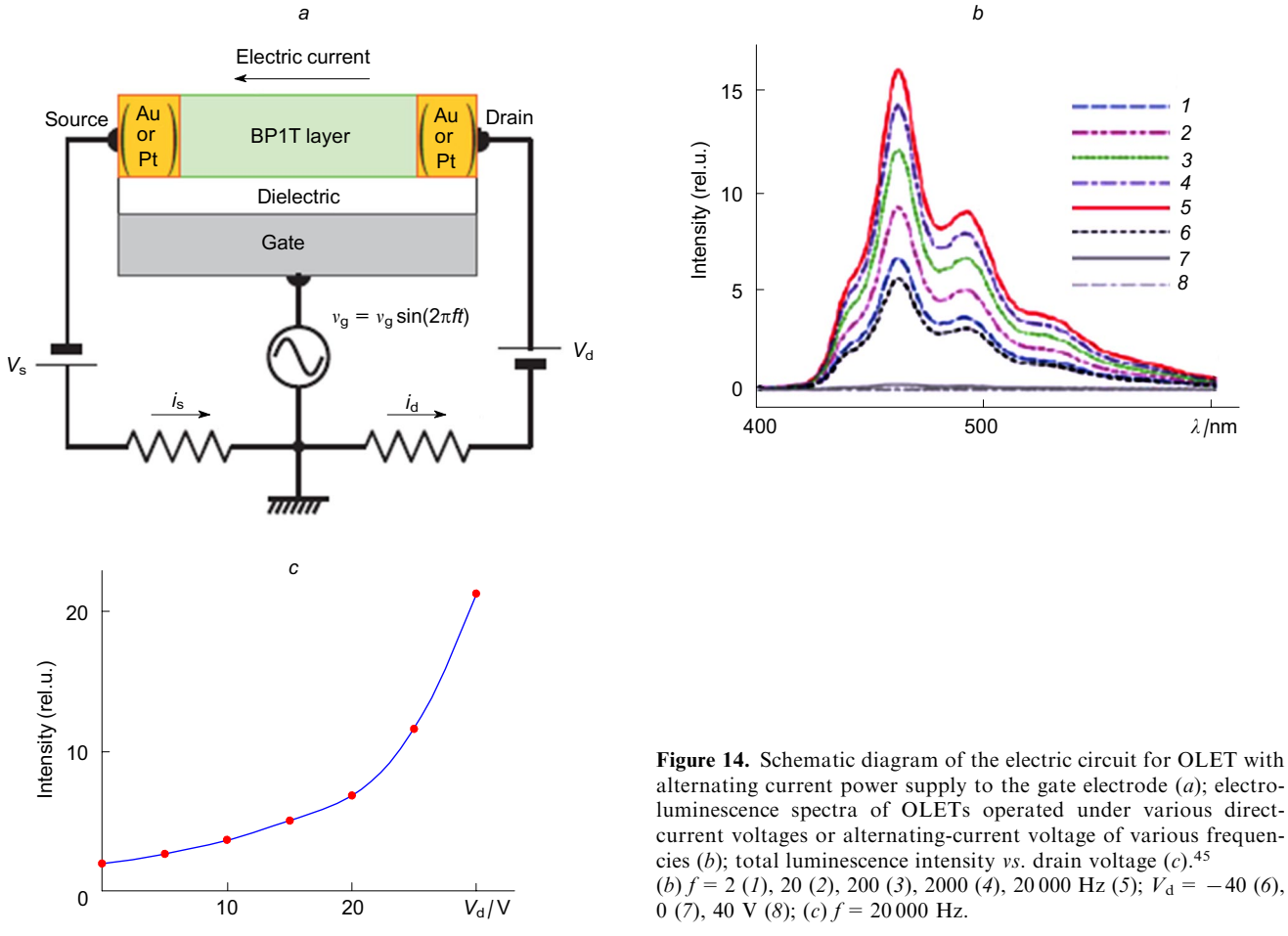


Figure 14. Schematic diagram of the electric circuit for OLET with alternating current power supply to the gate electrode (*a*); electroluminescence spectra of OLETs operated under various direct-current voltages or alternating-current voltage of various frequencies (*b*); total luminescence intensity *vs.* drain voltage (*c*).[45] (*b*) f = 2 (*1*), 20 (*2*), 200 (*3*), 2000 (*4*), 20 000 Hz (*5*); V_d = −40 (*6*), 0 (*7*), 40 V (*8*); (*c*) f = 20 000 Hz.

type of charge carriers injected from the given electrode. When the applied drain voltage was $V_d = 30$ V, the source voltage was $V_s = -30$ V, and the gate voltage amplitude was $V_g = 40$ V, the luminescence was visible by eye. At relatively low frequency (below 200 Hz), the light was intermittent, while at higher frequency, continuous luminescence was observed.

The luminescence spectra for different direct current gate voltage and for different frequencies of the modulated voltage V_g are shown in Fig. 14 *b*. It is important that even at low frequency $f = 2$ Hz, the luminescence intensity is higher than that in the case of direct current voltage V_d. As frequency increases (up to the maximum frequency accessible in the experiments, $f = 20$ kHz), the luminescence intensity monotonically increases. The authors also considered the dependence of the integrated emission intensity on the drain voltage: the V_d value was varied from 0 to 30 V, with the condition $V_d = -V_s$ being met. The shape of the obtained curves did not depend on frequency; a typical dependence is shown in Fig. 14 *c*. It is important that the device emitted light even at a zero drain voltage. In addition, the curve showed a monotonic growth, with a considerable increase in the intensity starting at $V_d = 20$ V.

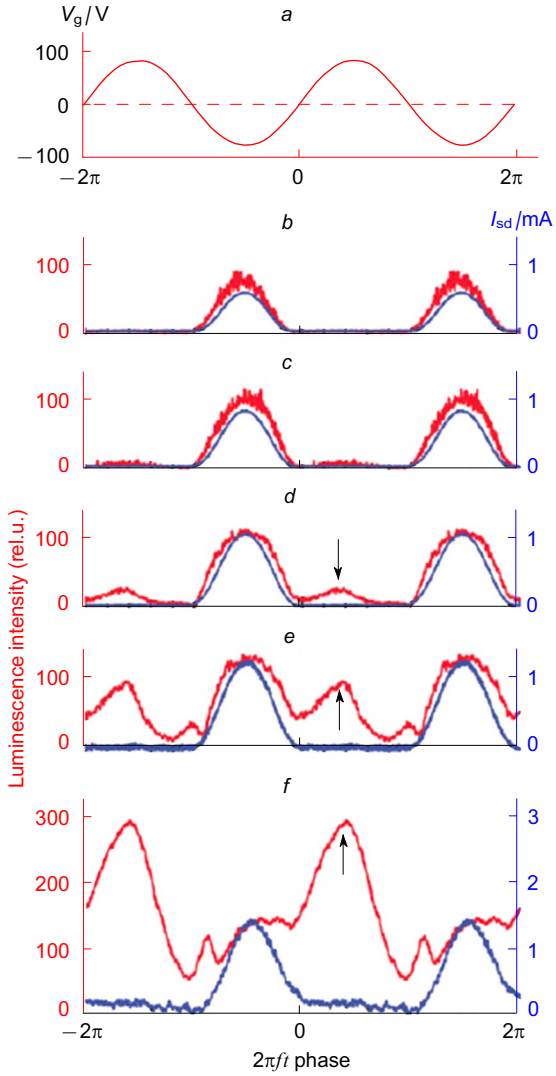


Figure 15. Shape of the gate voltage signal (*a*) and electroluminescence intensity and drain current of an OLET *vs.* gate voltage phase at various frequencies.[45]
$f = 20$ (*b*), 200 (*c*), 1000 (*d*), 5000 (*e*), 20 000 Hz (*f*).

For interpretation of the plotted dependences of the luminescence intensity on the gate voltage frequency, the authors investigated the time dependences of the electroluminescence intensity and current in the transistor channel on the voltage at various frequencies (Fig. 15). At low frequency ($f = 20$ Hz), luminescence was fully correlated with the current at negative voltages V_g. As the frequency f increased, one more weak luminescence peak (indicated by an arrow) appeared in the region of changing sign of V_g. Then the relative intensity of this peak increased, and at higher frequency, this peak determined the integral luminescence intensity. The authors attributed the appearance of this peak to the fact that charges of both signs should be present in the transistor channel for efficient luminescence to occur. In this case, in the region of positive V_g values, electrons are efficiently injected into the channel, while at negative V_g values, holes are injected. If the sign change is sufficiently fast (at high frequency), charge carriers do not have enough time to diffuse to the electrode, but interact instead with the charges of the opposite sign; finally, this interaction makes a contribution to the luminescence.

Thus, Yamao *et al.*[45] were able to attain the coexistence of high densities of opposite charges in an organic single crystal, which resulted in strong OLET luminescence. The results of this study demonstrated high potential of single crystals based on oligothiophenephenylenes for organic optoelectronic applications.

In the conclusion of this Section, we would like to note that oligothiophenes, benzothienobenzothiophenes and oligothiophenephenylenes are promising classes of organic compounds for the design of efficient self-assembled semiconducting monolayers by fast and technology-adaptable solution processing techniques. The first two indicated classes of compounds have high thermooxidative stability and charge carrier mobility in thin films. Compounds of the last-mentioned class combine moderate electron transport properties with high efficiency of photo- and electroluminescence.

5. Organic field-effect transistors based on self-assembled semiconducting monolayers

It was noted in the Introduction that the conductive layer in OFETs is 3 – 5 nm thick, which corresponds to 1 or 2 monolayers of conjugated oligomers. Experimental evidence for this fact was first reported by Dinelli *et al.*[7] and subsequently confirmed by other researchers.[46,47] Dinelli *et al.*[7] investigated thin films of sexithiophene supported on silicon with a thermally grown 200 nm-thick SiO_2 dielectric layer. Prior to the thermal deposition of the organic semiconductor, interdigitated Au/Ti electrodes were applied on the substrate to form a transistor channel with a length of 1 to 40 μm and a width of 1000 to 20 000 μm. They obtained two series of films differing in the substrate temperature and deposition rate: the first series was prepared at 150 °C and $F = 0.6$ nm min^{-1} and the second one was obtained at 120 °C and $F = 0.12$ nm min^{-1}. For both series, layer-by-layer film growth took place, which was characterized by the substrate coverage (Θ) measured as the number of monolayers (for sexithiophene, the monolayer thickness is

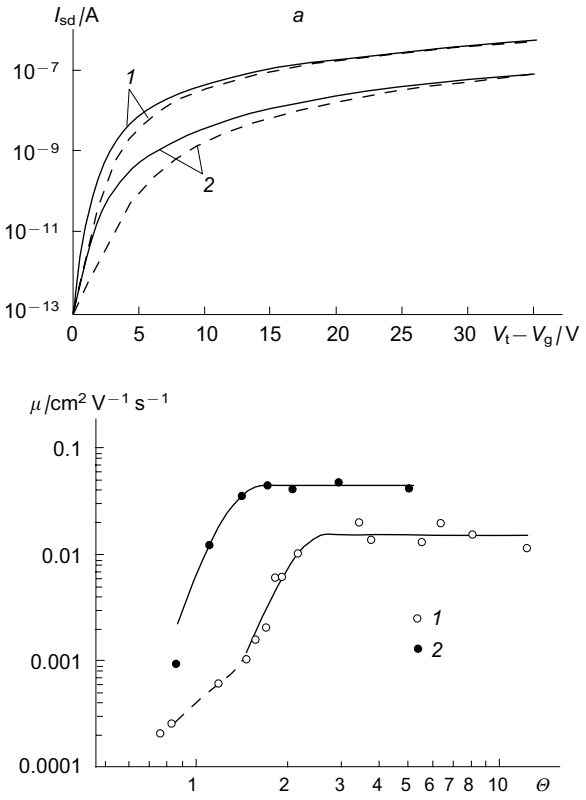


Figure 16. Transfer characteristics of OFETs based on sexithiophene (second series of films) measured at $V_{sd} = -1$ V (*a*) and charge carrier mobility *vs.* coverage Θ for the first and second series of films (*b*).[7]
(*a*) linear regime, Θ = 3 (*1*) and 1.1 (*2*), continuous and dashed lines describe the forward and backward sweeps, respectively; (*b*) (*1*) the first series of films (T = 150 °C and F = 0.6 nm min^{-1}), (*2*) second series of films (T = 120°C and F = 0.12 nm min^{-1}).

2.4 nm). The transfer characteristics of the OFETs of the second series with different Θ values are shown in Fig. 16 *a*. All of the transistors successfully operated both in vacuum and in air. In the case of measurements under ambient conditions, organic field-effect transistors demonstrated a positive shift of the threshold voltage by 8 – 10 V and a weak hysteresis of the volt – ampere curves. Furthermore, the electrical properties of devices with different Θ values were different. The dependence of the charge carrier mobility on Θ is depicted in Fig. 17 *b*. For films of the first series in the region $\Theta < 1.5$, the mobility increases exponentially; in the region $1.5 < \Theta < 2$, the mobility also increases by an exponential law, but the curve $\mu(\Theta)$ is steeper; when $\Theta \geqslant 2$, the curve is saturated. For films of the second series, the general pattern of dependence is the same; however, saturation occurs earlier (at Θ = 1.3) and the mobility is higher. Dinelli *et al.*[7] concluded that the charge transport in the OFETs occurs in one or two monolayers of the compound, while the subsequent layers make no contribution to the electric current.

5.1. Self-assembled semiconducting layers based on organic compounds with an anchor group

Currently, semiconducting monolayers are often manufactured by self-assembly of functional organic molecules.[48 – 50]

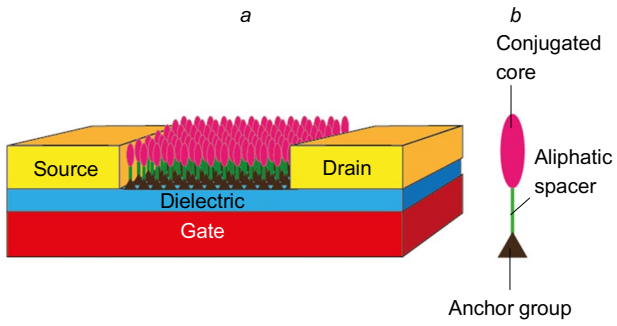


Figure 17. Schematic diagrams of a self-assembled monolayer functional anchor field effect transistor (SAMFET) (*a*) and an organic semiconductor used for the formation of the SASM (*b*).

The concept of self-assembled monolayers was proposed in 1946;[51] however, only at the end of the 1970s, a good monolayer based on organosilicon compounds was prepared.[52, 53] For the formation of SASMs, the initial compound should contain an functional anchor group, which chemically reacts with the substrate, a conjugated core, which is responsible for the semiconducting properties, and an aliphatic spacer, which allows some of the molecules to form a crystalline layer, thus compensating the substrate roughness (Fig. 17). It should be noted that the formation of SASMs accompanied by crystallization of conjugated moieties can also be classified as a self-organization process, because the crystalline monolayer thus formed has a higher ordered level than that observed in the initial system. Nevertheless, since amorphous films based on conjugated organic compounds can exhibit semiconducting properties and the degree of crystallinity of a monolayer is unknown *a priori* during the monolayer growth, organic semiconducting monolayers should be more correctly called self-assembled.

Tulevski *et al.*[54] were the first to obtain a SASM. In the proposed compound, tetracene served as the semiconductor core, hydroxyl groups performed the anchor function (structure **10**), and the aliphatic spacer was absent (Fig. 18). The authors studied the self-assembly of these molecules on the Al_2O_3 surface. The monolayer was studied by X-ray reflectivity, IR spectroscopy and X-ray photoelectron spectroscopy. It was found that the layer has a dense structure composed of vertically oriented molecules. Transistors based on the self-assembled monolayers demonstrated a dependence of the VAC on the gate voltage, which attested to the presence of a field effect. It is noteworthy that the shape of the curves in the low drain voltage region (linear operation regime of the transistor) attested to high contact resistances; a saturation regime was not attained, which precluded evaluation of the mobility for such devices. In addition, high substrate roughness and the absence of an aliphatic spacer in the structure of the initial compound allowed operation only for devices with very small conducting channel lengths (< 60 nm). This substantially restricted the scope of practical applications of these monolayers. The reproducibility of electrical characteristics was low (~ 50% of the devices operated) and the on-state current did not exceed 3 nA.

Mottaghi *et al.*[55] were the first to use compounds with aliphatic spacers for the design of SASMs. The conjugated

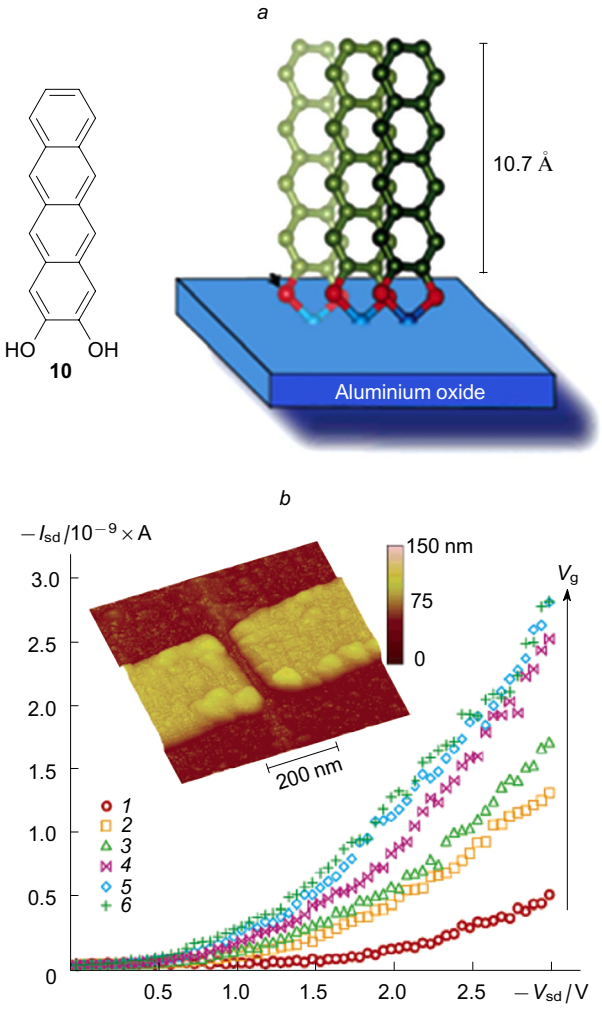
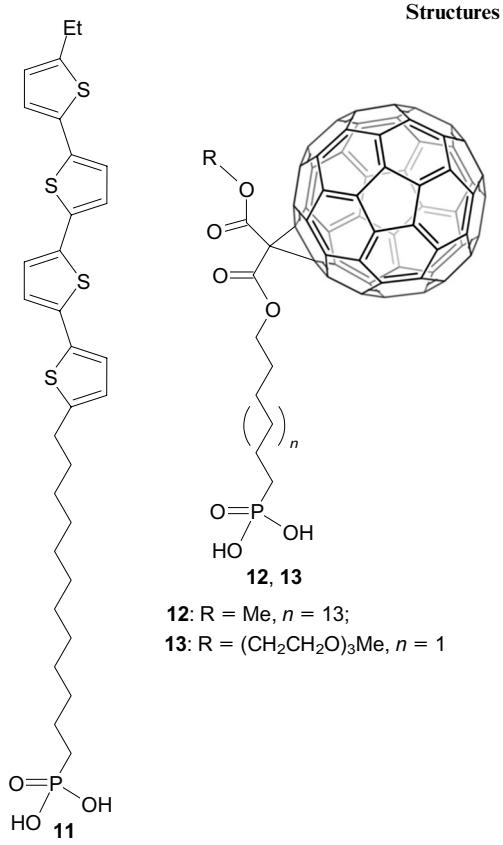


Figure 18. Schematic view of a SASM (*a*), volt – ampere (output) curves of a SAMFET based on tetracene **10** (*b*).[54]
b: $-V_g =$ 0 (*1*), 0.5 (*2*), 1 (*3*), 1.5 (*4*), 2 (*5*), 2.5 V (*6*). The inset shows the AFM-derived SAMFET morphology.

core was represented by ter- and quaterthiophenes, while a carboxylic acid moiety served as the functional anchor group. Devices based on these monolayers demonstrated the field effect and the carrier mobilities were calculated to be 8×10^{-4} for terthiophene and 0.0035 $cm^2\ V^{-1}\ s^{-1}$ for quaterthiophene. These values proved to be lower than in the case of compounds with a similar semiconducting core formed by vapour deposition. This was attributed to the fact that in the case of SASMs, the molecular packing is less dense than that in vapour deposited films, resulting in poorer electrical properties. The percentage of operating transistors was very low (4%) and measurement of electrical characteristics was possible only in an inert atmosphere. Among the factors reducing the electrical properties of the transistors, the authors listed high concentration of defects in the transistor channel and high contact resistance at the metal/semiconductor interface. Furthermore, semiconductor properties were displayed only by devices with very short channels ($\leqslant$100 nm), probably, because of high roughness of aluminium oxide surface; this markedly restricted the practical applicability of the devices.

A promising approach is the use of phosphonic acid residue as the reactive group in an organic self-assembled semiconductor, because these functional oligomers form dense SAMs (including semiconductor ones) on the aluminium oxide surface, which gives rise to SAMFETs with enhanced electrical characteristics. Novak *et al.*[49] reported SASMs based on phosphonic acid derivative C_2-4T-C_{12}-PA (5′-ethyl-2,2′:5′,2″:5″,2‴-quaterthiophene-5‴-yldodecylphosphonic acid (structure **11**) and two fullerene C_{60} derivatives with different spacers and substituents (structures **12** and **13**). The choice of these compounds as semiconductor oligomers is caused, on the one hand, by the ability of phosphonic acid residue to react with the substrate (aluminium oxide) surface to form SASMs and, on the other hand, by the presence of hole and electron conductivity in the known quaterthiophene and fullerene C_{60} derivatives, respectively. Self-assembled semiconducting monolayers were grown by keeping the substrate in THF solutions of these compounds with initial concentration of 1 mmol $litre^{-1}$. The formation of monolayers was confirmed by contact angle measurements, X-ray photoelectron spectroscopy, transmission electron microscopy and atomic force microscopy. The semiconducting properties of these layers were tested in SAMFETs for which densely packed SASM is necessary for efficient operation.

Structures 11 – 13



12: R = Me, *n* = 13;
13: R = $(CH_2CH_2O)_3Me$, *n* = 1

The authors[49] tested devices of two types — bottom-contact short (500 nm) channel transistor (upper part of Fig. 19 *a*) and top-contact long (10 μm) channel transistor (lower part of Fig. 19 *a*). In the bottom-contact topology, SASMs based on compound **11** showed a hole mobility of 10^{-5} $cm^2\ V^{-1}\ s^{-1}$, $I_{on/of} = 10^3$ and a relatively high thresh-

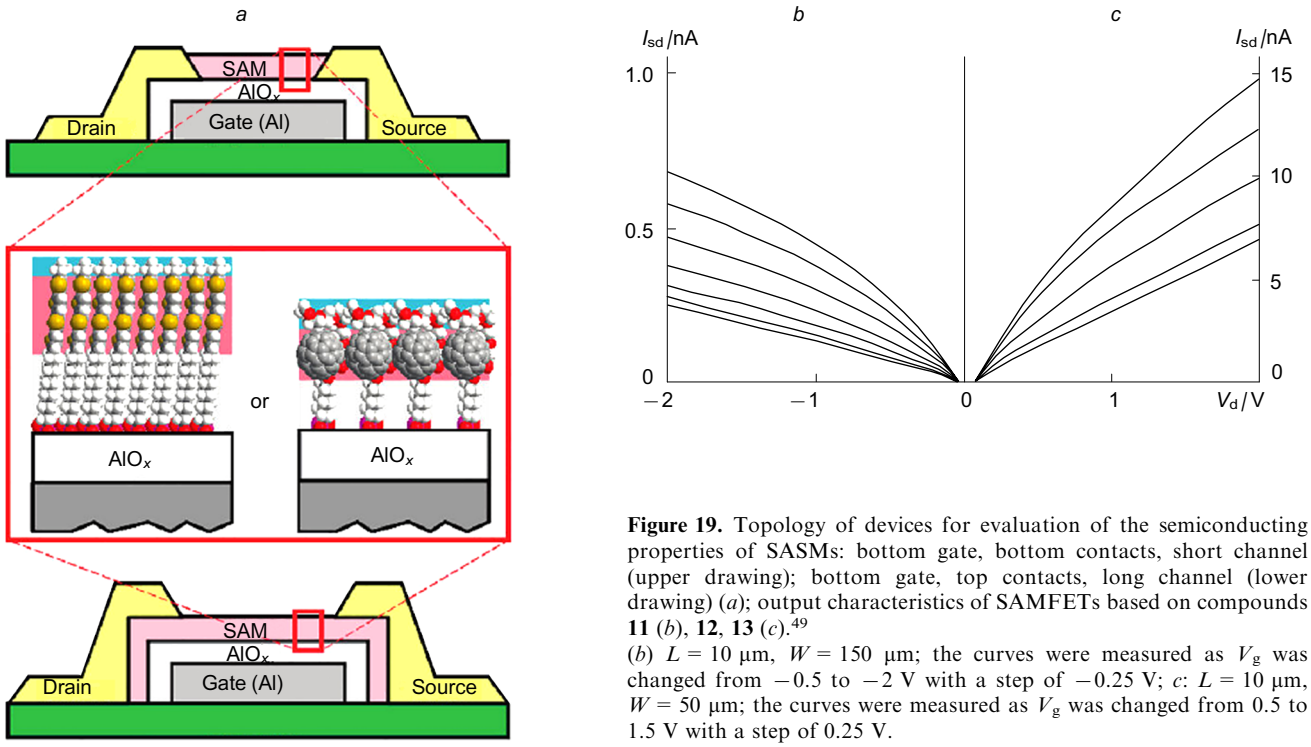


Figure 19. Topology of devices for evaluation of the semiconducting properties of SASMs: bottom gate, bottom contacts, short channel (upper drawing); bottom gate, top contacts, long channel (lower drawing) (*a*); output characteristics of SAMFETs based on compounds **11** (*b*), **12**, **13** (*c*).[49]
(*b*) $L = 10$ μm, $W = 150$ μm; the curves were measured as V_g was changed from −0.5 to −2 V with a step of −0.25 V; *c*: $L = 10$ μm, $W = 50$ μm; the curves were measured as V_g was changed from 0.5 to 1.5 V with a step of 0.25 V.

old voltage $V_t = -2.5$ V. The layers based on compound **12** showed poor electrical conductivity and rapidly degraded during testing due to high fullerene sensitivity to environmental oxygen and moisture. Meanwhile, layers based on compound **13** were more stable owing to the long ethylene glycol substituent. The measured carrier mobility was 10^{-4} cm^2 V^{-1} s^{-1}, $I_{on/of}$ was 2×10^4 and the threshold voltage V_t was 3 V. The authors attributed the low charge carrier mobility observed for the SASM based on the oligothiophene derivative to high roughness of the substrate. It was noted that in the case of oligothiophenes, efficient charge carrier transport requires π–π conjugation and long-range order to exist in the monolayer structure. Meanwhile in the case of fullerene C_{60}, the semiconducting behaviour is less sensitive to substrate roughness because of the spherical shape of the fullerene molecule, which accounts for good electron mobility of fullerene-based SASMs. It is important that both types of phosphonates allowed the researchers to produce transistors with relatively long channels (10 μm). These devices showed charge carrier mobilities close to those attained for short-channel transistors. Thus, it was concluded that the electron conductivity of SAMFETs based on phosphonate monolayers is rather limited by the substrate roughness than by the length of the OFET channel.

A semiconducting layer for SAMFETs based on phosphonic acid derivatives has been reported by Ringk *et al.*[50] The authors synthesized an organic semiconductor, 11-[*N*′-(1-hexylheptyl)perylene-3,4,9,10-tetracarboxylbisimid-*N*-yl)-undecylphosphonic acid (structure **14**), which was able to form SAMs on the aluminium oxide surface. Self-assembled monolayers were formed using silicon wafers with a deposited 100-nm-thick aluminium oxide layer. The self-assembled monolayers of compound **14** were fabricated by keeping these substrates in a THF solution of the starting compound with a concentration of 1.5×10^{-5} mol litre^{-1} for 24 h and subsequent annealing in a nitrogen atmosphere at 120 °C. The presence of dense SASM layer with a vertical orientation of conjugated moieties on the substrate was confirmed by AFM, X-ray photoelectron spectroscopy and grazing incidence X-ray diffraction. The output and transfer characteristics of SAMFETs are shown in Fig. 20. The shape of the curves is typical of n-type semiconductors in which the linear and saturation regimes of transistor operation can be distinguished; non-linearity is observed in the region of low drain-to-source voltage, which is indicative of high contact resistances. The authors attributed their appearance to the mismatching the LUMO level of the organic semiconductor (3.8 eV) and the work function of the gold electrode (~5 eV); nevertheless, this did not interfere with the device operation as a whole. The considerable dependence of current on the gate voltage illustrates the presence of field effect. The charge carrier mobilities in the saturation regime and the on/off current ratio were 1.5×10^{-3} cm^2 V^{-1} s^{-1} and 10^4, respectively; the yield of operating devices was 100%.

It should be noted that Ringk *et al.*[50] were the first to demonstrate the efficient operation of long-channel (100 μm) SAMFETs based on phosphonic acid derivatives. The dependence of carrier mobility on the channel length in the range from 2 to 100 μm is shown in Fig. 21 *a*. When the channel is short, the charge transport is restricted by contact resistance, which affects the measured mobility value. When the channel length is $L \geqslant 40$ μm, the mobility is constant, which is indicative of efficient charge transport in a densely packed monolayer. The transport is not limited by barriers that may arise at the domain boundaries in the semiconducting structure or due to incomplete substrate coverage with the SASM.

An important achievement of the study being considered[50] is the design of logic gates based on complementary n- and p-type SAMFETs. Previously fabricated[56]

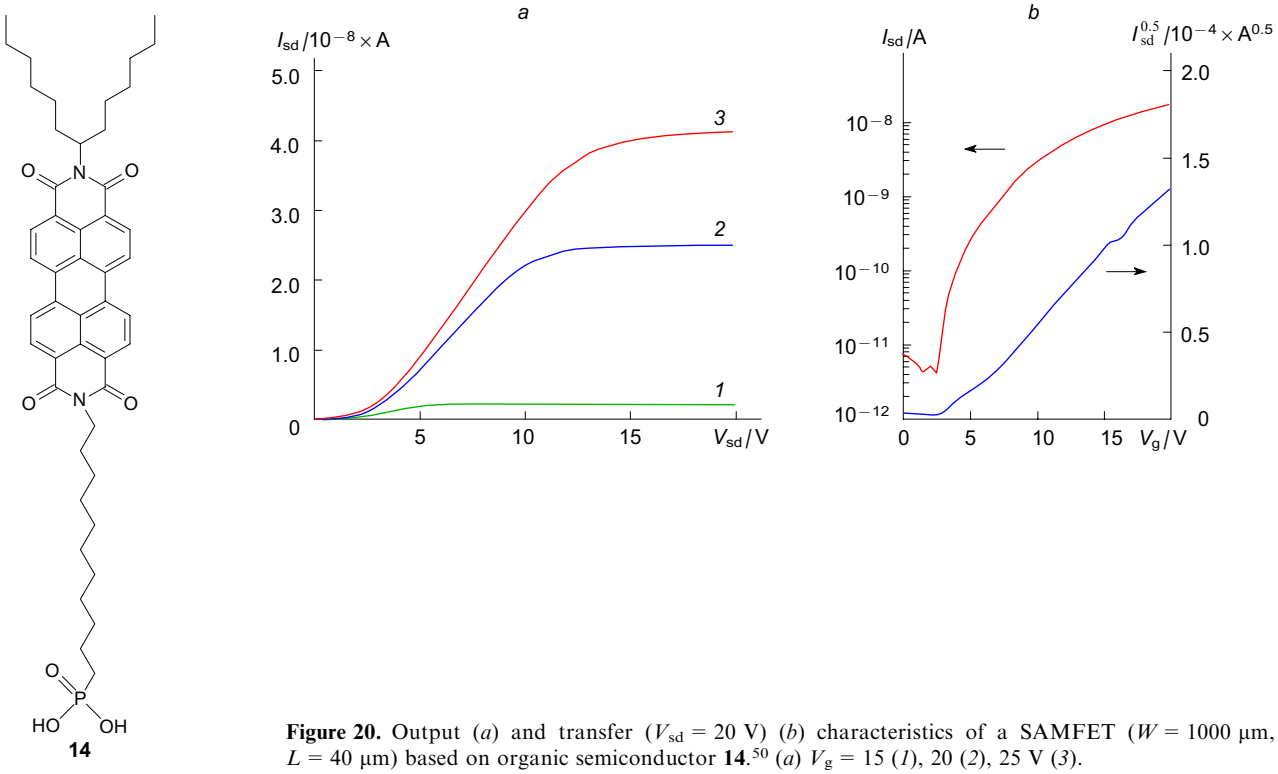


Figure 20. Output (*a*) and transfer (V_{sd} = 20 V) (*b*) characteristics of a SAMFET (W = 1000 μm, L = 40 μm) based on organic semiconductor **14**.[50] (*a*) V_g = 15 (*1*), 20 (*2*), 25 V (*3*).

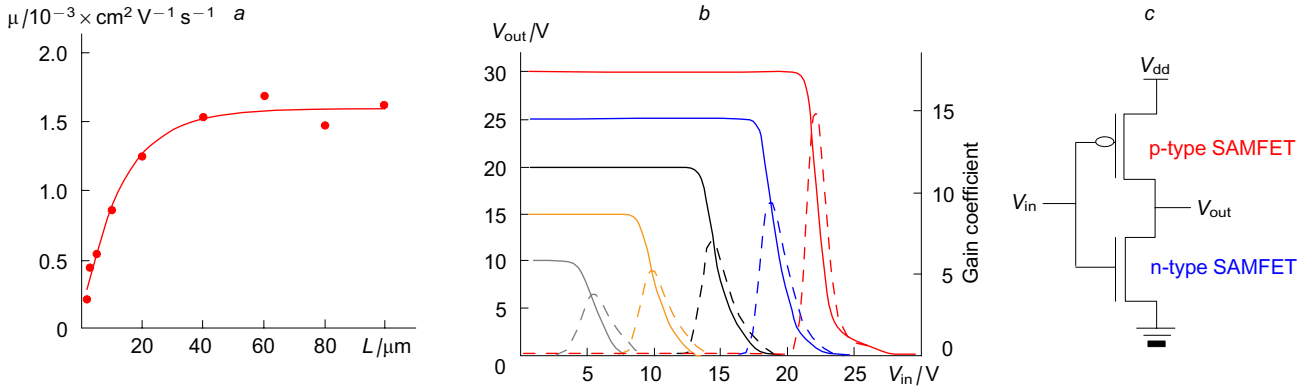


Figure 21. Charge carrier mobility in the saturation regime *vs.* SAMFET chain length (*a*), output voltage (continuous lines) and amplification coefficient (dashed lines) for an inverter based on two complementary n- and p-type SAMFETs *vs.* input voltage (*b*), electric circuit of the inverter (*c*).[50]

SAMFETs were used as p-type transistors. The logic gate was represented by an inverter. To make up for the difference in the carrier mobility of the semiconductors, devices with different channel lengths were used, particularly, 40 μm for p-type transistors and 2 μm for n-type transistors. Figures 21 *b*,*c* show the output signals of this inverter at different supply voltages in the range from 10 to 30 V with a 5 V step and the corresponding electric circuit. The device efficiently operated over the whole range of supply voltages and demonstrated a higher noise margin[57] than unipolar p-type SAMFET inverters.

Fabrication of a SAMFET based on phosphonic acid derivatives on a silicon or a flexible polymer substrate has been reported by Schmaltz *et al.*[58] The authors used [12-([1]benzothieno[3,2-*b*][1]benzothiophen-2-yl)dodecyl)]phosphonic acid (BTBT-C_{12}-PA) as the organic semiconductor and 12-sulfanyldodecylphosphonic acid (HS-C_{12}-PA) as the dielectric. The fabrication technique of the device is shown in Fig. 22. In the first stage, a 30 nm-thick aluminium layer was evaporated onto a silicon substrate with thermally grown SiO_2 or onto a poly(ethylene naphthalate)-based substrate and photolithographic patterning was carried out (see Fig. 22 *a*). The second stage was plasma treatment of the surface to form a dense AlO_x layer (see Fig. 22 *b*). On the substrate thus fabricated, self-assembly of the 12-sulfanyldodecylphosphonic acid molecules was conducted in order to generate a hybrid dielectric HS-C_{12}-PA + AlO_x layer (see Fig. 22 *c*). The functions of HS-C_{12}-PA included, on the one hand, reducing of the leakage current through the gate electrode and, on the other hand, increasing

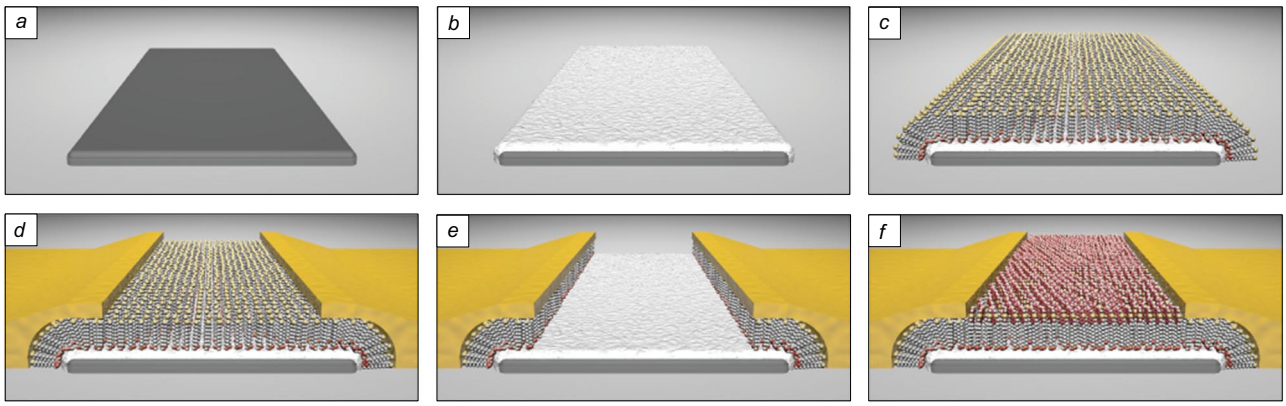


Figure 22. Fabrication process of a SAMFET based on BTBT-C_{12}-PA.[58] For (*a*–*f*), see text.

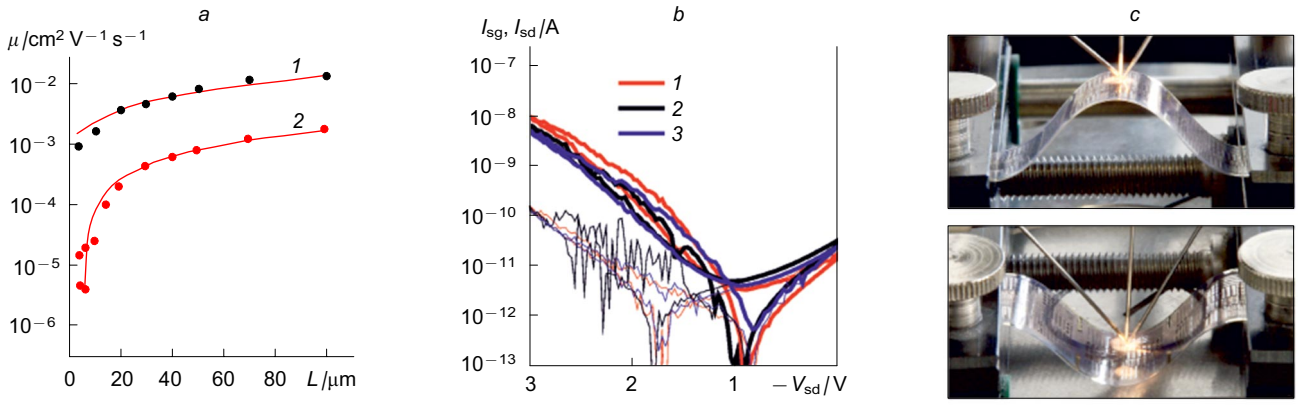


Figure 23. Hole mobility *vs.* transistor channel lengths for silicon and polymer substrates (*a*); transfer characteristics of the SAMFET on the polymer substrate without mechanical strain and with concave and convex bendings (*b*); optical photographs of the SAMFET with bent substrate and during electrical testing (*c*).[58]
(*a*) (*1*) SiO_2 substrate, (*2*) PEN substrate; (*b*) (*1*) concave bending, (*2*) no strain, (*3*) convex bending.

adhesion of the gold electrodes to the substrate. The resulting dielectric layer had a high electric capacitance ($C = 0.68$ μF cm^{-2}) and was 5.1 nm thick; this layer allowed operation of the device at low voltage (below 3 V). Then thermal evaporation of gold drain and source electrodes was carried out (see Fig. 22 *d*) followed by one more plasma treatment for removal of HS-C_{12}-PA from the SAMFET channel (see Fig. 22 *e*). The last stage was self-assembly of BTBT-C_{12}-PA from a solution on the fabricated substrate to generate a SAMFET active semiconducting layer (see Fig. 23 *f*).

The dependences of hole mobility on the SAMFET channel length in the saturation regime for the silicon and polymer substrates are shown in Fig. 23 *a*. In both cases, the channel length was varied from 2 to 100 μm. The highest charge carrier mobilities were 1.2×10^{-2} and 1.7×10^{-3} cm^2 V^{-1} s^{-1} for silicon and polymer substrates, respectively. The found mobilities were of the same order of magnitude as the best characteristics found for monolayer devices;[56] however, they were markedly inferior to OFETs based on benzothienobenzothiophene derivatives that were not covalently bound to the substrate.[33,34] This was explained by considering the following factors suppressing the electric transport in SAMFETs:

— the monolayer morphology and molecular packing differ from those of mutilayer BTBT films and are characterized by the absence of crystalline 2D structure;

— the absence of a second semiconducting layer that can form additional charge transfer pathways when the lower layer is defective; [7]

— high contact resistances (10^{11} Ω μm for the silicon substrate and 10^{12} Ω μm for the polymer substrate).

Schmaltz *et al.*[58] also studied variation of the electrical properties of SAMFETs upon mechanical strain of the substrate. The transfer characteristics for the transistor with channel length and width of 5 and 300 μm, respectively, with concave and convex bending of the polymer substrate and without bending are shown in Fig. 23 *b*. It was found that for the bending radius of 6 mm, the characteristic drain and gate currents and the shape of the curves as a whole do not change, which is indicative of SAMFET stability to mechanical strain. However, the authors noted that they did not evaluate the reproducibility of electrical properties upon repeated cyclic strain. The optical photographs of the transistors during electrical testing are shown in Fig. 23 *c*.

Ponomarenko *et al.*[56] proposed a number of organosilicon oligothiophene derivatives for the fabrication of

Table 1. Electrical properties of SAMFETs based on organosilicon oligothiophene derivatives.[56]

Anchor group	Aliphatic spacer	Semiconducting core [a]	Terminal group	Semiconducting properties	
				μ /cm^2 V^{-1} s^{-1}	I_{on-off}
$(EtO)_3Si$	$C_{11}H_{22}$	4T	Et	Amorphous dielectric	
$MeOSiMe_2$	C_6H_{12}	4T	C_6H_{13}	No SASM due to the low reactivity of the anchor group	
$ClSiMe_2$	$C_{11}H_{22}$	4T	Et	3×10^{-3}	10^6
$ClSiMe_2$	C_6H_{12}	4T	C_6H_{13}	3×10^{-3}	10^5
$MeOSiMe_2$	$C_{11}H_{22}$	5T	Et	No SASM due to the low reactivity of the anchor group	
$ClSiMe_2$	$C_{11}H_{22}$	5T	C_2H_5	4×10^{-2}	10^8
$ClSiMe_2$	C_6H_{12}	5T	C_6H_{13}	2×10^{-2}	10^7
$ClSiMe_2$	C_6H_{12}	6T	C_6H_{13}	No SASM due to low solubility of the starting compound	

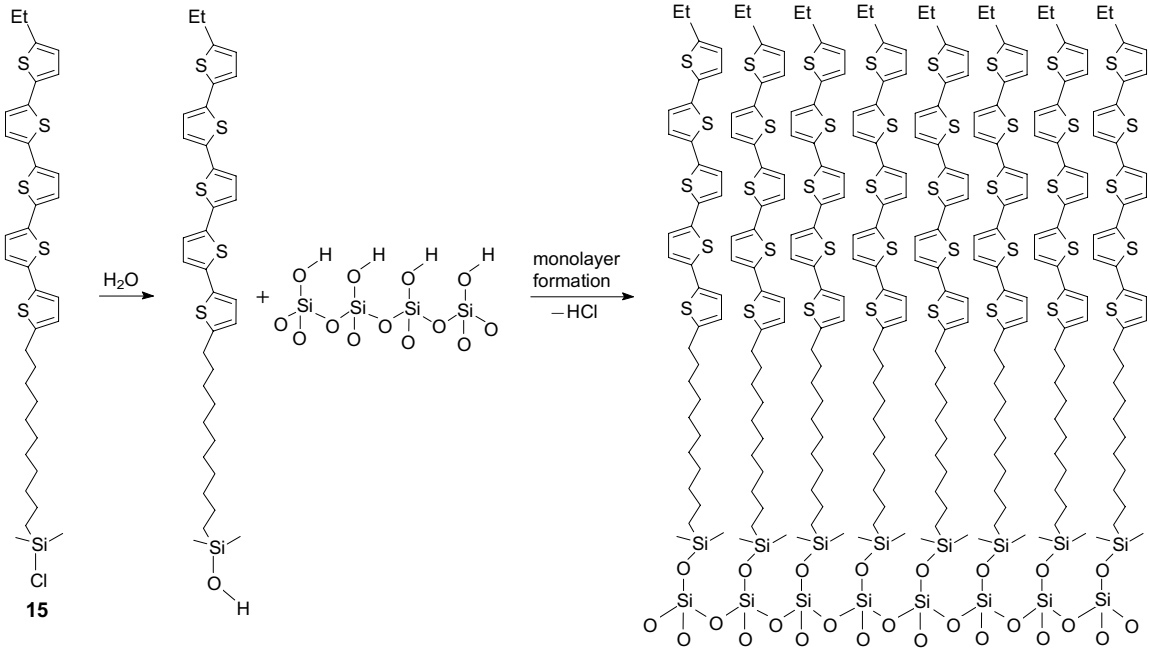
[a] The number of thiophene rings is indicated (T).

SASMs (Table 1). Semiconducting monolayers were formed from organic compounds with chlorosilyl anchor groups, a long aliphatic spacer, π-conjugated oligothiophene mesogenic group and terminal alkyl substituent in the molecule. It was shown that the formation of dense SASM on the silicon substrate is possible only when the initial compound contains a monochlorosilyl functional group. The authors varied the number of thiophene moieties in the conjugated core (from 4 to 6). They found that the length of conjugation affects the electrical properties of the transistor: upon the addition of one thiophene moiety (on going from quater- to quinquethiophenes), the SAMFET carrier mobility increased by an order of magnitude. However, the fabrication of devices based on sexithiophene was impossible because of their low solubility. It was also shown that the length of the alkyl spacer virtually does not affect the carrier mobility or the on/off current ratio of the OFET. The best electrical properties were shown by SAMFETs based on chloro[11-(5‴′-ethyl-2,2′:5′,2″:5″,2‴:5‴,2⁗:5⁗,2⁗′-quinquethien-5-yl)undecyl]dimethylsilane (compound **15**).

The process of fabrication of SASMs from chloro(quinquethiophene)silane on the silicon substrate is reflected in Scheme 1.[48] In the first stage, hydrolysis of the chlorosilyl group by traces of water takes place to give silanol. In the second stage, a covalent bond is formed between the substrate and the SASM molecule.

The electrical characteristics of SAMFETs based on chloro(quinquethiophene)silane are presented in Fig. 24. The shape of the curves corresponds to a p-type transistor with clearly discernable linear and saturation operation regimes and small hysteresis. The output curves (see Fig. 25 *b*) in the low V_{sd} region are straight lines, which is indicative of a minor influence of the contact resistances on the electrical properties of OFETs. The carrier mobility in the SAMFETs calculated from the transfer characteristics (see Fig. 25 *a*) reaches 4×10^{-2} cm^2 V^{-1} s^{-1}, the threshold voltage was close to 0 V and the on/off current ratio was

Scheme 1



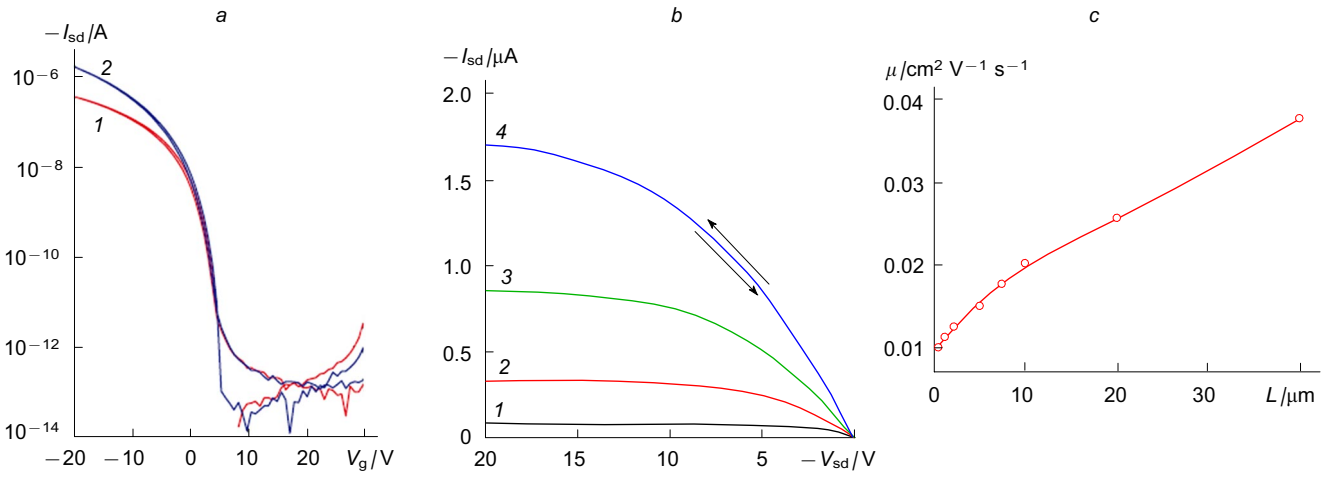


Figure 24. Transfer (*a*) and output (*b*) characteristics of a SAMFET based on chloro(quinquethiophene)silane **15**.[48] (*a*) $-V_{dd}$ = 2 (*1*), 20 V (*2*); (*b*) $-V_{dd}$ = 5 (*1*), 10 (*2*), 15 (*3*), 20 V (*4*); (*c*) mobility *vs.* transistor channel length.

10^8. These are record-high characteristics for SAMFETs based on organic molecules with an anchor group. In addition, the charge carrier mobility of the chloro(quinquethiophene)silane-based SAMFETs was close to the mobility obtained for polycrystalline α-quinquethiophene films.[59]

Thus, Smits *et al.*[48] reported one more experimental proof for the statement that the major charge transport in OFETs takes place in a several nanometre-thick layer adjoining the dielectric (for the oligomers in question, this corresponds to a monolayer). From the practical standpoint, it is significant that high crystallinity and low defect concentration of the obtained self-assembled monolayer allow operation of devices with longer channels (up to 40 μm); this could not be attained in earlier works. The applicability of long SAMFET channels is an important issue, since they can be fabricated by inexpensive scalable printing methods, whereas fabrication of short channels requires energy-demanding and expensive vacuum processes.

Special mention should be made of the dependence of mobility on the length of the SAMFET channel (see Fig. 24 *c*). As noted above, in an ideal OFET, the mobility does not depend on the channel length. When significant contact effects are involved, the mobility becomes dependent on the channel length. If the charge transport is dictated by the domain structure of the films (loss at the domain boundary), the mobility decreases with increasing channel length. The dependence of the mobility observed in this case indicates that the SASM is relatively uniform and the loss at the domain boundaries is insignificant.

The fabricated transistors showed a small spread of the key parameters — carrier mobilities, on/off current ratios and threshold voltages. The authors[48] demonstrated that these devices can be used to fabricate simple integrated circuits such as unipolar inverters consisting of two SAMFETs connected in series. Figure 25 *a*–*c* shows the circuit and volt–ampere characteristics for such inverter following the change in the supply voltage V_{dd} in the range from −10 to −20 V with a 5 V step. The device efficiently operated over the whole range of supply voltages, with the gain coefficient reaching six. Owing to high reproducibility of the technique of SAM formation from solutions, it was possible to fabricate integrated circuits such as a 15-bit code generator composed of ~300 SAMFETs (see Fig. 25 *d*). The output of this circuit corresponded to the programmed code; thus, SAMFETs can be used for fabrication of end-user organic electronic devices such as radio frequency identification (RFID) readers.

Mathijssen *et al.*[24] studied the electrical properties of SAMFETs based on the monochlorosilyl derivative of chloro(quinquethiophene)silane **15** as functions of monolayer coverage of the substrate. It was found that SAM is fabricated on the silicon dioxide surface *via* the formation and subsequent growth of monolayer islands. The substrate coverage considerably depended on the immersion time in the solution, with 100% coverage being attained in ~15 h (Fig. 26). According to grazing incidence X-ray diffraction data, the monolayer was crystalline and highly ordered throughout the whole growth process, which is responsible for good electrical properties of these monolayers.

The authors also studied the carrier mobility as a function of the transistor channel length for different monolayer coverages of the substrate. It followed from the proposed theoretical model that in the case of partial coverage, the measured mobility decreases exponentially with increasing channel length. This is due to the lack of a continuous conducting layer in the channel. Separate domains form a percolation path for the charge carriers, thus decreasing their efficient (measured) mobility. However, for the completely formed monolayer, the mobility somewhat increases with increasing channel length; this is caused by decreasing contribution of the contact resistance to the total transistor resistance. This model was confirmed by experimental electrical measurements of the SAMFETs.

Thus, high electrical characteristics of monolayer transistors fabricated *via* self-assembly from solutions can be attained if the substrate is fully covered by the monolayer; for this purpose, the substrate must be kept in a solution of an organic semiconductor for tens of hours. This approach is not industrially feasible and restricts the application prospects for SAMFETs.

Flesch *et al.*[60] considered the structure and the phase behaviour of SAMs based on chloro(quinquethiophenesilane) **15**. It was found that molecules in the monolayers are

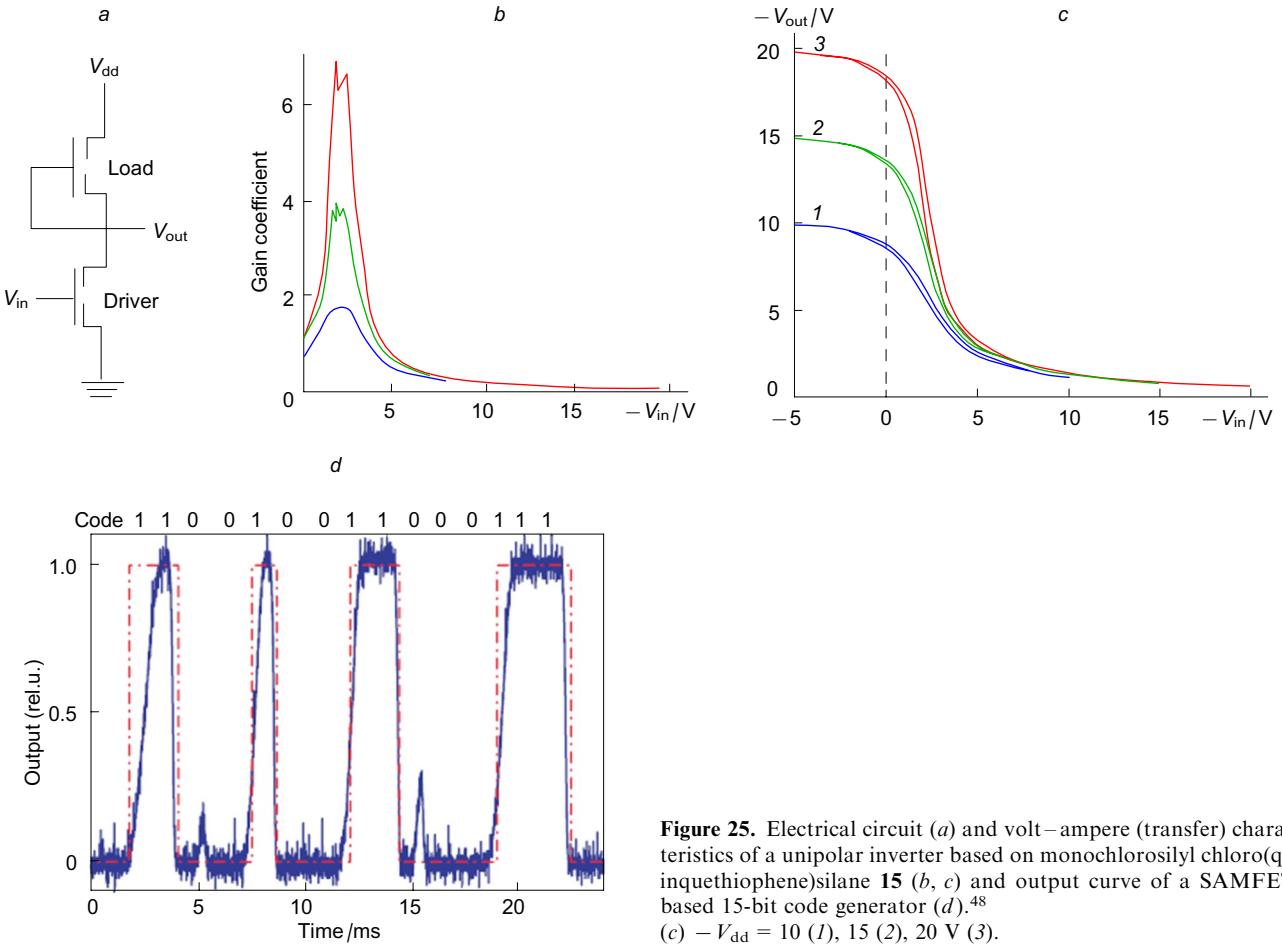


Figure 25. Electrical circuit (*a*) and volt – ampere (transfer) characteristics of a unipolar inverter based on monochlorosilyl chloro(quinquethiophene)silane **15** (*b*, *c*) and output curve of a SAMFET-based 15-bit code generator (*d*).[48]
(*c*) $-V_{dd}$ = 10 (*1*), 15 (*2*), 20 V (*3*).

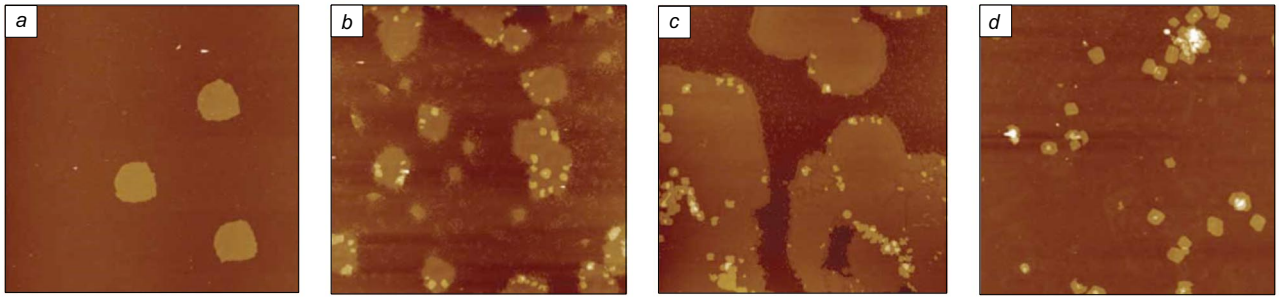


Figure 26. SAM morphology for immersion times in solution of 0.25 (*a*), 0.5 (*b*), 1 (*c*), 15 h (*d*).[24]
Image size: 20 × 20 μm.

packed into a herringbone structure, which is typical of oligothiophenes. The unit cell parameters immediately after the self-assembly were a = 5.6, b = 7.2 Å, γ = 90°. After annealing at 400 K for 60 min *in vacuo*, the unit cell parameters were a = 5.6, b = 8.1 Å, γ = 90°; this was interpreted as increasing tilt angle of the molecules from 0° to 13° upon appealing. It is noteworthy that SAMFETs based on a layer tilted by 13° had the highest carrier mobility.

Gholamrezaie *et al.*[61] reported the fabrication of a SASM based on chloro(quinquethiophene)silane **15** on a flexible polymer substrate coated by a dielectric SU8 layer (Fig. 27 *a*). The choice of the dielectric was caused by its wide use in electronic devices and by the presence of epoxide groups, which can be converted to hydroxyl groups by oxygen plasma treatment of the layer. As in the study of Choi *et al.*,[25] the plasma-treated sample was kept in a solution of the organic semiconductor for the formation of SAM. The investigation of the resulting monolayers by AFM, X-ray photoelectron spectroscopy and grazing incidence X-ray diffraction revealed the presence of highly ordered densely packed SAMs. Unlike self-assembly on the SiO_2 surface, in this case, only some molecules were chemically bound to the SU8 surface upon the reaction with the OH groups. The molecules chemically bound to the dielectric served as the growth points for the monolayer. The driving force of the self-assembly was due to intermo-

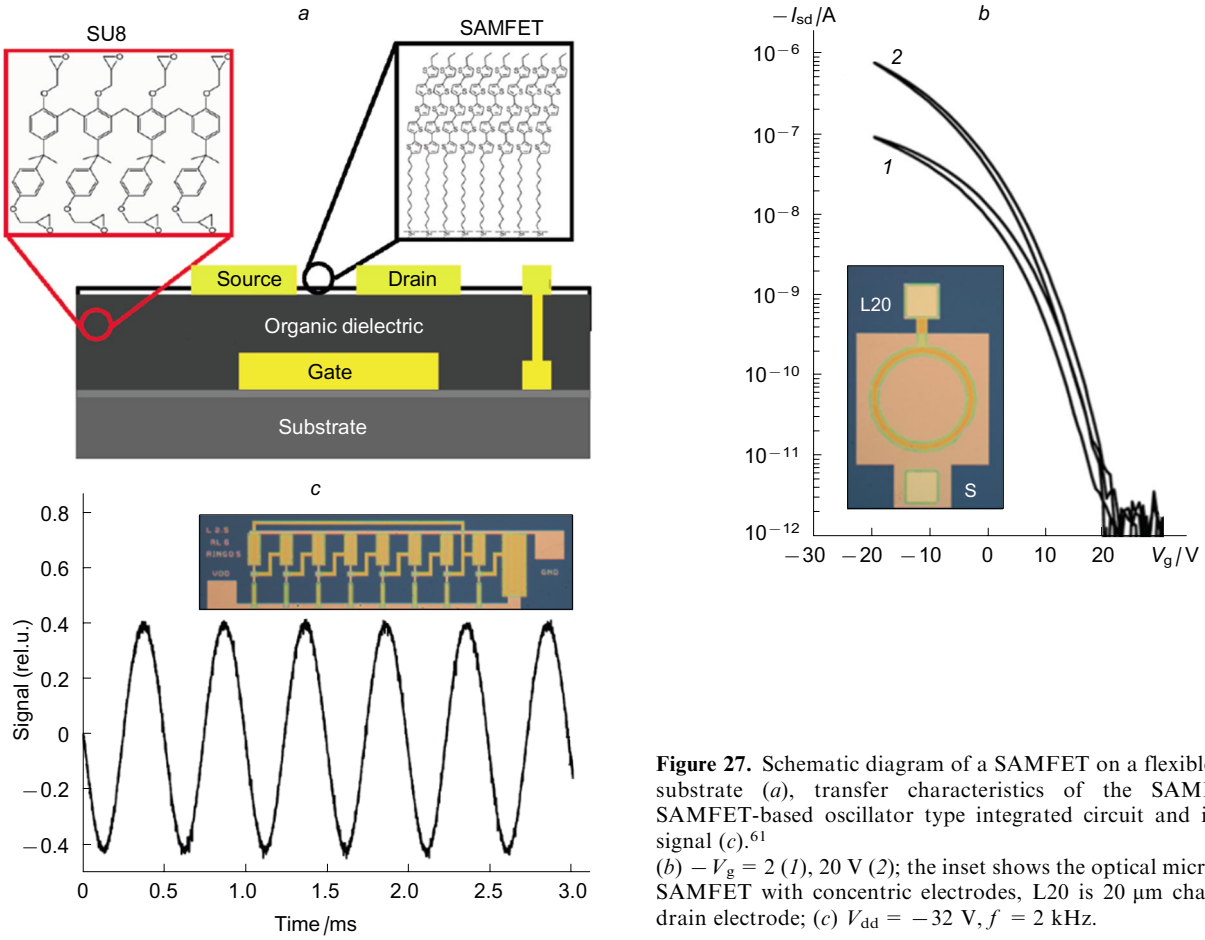


Figure 27. Schematic diagram of a SAMFET on a flexible polymer substrate (*a*), transfer characteristics of the SAMFET (*b*), SAMFET-based oscillator type integrated circuit and its output signal (*c*).[61]
(*b*) $-V_g$ = 2 (*1*), 20 V (*2*); the inset shows the optical micrograph of SAMFET with concentric electrodes, L20 is 20 μm channel; S is drain electrode; (*c*) $V_{dd} = -32$ V, $f = 2$ kHz.

lecular interaction between alkyl groups and π–π interaction of the conjugated thiophene moieties.

The transfer characteristics for linear and saturation SAMFET operation regimes are presented in Fig. 27 *b*. The measured carrier mobility was 2×10^{-2} cm^2 V^{-1} s^{-1}, which is close to the value found for the silicon dioxide-supported SAM. It is noteworthy that the OFET threshold voltage was 20 V, which differed from the same characteristics for SiO_2 . The SAMFETs showed a small spread of the key parameters; hence, they were used to fabricate an oscillator type integrated circuit (see the inset in Fig. 27 *c*). The measured oscillation frequency was 2 kHz.

A highly promising practical application of SAMFETs is the design of highly sensitive gas sensors.[62] The operation principle of these devices is the selective sorption of the target gas (analyte) on the semiconductor surface. Since the thickness of the semiconductor layer in SAMFETs is a few nanometres, the gas molecules interact directly with the OFET conducting channel; hence, even a minor concentration of the analyte considerably influences the electrical properties of SAMFETs. Therefore, such transistors can be used to detect ultralow concentrations (down to tens of ppb) of hazardous gases. Note also that in the general case, OFET is a multi-parameter gas sensor, because all key characteristics of the transistor may vary independently of one another upon a change in the environmental parameters.

A drawback of SAMFET gas sensors is a drift of the threshold voltage upon interaction of the transistor with various gases present in the atmospheric air. In order to increase the sensitivity to a particular gas, nitric oxide, the authors proposed to overlay the semiconducting monolayer with a receptor film composed of an iron(III) porphyrin chloride complex (Fig. 28). This particular receptor was chosen because of its ability to selectively bind to nitric oxide molecules. The threshold voltage shifts with time for SAMFETs with and without the receptor layer are depicted in Fig. 28 *b*. Without the receptor, the threshold voltage shift in the presence of NO differed little from the basic value, whereas attachment of the receptor layer enhanced the sensing properties.

A series of transfer curves of the transistor with the additional receptor layer kept in a nitrogen atmosphere with different nitrogen oxide contents are presented in Fig. 28 *c*. The threshold voltage changed most appreciably, which was attributed to the electrostatic interaction of the sorbed analyte with the receptor layer. In turn, this led to semiconductor doping and shifted the threshold voltage. The threshold voltage shift as a function of NO concentration is presented in Fig. 28 *c* (inset). The curve has a saturation shape and the sensor sensitivity limit is 50 ppb. This value is lower than the previously reported sensitivity limit for OFET-based sensors (2.5 ppm).[63]

Agina *et al.*[64] tested the possibility of SAM fabrication from chloro(quinquethiophene)silane **15** using fast solution techniques. It was shown that spin coating and Langmuir–Blodgett methods are promising for the fabrication of highly ordered crystalline monolayers from the chlorosilyl

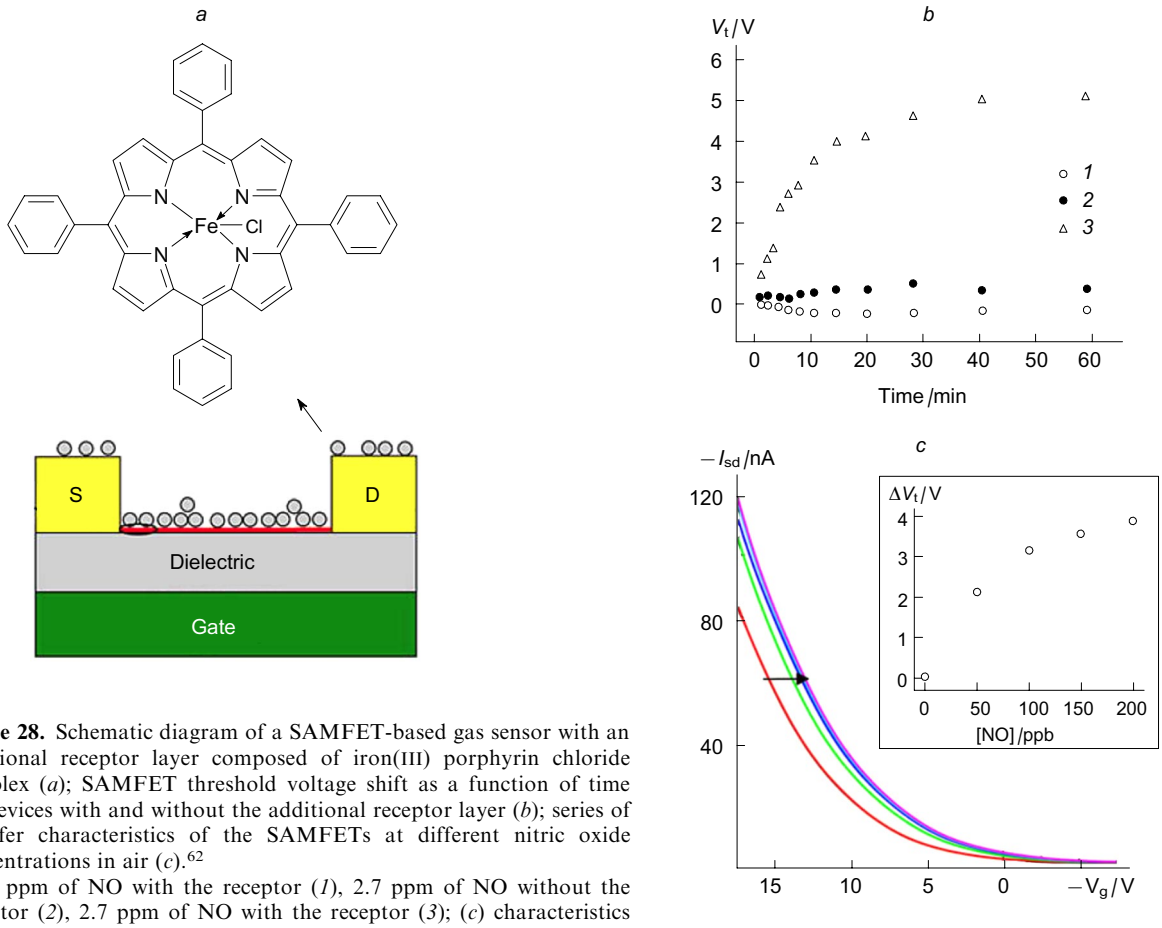


Figure 28. Schematic diagram of a SAMFET-based gas sensor with an additional receptor layer composed of iron(III) porphyrin chloride complex (*a*); SAMFET threshold voltage shift as a function of time for devices with and without the additional receptor layer (*b*); series of transfer characteristics of the SAMFETs at different nitric oxide concentrations in air (*c*).[62]
(*b*) 0 ppm of NO with the receptor (*1*), 2.7 ppm of NO without the receptor (*2*), 2.7 ppm of NO with the receptor (*3*); (*c*) characteristics were measured under the same conditions; their dynamics with time is reflected; the inset shows the threshold voltage shift *vs.* NO concentration.

quinquethiophene derivative. X-Ray diffraction, X-ray scattering and molecular modelling methods were used to elucidate the dependence of the monolayer structure on the fabrication method; this allowed the selection of the optimal conditions for monolayer film formation. It was noted that the LB method is inapplicable for the fabrication of monolayers of linear non-functional oligomers (such as α,α′-dialkyloligothiophenes), *i.e.*, the presence of the chlorosilyl group is necessary for the LB monolayer formation. One more conclusion is that the proposed approach can be used to generate Langmuir monolayers based on organosilicon compounds with any type of conjugated moieties; therefore, this approach is universal.

Agina *et al.*[64] also considered the phase behaviour of chloro(quinquethiophene)silane **15** at the water/air interface. The Langmuir isotherms of this compound on the water surface in the first and second layer compression – decompression cycles are shown in Fig. 29. First of all, they noted the fact that the two cycles do not coincide and show a significant hysteresis. This can be attributed to spontaneous crystallization of the conjugated moieties of the molecule or, more likely, the formation of bilayers of siloxane dimers *via* hydrolysis of chlorosilane and subsequent dimerization of the resulting silanol. The authors suggested that in the first compression – decompression cycle, the Langmuir monolayer mainly consists of silanol resulting from chlorosilane hydrolysis; layer compression

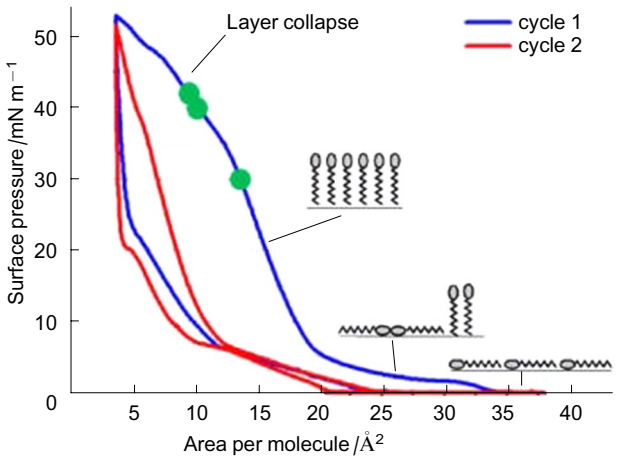
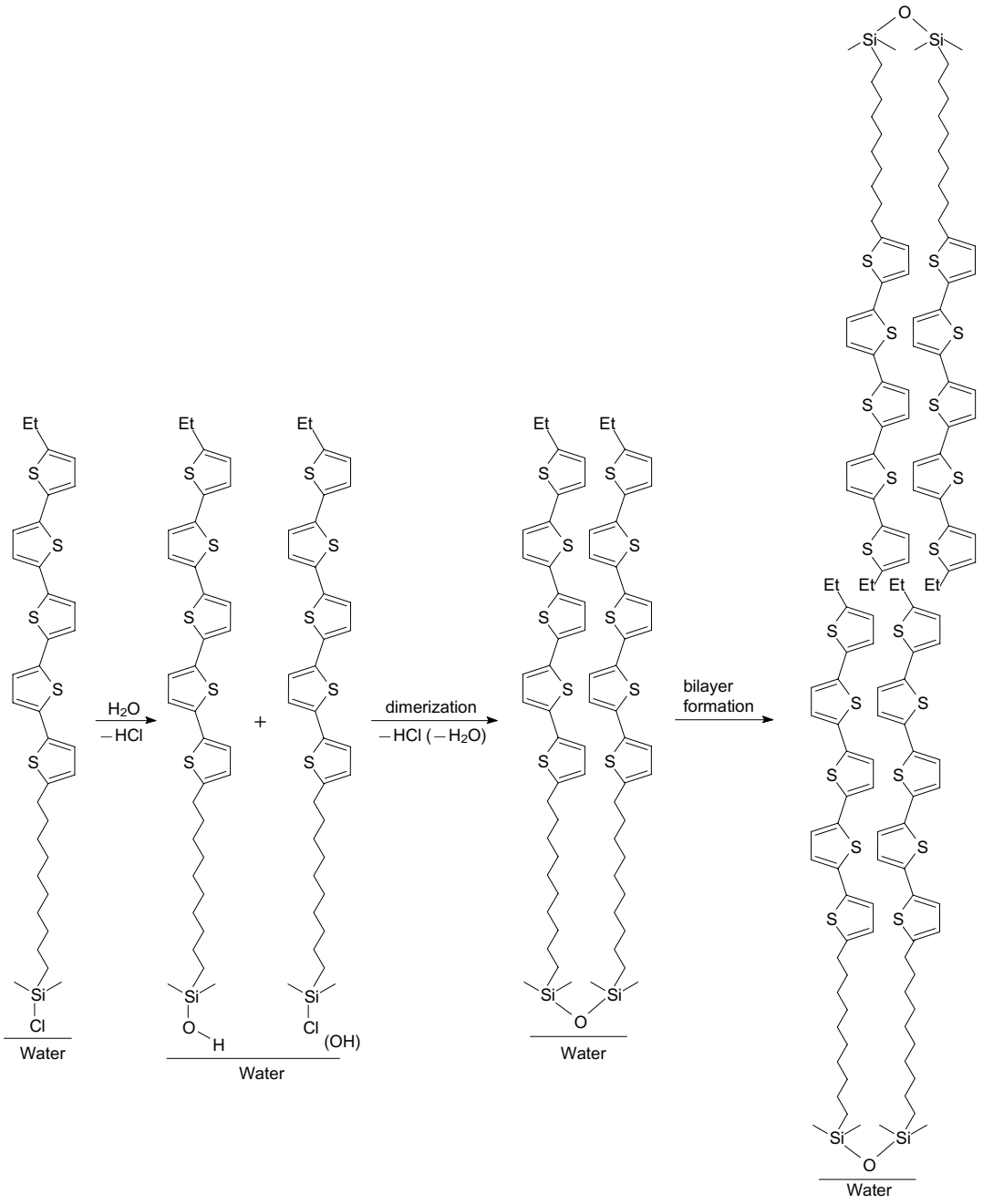


Figure 29. Langmuir isotherms for chloro(quinquethiophene)silane on a water surface.[64]

promotes dimerization to give the siloxane dimer, which is less strongly bound to water than siloxane; therefore, some of the molecules depart from the water surface to form a bilayer (Scheme 2).

According to the proposed model of molecular packing in the Langmuir monolayer (see Fig. 29), the layer com-

Scheme 2



pression is accompanied by reorientation of the molecules from the initial horizontal position, in which hydrogen bonds with water molecules are formed by not only oxygen atoms, but also thiophene sulfur atoms, to a vertical position as a result of detachment of thiophene moieties from the water surface followed by crystallization in monolayers. Using Brewster microscopy at different pressures, collapse of the chloro(quinquethiophene)silane monolayer on the water surface was found to start at a surface pressure of 45 mN m^{-1}; in the subsequent experiments, LB monolayers were transferred at surface pressures as close as possible to, but below, the collapse pressure. Analysis of the X-ray reflectivity data demonstrated that the thickness of an LB monolayer transferred on silicon was 39.6 Å, which was well-correlated with the calculated length of the chloro(quinquethiophene)silane molecule. By electron density reconstruction, it was found that the conjugated thiophene moiety deviates from the perpendicular to the substrate by an angle of 13°, which correlates with the tilt angle of the thiophene moiety found for monolayers self-assembled from solutions and then annealed.[60] The results allowed the authors[64] to expect that the LB monolayers of chloro(quinquethiophene)silane would show high electrical properties when used in OFETs.

Sizov *et al.*[65] investigated the semiconducting properties of the self-assembled LB monolayers based on chloro(quinquethiophene)silane **15**, which were used to fabricate OFETs and simple electronic microcircuits. The output curves of SAMFETs at different gate voltages, which illustrate the field effect, are shown in Fig. 30 *a*. The devices exhibited characteristics typical of unipolar p-type transistors, with the key OFET parameters being as follows:

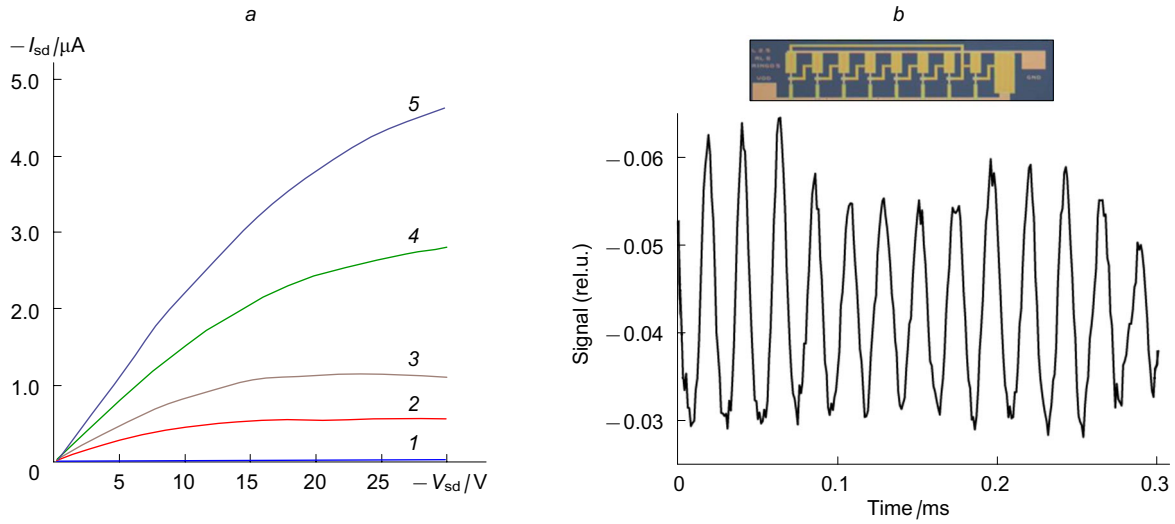


Figure 30. Output characteristics of the SAMFET based on chloro(quinquethiophene)silane **15** LB monolayer (*a*), an oscillator circuit based on ten SAMFETs fabricated on one substrate and its output signal (*b*).[65]
(*a*) $-V_g = 0$ (*1*), 10 (*2*), 20 (*3*), 30 (*4*), 40 V (*5*); (*b*) $V_{dd} = -30$ V.

charge carrier mobility of up to 1.1×10^{-2} cm^2 V^{-1} s^{-1}; on/off current ratio of 10^6, and threshold voltage of approximately −3 V. It is worth noting that the threshold voltage varied from 10 to −10 V for transistors on the same substrate. The measured electrical parameters of LB film-based OFETs differed only slightly from those established for the chloro(quinquethiophene)silane monolayer self-assembled from solutions:[25,48,56,61,62] $\mu = 4 \times 10^{-2}$ cm^2 V^{-1} s^{-1}, $V_t = 0$, $I_{on-of} = 10^6$. The minor difference between the mobilities was attributed to the domain structure of the LB monolayer and, as a consequence, substrate coverage of <100%. Owing to high uniformity of the LB monolayers, it was possible to fabricate several operative OFETs on the same substrate. Out of ten tested devices, all ten demonstrated acceptable electrical properties, which enabled the manufacture of organic electronic devices such as oscillator type integrated circuits with an oscillation frequency of 50 kHz (see Fig. 30 *b*). Since the electrical properties of OFETs formed by LB monolayers are close to the properties of SAMFETs self-assembled from solutions, but LB monolayers are formed much faster (a few minutes) than self-assembly occurs (tens of hours), the authors concluded that the Langmuir methods are fairly promising for the fabrication of SAMFETs and devices based on them.

Note that the study of Sizov *et al.*[65] is not the first one to attempt using the LB monolayers as semiconducting SAMs. For example, Cao *et al.*[66] used copper phthalocyanine transferred to a silicon substrate by the LB method as a semiconductor. It is noteworthy that the electrodes in these OFETs were made of graphene. The electrodes were manufactured using high-precision photolithography and oxygen plasma etching. The drain and source electrodes thus formed were separated by a channel with a length varying from 20 to 100 nm. After electrode fabrication, the copper phthalocyanine LB layer was transferred to the whole

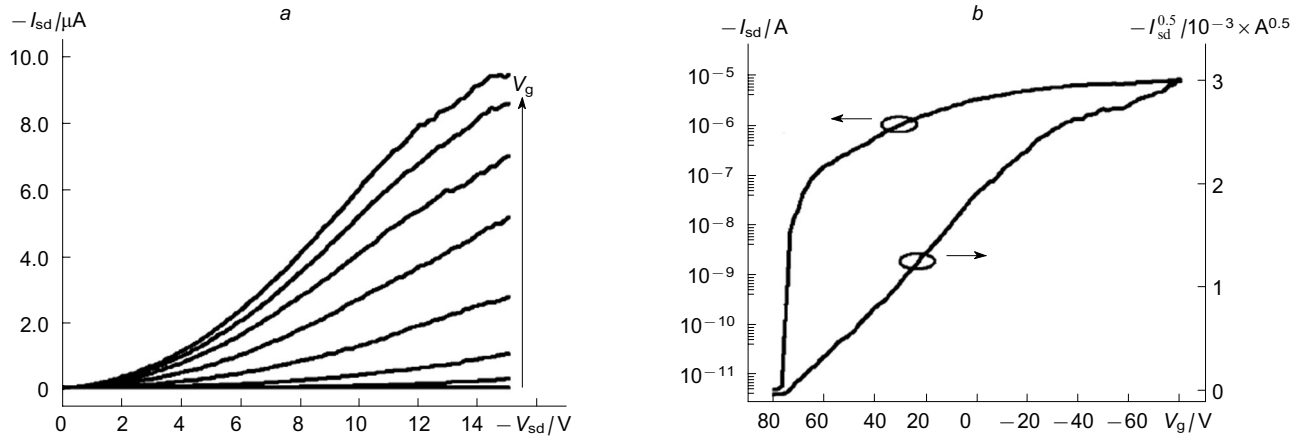


Figure 31. Output (*a*) and transfer (*b*) characteristics of OFET based on a copper phthalocyanine LB monolayer.[66]
The series of output curves was obtained for $V_g = 80 \rightarrow -88$ V with a step of 24 V (the vertical arrow corresponds to increasing absolute magnitude of V_g). The transfer curve was measured for $V_d = -15$ V.

substrate. According to optical microscopy and atomic force microscopy, the layers were homogeneous and the substrate coverage was high. The calculated LB monolayer thickness was 1.3 nm, which was consistent with the data for the Langmuir layers of the same compound formed on the silicon dioxide surface.[67]

A series of output curves for OFETs based on the copper phthalocyanine LB monolayer are shown in Fig. 31 *a*. The OFET channel was 50 nm long and 2 μm wide. The shape of the curves depended on the gate voltage, which was indicative of the field effect. The calculated carrier mobilities in the linear and saturation regimes were 4×10^{-2} and 10^{-2} cm^2 V^{-1} s^{-1}, respectively; this is around the best values known for monolayer OFETs at the time of publication of this study. However, it is necessary to mention a pronounced S-shaped bend of the output characteristics of the transistor in the low drain voltage region (see Fig. 31 *a*); this attests to considerable contact effects at the electrode/semiconductor interface. One more specific feature of these SAMFETs is a high on/off current ratio visible in the transfer curve of OFETs (see Fig. 31 *b*). The authors interpreted this effect as being due to the use of ultrathin electrodes based on graphene monolayers.

Despite the high electrical characteristics of the OFETs based on the copper phthalocyanine LB films, the devices operate only in the case of very short channel lengths (< 100 nm), which hampers their practical application, whereas more promising SASMs show higher mobility, in particular, at large channel lengths.

Sizov *et al.*[68] proposed for the first time chemically inert disiloxane semiconducting oligomers as the base for LB SAMFETs. The authors noted that unlike chlorosilanes studied previously, disiloxanes cannot form semiconducting monolayers *via* self-assembly from solutions, as they lack functional groups capable of forming covalent bonds with the SiO_2-coated substrate. However, disiloxanes are amphiphilic compounds, because they contain a hydrophilic siloxane anchor group and a hydrophobic conjugated oligothiophene moiety; therefore, they can form Langmuir monolayers on the water surface.

The manufactured LB monolayers of 1,3-bis[11-(5‴-hexyl-2,2′:5′,2″:5″,2‴-quaterthiophen-5-yl)undecyl]-1,1,3,3-tetramethyldisiloxane [O(Si-Und-4T-Hex)$_2$][68] were examined by polarizating optical microscopy, atomic force microscopy, X-ray diffraction analysis and X-ray photoelectron spectroscopy. The whole set of the results indicates that LB monolayers are macroscopically homogeneous with small numbers of macrodefects; the layer thickness is 4 nm, which corresponds to a half of the calculated length of the siloxane dimer molecule. Therefore, the authors suggested that the orientation of molecules in the layer is nearly vertical. The grazing incidence X-ray diffraction and X-ray reflectivity data confirmed the crystal structure of the obtained monolayers with the unit cell parameters $a = 7.96$ Å and $b = 5.65$ Å and vertical orientation of the conjugated cores responsible for the semiconductor properties. It was concluded that the monolayer self-assembly at the water/air interface is due to the intermolecular π–π interactions giving a two-dimensional centred orthogonal herringbone type packing. The crystal unit cell parameters of the monolayer were close to those described previously for polythiophene.[69] A study of the LB monolayers by X-ray photoelectron spectroscopy also confirmed the correspondence of the atomic composition of the monolayers to the calculated one.[70]

The self-assembled semiconducting monolayers based on O(Si-Und-4T-Hex)$_2$ were tested as active semiconducting layers for OFETs. The output and transfer characteristics of LB SAMFETs based on this compound with 30 μm channel length are presented in Fig. 32. The curves have a shape typical of p-type transistors: at low negative voltages, the current is proportional to the voltage; when the voltage increases, the current is saturated. The shape of the output curves (see Fig. 32 *a*) considerably depended on the gate voltage, which illustrated the field effect. The authors noted a weak influence of the contact effects on the electrical characteristics of OFETs; this is manifested as a high linearity of output curves in the vicinity of zero voltage.[71] An important feature of electrical characteristics is a positive threshold voltage (~15 V, see Fig. 32 *b*), which was attributed to doping of the semiconducting monolayers under ambient conditions. The found carrier mobility values reached 3×10^{-3} cm^2 V^{-1} s^{-1} in the linear regime, while the on/off current ratio was about 10^5 and was

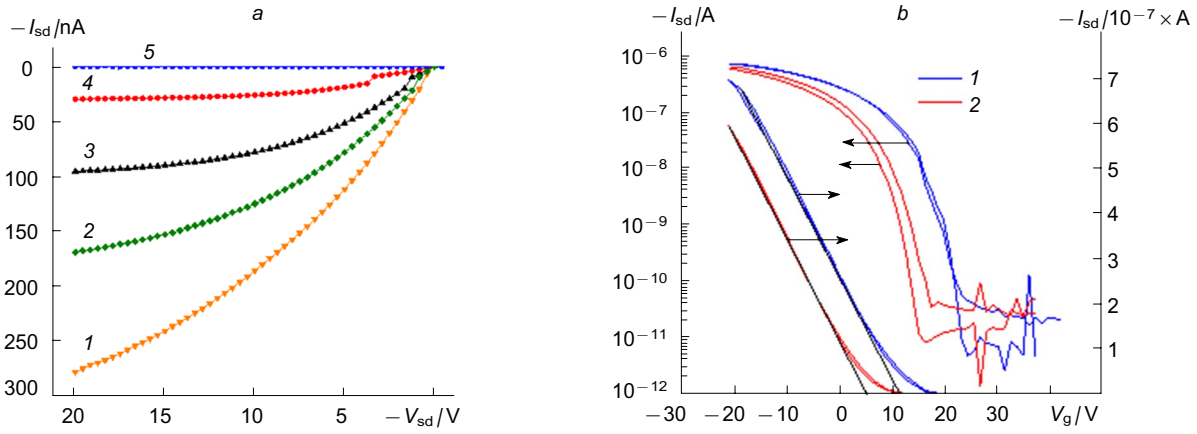


Figure 32. Output (*a*) and transfer (*b*) characteristics of SAMFET based on an O(Si-Und-4T-Hex)$_2$ LB monolayer. (*a*) $V_g = 0$ (*1*), 5 (*2*), 10 (*3*), 15 (*4*), 30 V (*5*); (*b*) (*1*) after the transfer, (*2*) after a month of storage under ambient conditions. The Figures were drawn by the authors using the data of Ref. 68, including SI.

determined by very low off-state currents in the transistor channel. Another important feature is the presence of a very small hysteresis of the curves visible in the region of small currents.

The manufactured SAMFETs showed high stability and reproducibility of electrical properties. After storage for 3 months under ambient conditions, the charge carrier mobility virtually did not change. The authors noted that storage in air is accompanied by a slow shift of the threshold voltage towards negative values (~8 V within a month of storage). This effect can be due to sorption of the charged particles in the transistor channel, which in turn induces doping of the semiconducting layer.[72,73] Since the initial threshold voltage is positive, its shift towards the negative region allows for the transistor operation at low voltage. Nevertheless, this fact must be borne in mind for the design of organic electronic devices based on LB monolayers. For example, in the SAMFET-based sensors,[62] the electrical response is defined by the rate of threshold voltage shift at a particular gas concentration in the environment and is insensitive to the absolute voltage value. It is more important to preserve the general operability of the device and the mobility of its charge carriers.

An important feature of LB monolayers obtained by Sizov *et al.*[68] is the absence of covalent bonds between the semiconducting layer and the substrate, because the siloxane dimer molecule O(Si-Und-4T-Hex)$_2$ has no reactive groups. A similar situation was reported in other studies[74,75] in which the semiconducting oligomer formed thin (including monolayer) films on the substrate *via* physisorption. However, the presence of a siloxane group able to form hydrogen bonds enables self-assembly of a monolayer at the water/air interface; this is a more economically and industrially feasible process. The similarity of the electrical properties of the LB SAMFETs based on the siloxane dimer and chlorosilane-based SAMFETs self-assembled from solution in which the semiconducting layer was covalently linked to the substrate [56] led the authors to conclude that the chemical nature of the anchor group has a minor effect on the morphology and electrical properties of the semiconducting monolayers composed of conjugated organosilicon oligomers. From the practical standpoint, disiloxanes are more easy-to-handle materials for application in organic electronic devices, because they require no inert atmosphere for storage or processing.

Trukhanov *et al.*,[76] who investigated the photophysical properties of monolayer OFETs based on the LB monolayers of O(Si-Und-4T-Hex)$_2$, ascertained that a photocurrent can be recorded in such devices upon irradiation of the active layer with modulated laser light at 405 nm. It was also noted that photocurrent increased with increasing optical modulation frequency, which is attributable to one of the following factors:

— the electronic structure of the organic semiconductor may have low-lying energy states, which act as traps for photoinduced charges, thus being responsible for the observed trend;

— reaching the limiting density of charge carriers in the semiconductor layer.

The authors proposed a simple numerical model of a photosensitive OFET based on Poisson's equation. This approach demonstrated that in p-type transistors, the photocurrent is formed in a small region near the OFET drain. The authors noted good prospects of the model for describing experiments on SAMFET photosensitivity measurements.

Agina *et al.*[77] studied the Langmuir monolayers of diphenylbithiophene derivatives. The interest in these compounds is due to the fact that the oligothiophenephenylene single crystals may combine high electrical transport and luminescent properties in organic electronic devices.[42,45,78,79] Meanwhile, in the 1,3-bis[11-(4-{5-[4-(trimethylsilyl)phenyl]-2,2-bithien-5-yl}phenyl)undecyl]-1,1,3,3-tetramethyldisiloxane [O(Si-Und-PTTP-TMS)$_2$] monolayer films, the carrier mobility was 1.0×10^{-5} cm^2 V^{-1} s^{-1} and the threshold voltage was −25 V.[77] These characteristics are not the highest, but it is important that using this compound, the authors succeeded in fabricating a monolayer that combined semiconducting and luminescence properties.

The photoluminescence spectra of the Langmuir–Schaefer monolayer, a spin-cast multilayer film and a solution of O(Si-Und-PTTP-TMS)$_2$ in toluene are shown in Fig. 33 *a*. The spectra of the mono- and multilayer films are shifted by ~0.15 eV with respect to the solution spectrum, which is indicative of strong intermolecular

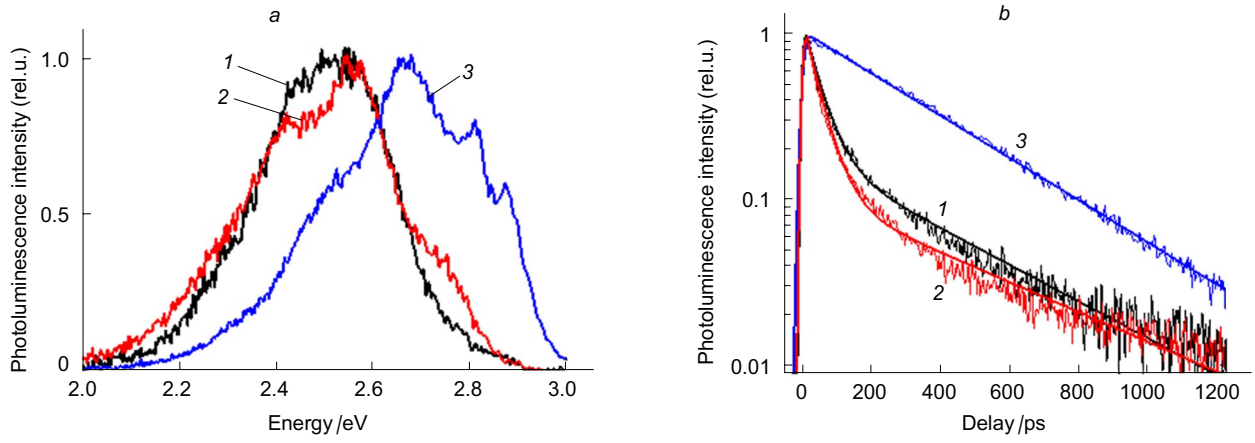
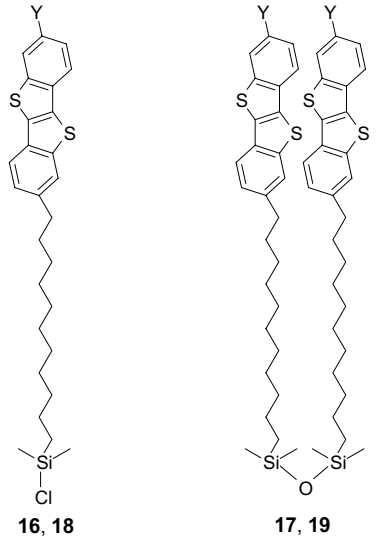


Figure 33. Photoluminescence spectra (*a*) of O(Si-Und-PTTP-TMS)$_2$ in LS monolayers (*1*), multilayer spin-coated films (*2*) and toluene solution (*3*); time-resolved photoluminescence kinetic curves (*b*).[77]

interaction both in the monolayer and in the multilayer film. The photoluminescence intensities of the films obtained by SC and LS methods were similar, despite the difference in the layer thickness; the authors attributed this to higher luminescence quantum yield for the monolayer compared with the polycrystalline multilayer film. The time-resolved kinetic curves of luminescence (see Fig. 33 *b*) for the monolayer and multilayer films are described by biexponential decay with two characteristic times $\tau_1 \approx 50$ ps and $\tau_2 \approx 420$ ps. The first characteristic time (τ_1) was attributed to luminescence self-quenching in view of the dense molecular packing both in the monolayer and in the multilayer films. The second characteristic time (τ_2) was close to the monoexponential decay time measured in a dilute solution of O(Si-Und-PTTP-TMS)$_2$, which allowed the authors to assign this value to the excited state lifetime of the organosilicon oligomer molecule. The key conclusion is that the Langmuir methods are suitable for self-assembling of semiconducting organosilicon monolayers combining semiconducting properties with high luminescence efficiency.

Borshchev *et al.*[80] proposed organosilicon benzothienobenzothiophene derivatives as the base for self-assembled semiconducting monolayers (structures **16** – **19**). Compounds of this class are known owing to high charge carrier mobilities, which are demonstrated by single crystalline BTBT semiconductors in OFETs; this allowed the authors to assume the presence of high electrical characteristics in BTBT monolayers.[29,81] They studied four organosilicon benzothienobenzothiophene derivatives, which differed by the presence or absence of a terminal aliphatic group and by the type of anchor group (siloxane or chlorosilyl) in the starting chemical compound. Monolayers based on compounds devoid of terminal aliphatic groups [Cl-Si-Und-BTBT (**16**) and O(Si-Und-BTBT)$_2$ (**17**)] showed very low electrical characteristics (mobilities were less than 5.0×10^{-6} cm^2 V^{-1} s^{-1}), whereas LB monolayers based on compounds with a terminal hexyl moiety, Cl-Si-Und-BTBT-Hex (**18**) and O(Si-Und-BTBT-Hex)$_2$ (**19**), showed high semiconducting properties with mobilities of up to 1.3×10^{-2} cm^2 V^{-1} s^{-1}, which is close to the record-high values known for self-assembled monolayers with an anchor group.

Structures 16 – 19



16, **18** **17**, **19**

Y = H [**16**, Cl-Si-Und-BTBT; **17**, O(Si-Und-BTBT)$_2$],
n-C_6H_{13} [**18**, Cl-Si-Und-BTBT-Hex; **19**, O(Si-Und-BTBT-Hex)$_2$]

In order to elucidate the grounds behind the so significant influence of the terminal alkyl group on the semiconductor characteristics of LB monolayers, the authors examined the monolayer morphology by AFM. For all compounds studied by Borshchev *et al.*,[80] the substrate coverage was high, which was confirmed by AFM and polarizating optical microscopy data. According to AFM data, in the case of compounds without a terminal alkyl group, the monolayer thickness was 5 nm (Fig. 34 *a*), which does not correspond to a monolayer packing with a vertical arrangement of the conjugated moieties. For these compounds, the LB monolayer thickness proved to be greater than the calculated length of the chlorosilane molecule, but smaller than the length of the disiloxane molecule in the unfolded conformation. The results obtained for O(Si-Und-BTBT)$_2$ and Cl-Si-Und-BTBT suggested another molecular packing differing from the packing of analogues with a

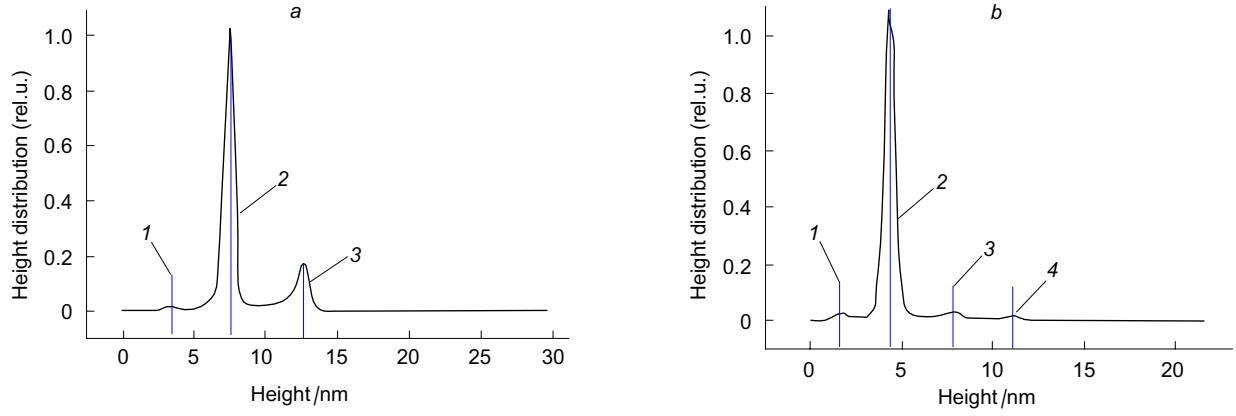
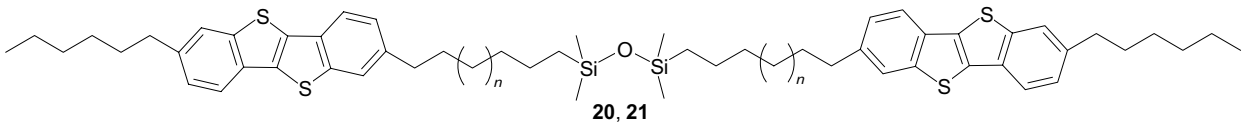


Figure 34. Height distribution for LB monolayers based on O(Si-Und-BTBT)$_2$ (*a*) and O(Si-Und-BTBT-Hex)$_2$ (*b*).[80]
(*1*) Substrate, (*2*) first monolayer, (*3*) second layer, (*4*) third layer.

Structures 20, 21



20, **21**

n = 1 [**20**, O(Si-Hex-BTBT-Hex)$_2$], 2 [**21**, O(Si-Hept-BTBT-Hex)$_2$]

terminal alkyl group. The molecular packings of O(Si-Und-BTBT)$_2$ and Cl-Si-Und-BTBT were responsible for their low semiconducting properties, whereas in the case of the BTBT derivative with a terminal alkyl group, the semiconducting molecules were vertically arranged in the monolayer, with the monolayer height being 3.3 nm (see Fig. 34 *b*). This value was well-correlated with the theoretically calculated size of the molecule and dictated high electrical characteristics. The vertical arrangement of the conjugated moieties was later confirmed by X-ray diffraction analysis and molecular modelling.[82]

Agina *et al.*[83] studied the effects of the alkyl spacer length of organosilicon BTBT derivatives (structures **20**, **21**) and thin film fabrication technique on the electrical properties of the resulting SAMFETs. Monolayer films were fabricated by the Langmuir–Blodgett, Langmuir–Schaefer, doctor blade and spin coating methods. It was shown that Langmuir methods are suitable for the formation of uniform monolayer films in which the arrangement of conjugated moieties is nearly vertical. The spin coating method allows fabrication of films with a thickness corresponding to two or three monolayers of the compounds. The length of the alkyl spacer insignificantly affects the morphology and electrical properties of monolayers formed by the Langmuir methods, whereas in the case of spin coating, an increase in the spacer length results in a change in the hydrophilic-hydrophobic balance of materials, which ultimately affects their electrical properties. The charge carrier mobility in the manufactured SAMFETs reaches 4×10^{-2} cm^2 V^{-1} s^{-1}, and the on/off current ratio reaches 10^5. The transistors show high reproducibility of electrical characteristics and stable operation under ambient conditions.

It has been noted above that the design of gas sensors is a promising application of self-assembled semiconducting organosilicon monolayers. Gas sensors based on OFETs have long been known.[84–86] By decreasing the thickness of the organic semiconducting layer to 3–5 nm, one can reduce the limit of detection (the minimum concentration that can be determined) and the response time. Trul *et al.*[82] described OFETs based on monolayers of the organosilicon BTBT derivative O(Si-Und-BTBT-Hex)$_2$ (compound **17**) and demonstrated detection of low concentrations of ammonia in dry air using devices of this type. The authors studied bottom-contact bottom-gate OFETs. Prior to the monolayer transfer, the silicon dioxide surface was treated with chlorodimethyloctylsilane; this treatment improved the operation stability of OFETs and increased the mobility of charge carriers.[71, 87–89]

The transfer characteristics of SAMFETs based on O(Si-Und-BTBT-Hex)$_2$ are shown in Fig. 35 *a*. The shape of the curves is typical of p-type transistors and the calculated mobility reaches 7×10^{-2} cm^2 V^{-1} s^{-1}. The response to a toxic gas (ammonia) was investigated by considering the time dependences of the on-state current during continuous SAMFET operation in dry air and upon addition of traces of ammonia into the transistor chamber. It was found that with direct-current voltage being applied

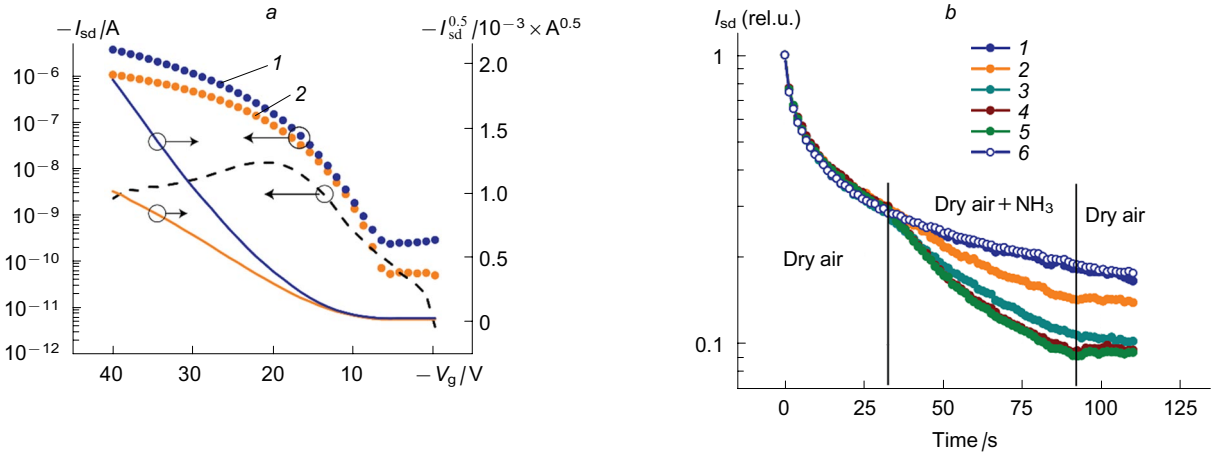


Figure 35. Transfer characteristics of SAMFET based on organosilicon BTBT derivative O(Si-Und-BTBT-Hex)$_2$ **17** (*a*) and time dependences of drain current at constant electrode voltages in dry air and with traces of ammonia added (*b*).[82]
(*a*) Dashed curve shows the leakage current through the OFET gate, V_{sd} = −10 (*1*), −40 V (*2*); (*b*) (*1*) dry air before NH_3 injection; (*2*) 400 ppb of NH_3, (*3*) 600 ppb of NH_3, (*4*) 800 ppb of NH_3, (*5*) 1000 ppb of NH_3, (*6*) dry air after NH_3.

to the OFET electrodes, the drain current decreased with time due to the so-called bias-stress effect of the organic semiconductor.[88] When ammonia was present in the chamber, the current decay rate was faster, which implied potential application of these SAMFETs as sensors (see Fig. 35 *b*). The authors also noted that the sensor proved to be reusable, as its electrical parameters returned to the initial values within 60 min after replacement of air containing the toxic gas by fresh air.

Thus, quite a few compounds able to form SASMs are currently known. The electric characteristics of these systems reached rather high values (for example, the charge carrier mobility is up to 7×10^{-2} cm^2 V^{-1} s^{-1}); however, they are inferior to organic semiconductors based on bulk films of chemical compounds with analogous conjugated moieties. First of all, this is due to the fact that in the case of OFETs, an important role is played by not only the bottom monomolecular semiconducting layer, which accommodates the major charge transport, but also by the next (second) layer, which is able to compensate for defects of the first layer.[7] In the case of molecules with an anchor group, formation of the second and subsequent electric layers introduces additional defects into the organic semiconductor such as chemically reactive or polar groups, which limits the electrical properties of SASM-based devices. As a result, among organic semiconductors with anchor groups, the best electrical properties are inherent in monolayer films, while deposition of the subsequent semiconducting layers does not improve the performance. Despite the moderate carrier mobilities, SASM-based transistors show high stability and operate on both silicon and flexible polymer substrates. A highly promising application of SASMs composed of organic molecules with an anchor group is the design of highly sensitive gas sensors suitable for detecting low concentrations (< 1 ppm) of low-molecular-mass toxic gases or volatile organic compounds in the environment.

5.2. Self-assembled semiconducting monolayers based on organic compounds without anchor groups

A significant current trend of organic electronics is the fabrication of self-assembled thin layers (including monolayers) based on short conjugated molecules containing no functional or polar anchor groups from solutions. This trend is being addressed in more and more publications. The electrical properties of the fabricated semiconducting films are usually rather high, despite the small semiconductor thickness (the carrier mobility can reach 1 cm^2 V^{-1} s^{-1}). The present Section of the review covers the most interesting results reported on this subject in recent years.

One of the first SASMs based on di(2-octyldodecyl)septithiophene has been described by Defaux *et al.*[90] Owing to the presence of long branched substituents, the solubility of the starting compound in toluene was relatively high (3 g litre^{-1}), which allowed spin coating fabrication of thin films. According to AFM data, the film morphology was macroscopically homogeneous and the monolayer thickness was ~ 4 nm (Fig. 36 *a*). The monolayer thickness was calculated from X-ray reflectivity data; the resulting value (41 Å) correlates with with AFM data. In addition, it was found that the electron density of the films can be successfully represented by a three-layer model (see Fig. 38 *b*) in which the central layer corresponds to thiophene cores, while the top and bottom layers correspond to alkyl substituents. According to the modelling results, the tilt angle of the thiophene cores was found to be 40°.

The transfer characteristics of a SAMFET based on the di(2-octyldodecyl)septithiophene monolayer measured in the saturation ($V_{sd} = -20$ V) and linear ($V_{sd} = -2$ V) regimes are depicted in Fig. 36 *c*. The charge carrier mobility in the linear regime reached 10^{-2} cm^2 V^{-1} s^{-1}, which is close to the record-high values known for semiconductors containing a reactive anchor group.[25]

Glushkova *et al.*[91] described ultrathin semiconducting single crystals based on two oligothiophenephenylenes differing in the length of the terminal substituents: 1,4-bis(5′-hexyl-2,2′-bithiophen-5-yl)benzene (DH-TTPTT) and 1,4-bis(5′-decyl-2,2′-bithiophen-5-yl)benzene (DD-TTPTT). The single crystals were grown on a silicon substrate by spin coating from a dichlorobenzene solution with a 0.4–1 g litre^{-1} concentration at 600–800 rpm during 30 s. The needle crystals thus formed were examined by

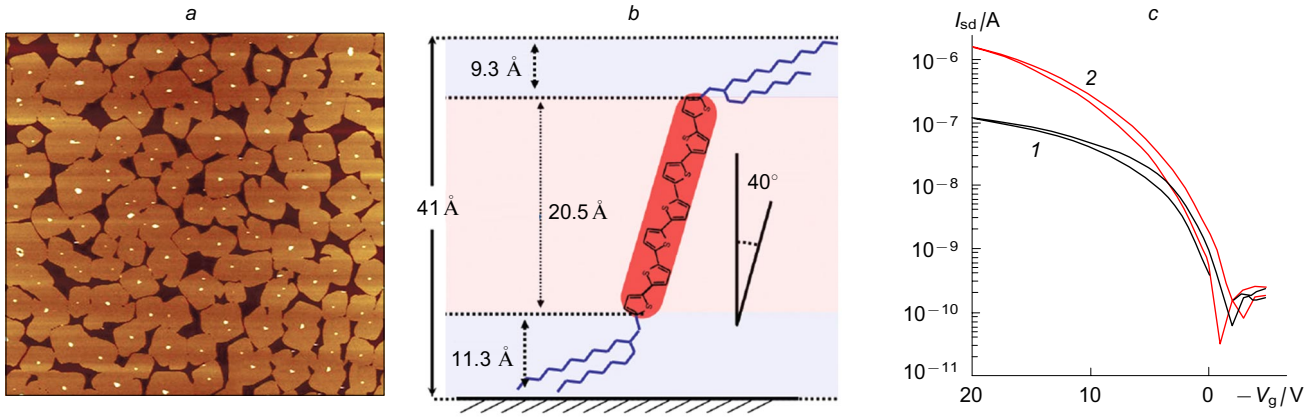


Figure 36. Morphology of the di(2-octyldodecyl)septithiophene monolayer on a silicon substrate (*a*), presumptive molecular packing of the monolayer (*b*) and transfer characteristics of SAMFET based on this monolayer (*c*).[90]
(*a*) Image size 12 × 12 μm^2; (*c*) $V_{sd} = -2$ (*1*), −20 V (*2*).

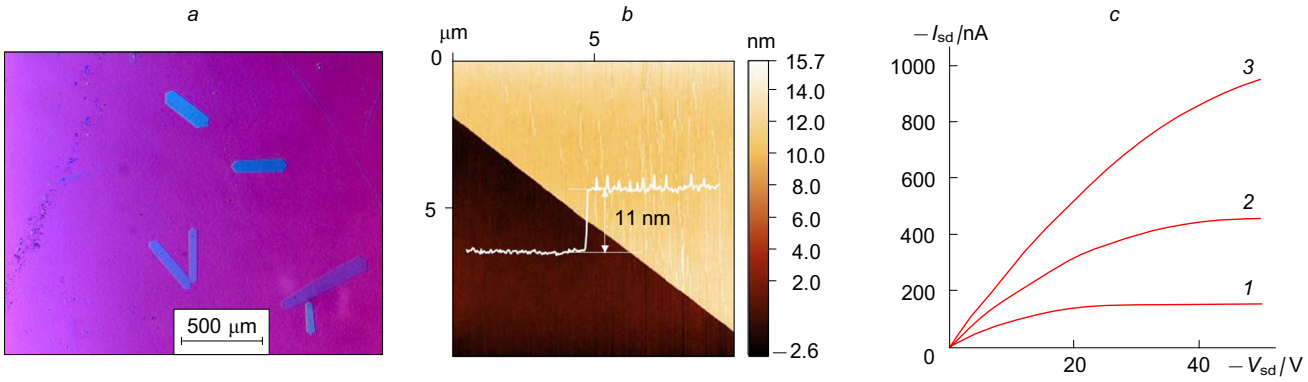


Figure 37. Optical micrograph (*a*) and morphology (*b*) of ultrathin DD-TTPTT single crystals and output curves of OFET based on them (*c*).[91]
(*b*) White colour designates the surface profile from AFM; (*c*) $-V_g$ = 10 (*1*), 20 (*2*), 50 V (*3*).

polarizating optical microscopy, atomic force microscopy and transmission electron microscopy.

An optical micrograph of the ultrathin DD-TTPTT single crystals taken by differential interference contrast microscopy is shown in Fig. 37 *a*. The absence of visible defects suggested that the image corresponded to single crystals. According to AFM data (see Fig. 37 *b*), the surface roughness did not exceed 0.3 nm. The thickness of a single crystal estimated from AFM data was 11 nm, which corresponded to several molecular monolayers. A series of output curves for the OFETs with a DD-TTPTT single crystal as the semiconductor is shown in Fig. 37 *c*. The VACs of the device were typical of a p-type transistors, while the mobility reached 0.2 $cm^2\ V^{-1}\ s^{-1}$ in the linear regime. However, in the case of DH-TTPTT single crystals, the mobility was lower, that is, up to 0.06 $cm^2\ V^{-1}\ s^{-1}$; the authors attributed this result to decreasing length of the alkyl chain compared with the chain of DD-TTPTT, which leads to less efficient spatial separation of the conductive layer and the dielectric surface containing energy traps for charge carriers.

Peng *et al.*[92] proposed an original technique for the fabrication of semiconducting monolayers based on the DB method with deposition from a supersaturated solution in two stages (dual solution-shearing). The monolayer was composed of 2,9-didecyldinaphtho[2,3-*b*:2′,3′-*f*]thieno[3,2-*b*]thiophene (C_{10}-DNTT). The essence of the method was as follows: first, C_{10}-DNTT was dissolved in tetralin to the concentration c_1 close to the concentration of a saturated solution (c_1 = 1 mg ml^{-1}). Then C_{10}-DNTT crystallization nuclei were formed by the DB method at 85 °C on a silicon substrate the surface of which was modified with trichloro(phenyl)silane (the concentration of the saturated C_{10}-DNTT solution at 85 °C was 0.9 mg ml^{-1}). According to optical microscopy data, the nuclei thus obtained had different crystallographic axis orientations and were multilayer crystallites. At the final stage, the second DB shearing process was performed at a temperature of 90 °C and at the solution concentration c_2 = 1 mg ml^{-1} (Fig. 38 *a*). The concentration of the saturated solution at this temperature was 1.1 mg ml^{-1} and the work of adhesion between the neighbouring C_{10}-DNTT layers is moderate (50 mN m^{-1}); hence, some of the mole-

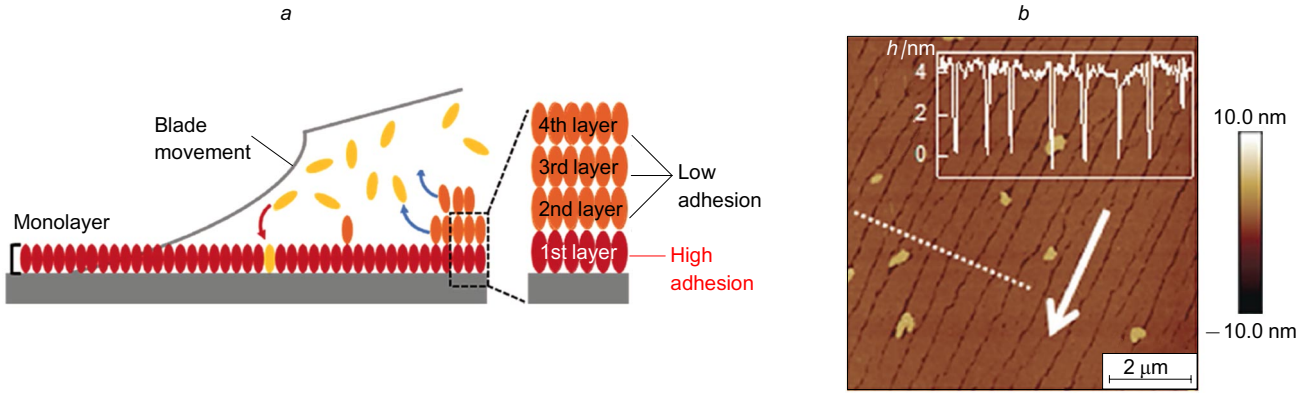


Figure 38. Schematic diagram of formation of monolayer semiconductors *via* DB technique with two-stage deposition from a supersaturated solution (*a*) and AFM morphology of the C_{10}-DNTT monolayer obtained by this method (*b*).[92]
(*b*) The inset shows the AFM-based surface profile.

cules occurring in the crystallites could return to the solution. However, the work of adhesion between the substrate and the first C_{10}-DNTT layer was greater than that between the neighbouring layers (64.3 mN m^{-1}); therefore, the dissolution of the bottom layer was relatively slow. The typical morphology of the C_{10}-DNTT film obtained in this way is illustrated in Fig. 38 *b*. The film thickness was ~4 nm, which corresponds to a vertical orientation of the organic semiconductor molecules on the silicon substrate. Thus, by controlling the substrate temperature and solution concentration, it is possible to fabricate high-quality C_{10}-DNTT monolayers, which can be used in high-performance SAMFETs.

The fabricated C_{10}-DNTT monolayers were tested as semiconducting layers of the bottom-gate top-contact OFETs. The charge carrier mobility in the OFETs reached 10.4 $cm^2\ V^{-1}\ s^{-1}$ for the measurement of electrical properties in an inert atmosphere or for the device encapsulated by deposition of a thin PMMA layer. However, the devices did not demonstrate electrical properties under normal conditions ($\mu = 0$), which restricted the practical application of the fabricated monolayers in the real organic electronic devices. Nevertheless, the so high charge carrier mobility attained in monolayer devices is an important scientific result, which makes the developed approach to the fabrication of monolayerss highly promising.

Currently, active research is in progress into soluble benzothienobenzothiophene derivatives capable of forming thin (including monolayer) semiconducting layers.[93–97] Among the publications, of special note is the paper of Wang *et al.*,[93] in which a two-dimensional molecular single crystal of dialkyl-substituted benzothienobenzothiophene C_8-BTBT-C_8 was formed on the silicon dioxide surface by dragging a drop of a solution of the compound in a mixture of solvent and antisolvent over the substrate surface by a flow of air. The basic idea behind the method was that the floating-coffee-ring effect was observed on the contour of the moving drop. Due to this effect, the C_8-BTBT-C_8 crystal growth was located in a small spatial area, which afforded highly ordered 2D crystals with a lateral size of the order of hundreds of micrometres within hundredths of a second (Fig. 39 *a*,*b*).

The single crystals thus obtained were tested as top-contact bottom-gate OFET semiconducting layers. A typi-

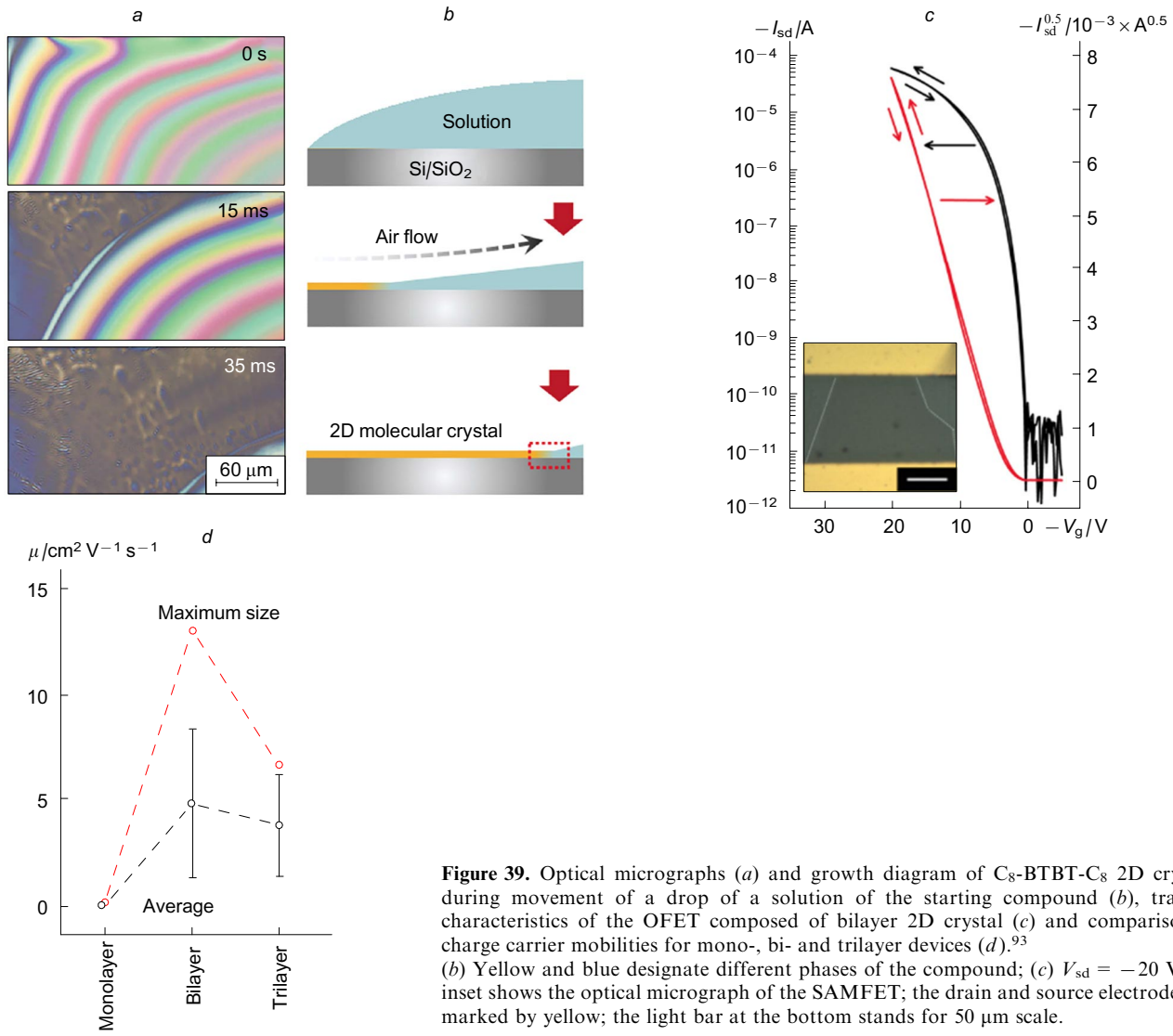


Figure 39. Optical micrographs (*a*) and growth diagram of C_8-BTBT-C_8 2D crystals during movement of a drop of a solution of the starting compound (*b*), transfer characteristics of the OFET composed of bilayer 2D crystal (*c*) and comparison of charge carrier mobilities for mono-, bi- and trilayer devices (*d*).[93]
(*b*) Yellow and blue designate different phases of the compound; (*c*) $V_{sd} = -20$ V; the inset shows the optical micrograph of the SAMFET; the drain and source electrodes are marked by yellow; the light bar at the bottom stands for 50 μm scale.

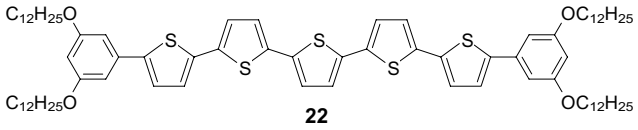
cal transfer characteristics of an OFET based on a bilayer single crystal measured in a vacuum is shown in Fig. 39 *c*. This curve was used to calculate the charge carrier mobility (5.2 $cm^2\ V^{-1}\ s^{-1}$), the on/off current ratio (10^6), the subthreshold slope (0.4 V per decade) and the threshold voltage (−3 V). The highest carrier mobility was 13.0 $cm^2\ V^{-1}\ s^{-1}$; this is the record-high value for several molecular layer thick semiconductors. Furthermore, the contact resistance at the electrode/semiconductor interface (0.4 kΩ) was also among the best values know for organic semiconductors. It is worthy of special note that the electrical properties of monolayer OFETs were relatively low (μ = 0.04 $cm^2\ V^{-1}\ s^{-1}$), whereas in the case of bi- and trilayer transistors, they were markedly higher and close to each other (see Fig. 39 *d*). Thus, this approach is suitable for the fabrication of molecular 2D crystals with high electrical characteristics using a fast solution procedure. However, the authors did not report the electrical properties of the films under ambient conditions and, hence, their practical applicability is still an open question.

One more case of formation of monolayer 2D crystals from the liquid phase was reported by Jiang *et al.*[98] As the starting compound, the authors used 1,4-bis[(5′-hexyl-2,2′-bithiophen-5-yl]ethynyl)benzene. The deposition of millimetre-size 2D crystals of the chosen compound from a solution was confirmed by polarizating optical, atomic force, scanning electron microscopy and X-ray diffraction. The crystal thickness varied from 1 to 21 monolayers upon a change in the film formation conditions. The charge carrier mobility in these crystals amounted to 0.3–1.0 $cm^2\ V^{-1}\ s^{-1}$ and was virtually independent of the semiconducting layer thickness. This was attributed to the presence of a conducting channel only in a thin layer at the semiconductor/dielectric interface. The high stability of electrical properties of the crystals during storage in air and simplicity of the semiconductor preparation procedure prompted the conclusion that this approach would be promising for practical applications.

Chen *et al.*[99] described photosensitive OFETs stable in water based on self-assembled monolayers of quinquethiophene derivative with bulky alkyl substituents (structure **22**). As the substrate, the authors used highly doped silicon with a thin (6 nm) HfO_2 oxide film grown by a sol–gel process (Fig. 40). The choice of the dielectric is caused by its small thickness (which decreased the operating voltage range of the transistor) and high dielectric permittivity. The resulting monolayers were studied by AFM, X-ray reflectivity, X-ray diffraction with the SLD model and transmission electron microscopy. The whole set of results led to the conclusion that the fabricated monolayers were highly ordered and the thiophene cores formed a crystalline layer tilted by 50° (see Fig. 40 *b*,*c*).

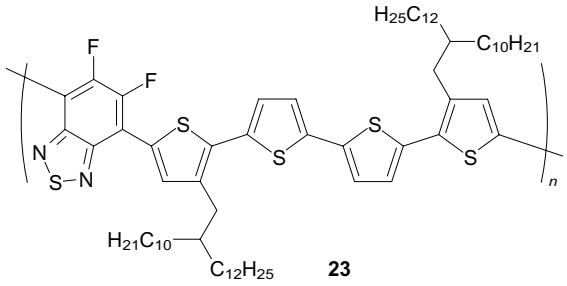
The monolayers of compound **22** were used as OFET semiconducting layers. A series of output curves for the transistor with operating voltages of 0–4 V is shown in Fig. 40 *c*. The linear and saturation operation regimes can be clearly seen in the curves. The average charge carrier mobility in the monolayers of compound **22** supported on HfO_2 was 0.08 $cm^2\ V^{-1}\ s^{-1}$, which is a typical value for oligothiophene films. The operability of monolayer transis-

Structure 22



22

Structure 23



23

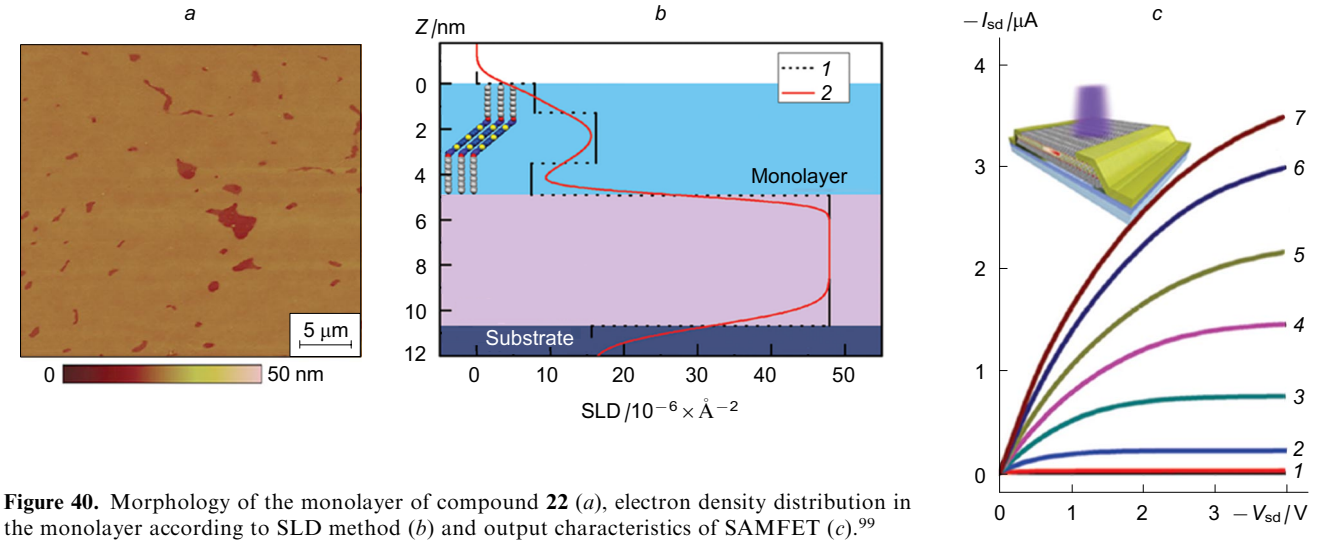


Figure 40. Morphology of the monolayer of compound **22** (*a*), electron density distribution in the monolayer according to SLD method (*b*) and output characteristics of SAMFET (*c*).[99] (*b*) (*1*) Model, (*2*) experiment; (*c*) $-V_g$ = 0.5 (*1*), 1 (*2*), 1.5 (*3*), 2 (*4*), 2.5 (*5*), 3 (*6*), 3.5 (*7*); the upper drawing is a 3D model of photosensitive SAMFET.

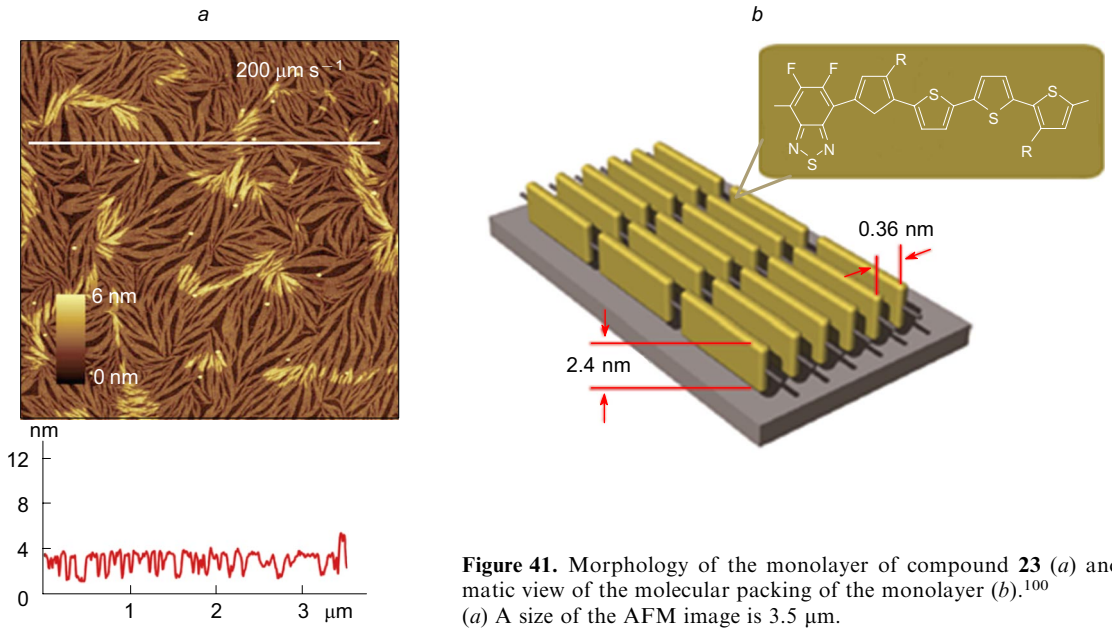


Figure 41. Morphology of the monolayer of compound **23** (*a*) and schematic view of the molecular packing of the monolayer (*b*).[100]
(*a*) A size of the AFM image is 3.5 μm.

tors in the deionized water deserves special mention. The carrier mobility was also high in this case: up to 0.06 cm^2 V^{-1} s^{-1}.

Li *et al.*[100] reported on integrated circuits based on a monolayer of the difluorobenzothiadiazole and oligothiophene **23** copolymer. The authors described a facile process for the fabrication of highly ordered polymer films using immersion into a solution. It was shown that the deposition rate was a key factor for the formation of homogenous monolayers. Deposition at a rate of 200 μm s^{-1} gave a 2.4 nm-thick polymer monolayer (Fig. 41 *a*). A grazing incidence X-ray diffraction study established a molecular packing of the polymer in the monolayer (see Fig. 41 *b*). The monolayers had high charge carrier mobilities (up to 3 cm^2 V^{-1} s^{-1}); they were highly homogeneous; therefore, they could be used to fabricate integrated circuits such as a ring oscillator and a 15-bit code generator.

Vladimirov *et al.*[101] investigated the effect of solvent characteristics [namely, surface tension (γ) and viscosity (η)] on the properties of semiconducting films deposited from solutions. The authors used (*N*,*N*′-di[(*S*)-1-methylpentyl]-1,7(6)-dicyanoperylene-3,4 : 9,10-bis(dicarboxamide) (PDI1MPCN2) as the starting compound. Depending on the solvent type, the same compound may form no film, being deposited as separate crystallites possessing no electrical properties; also, it may be deposited on the substrate

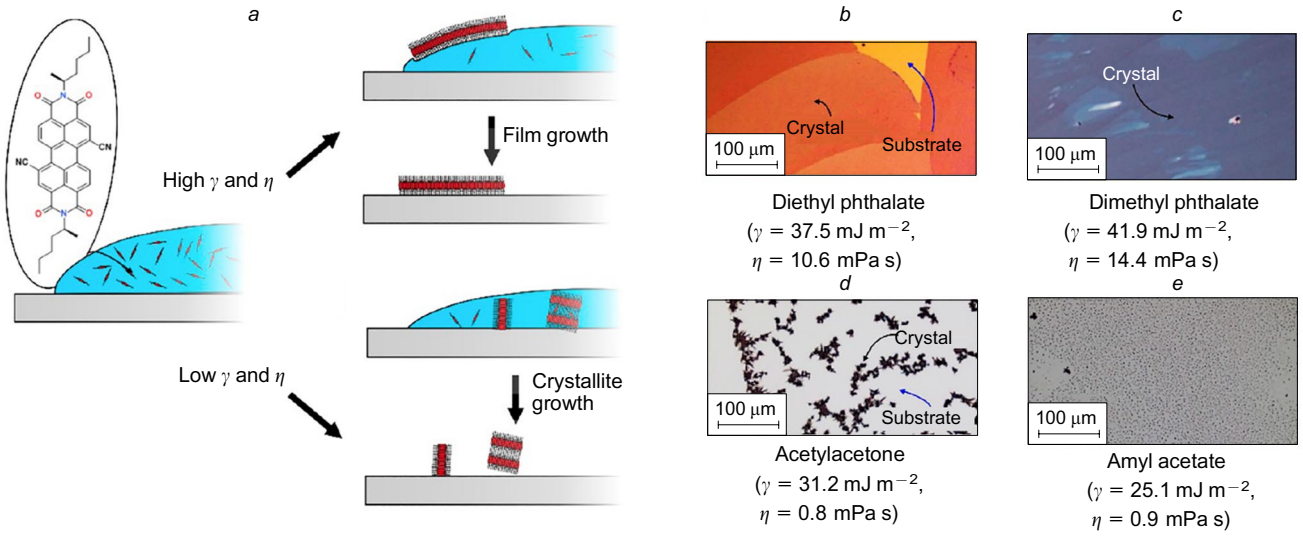


Figure 42. Illustration of the fabrication (*a*) and optical micrographs of the PDI1MPCN2 films deposited from various solvents (*b*–*e*).[101]
γ is the surface tension, η is viscosity.

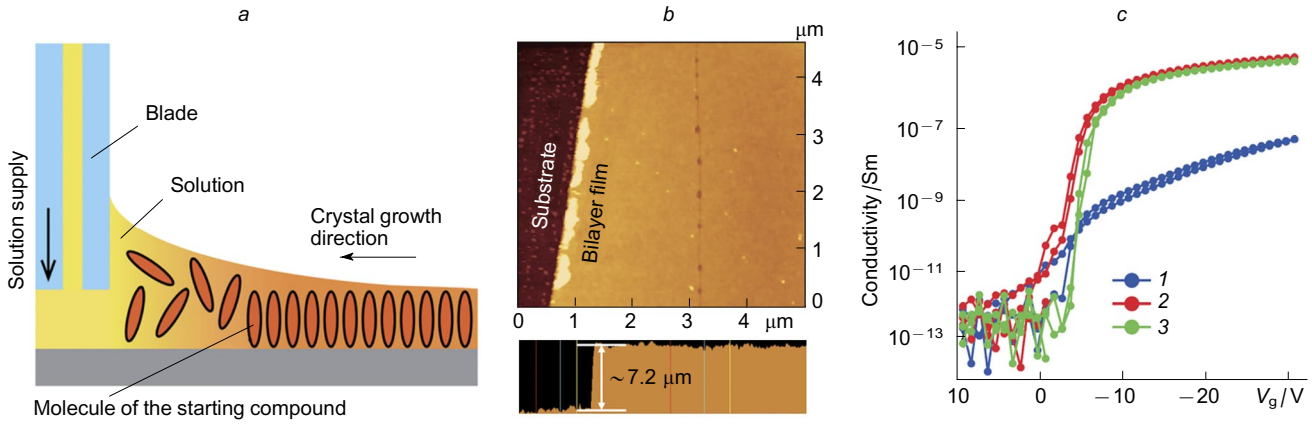


Figure 43. Schematic diagram of formation of monolayer single crystals (*a*), AFM morphology of the resulting films (*b*), transfer characteristics of OFETs based on mono-, bi- and trilayer single crystals (*c*).[102]
(*c*) $V_{sd} = -3$ V, (*1*) one layer, (*2*) two layers, (*3*) three layers.

as a high-quality polycrystalline film. The authors noted that in the case of solvents with high γ and η values, films were formed, whereas low γ and η values led to the formation of 3D crystallites (Fig. 42). The surface tension was found to have the crucial influence on the crystallization. An important practical result of this study is that the authors demonstrated how the electrical properties of semiconducting layers can be considerably changed by selection of the solvent. The charge carrier mobility can be increased to 4 $cm^2 V^{-1} s^{-1}$ in the case of PDI1MPCN2. The film stability evaluated by the characteristic time over which the current decays on application of an external voltage can vary from 10^3 to 10^{13} s. This result is very important, because increase in the OFET stability is a challenge of organic electronics.

Yamamura *et al.*[102] described the procedure of formation of centimetre-sized ultrathin single crystals of 3,11-dioctyldinaphtho[2,3-*d*:2′,3′-*d*′]benzo[1,2-*b*:4,5-*b*′]dithiophene (C_8-DNBDT-NW) possessing charge carrier mobilities of up to 13 $cm^2 V^{-1} s^{-1}$ and ultralow electrode/semiconductor contact resistance (46.9 Ω cm). The single crystal formation procedure is based on crystallization of the compound in the front of a moving solvent drop. A solution of the starting compound was continuously injected into the bulk of the moving drop with a DB technique (Fig. 43 *a*). The films obtained in this way were studied by polarizating optical microscopy, atomic force microscopy, transmission electron microscopy, Raman spectroscopy and electron diffraction. The set of obtained data confirmed the single crystalline nature of the films. This is exemplified in Fig. 43 *b*, which shows the AFM morphology of the obtained single crystal with a thickness of 7.2 nm, which corresponded to a bilayer film. The authors noted that bi- and trilayer single crystals demonstrated high semiconducting properties, whereas multilayer OFETs showed poorer characteristics. This result was attributed to the presence of defects in the semiconducting bottom layer, which was formed during the monolayer crystallization, whereas in bi- and trilayer devices, the density of these defects was lower.

We would like to note in conclusion that SASMs based on organic compounds containing no anchor groups are under vigorous research. Such monolayers are of high interest, as they can be formed by a broad range of solution methods. Organic semiconductors containing no anchor groups are normally characterized by high charge carrier mobilities and, hence they are suitable for fabrication of integrated circuits. However, only a few papers present data on air stability of the devices, which leaves open the question of their applicability without an additional encapsulating layer.

* * *

The presented literature review has shown that self-assembled monolayer organic semiconductors are of high interest for both fundamental research and practical applications. They represent convenient objects for a variety of *in situ* experiments aimed at investigating the charge transport mechanisms in organic semiconductors. This is due to the fact that the organic current-carrying layer in SASMs is in contact with the environment and can be easily affected by external factors. As regards practical applications, the high charge carrier mobilities achieved in recent years for organic monolayers enabled the fabrication of various microelectronic devices based on them such as digital microcircuits and highly sensitive gas sensors. The latter devices have several competitive advantages over other types of chemical sensors; therefore, one may expect that commercial prototypes of sensors based on organic monolayers will appear in the near future.

This review was prepared within the framework of the support programme to leading scientific schools NSh-5698.2018.3 and with the support of the Russian Foundation for Basic Research (Project Nos 16-29-05321 and No. 18-33-01210).

Figures 2, 4–6, 30 are courtesy of AIP Publishing; Figs 3, 12–14, 20–23, 31, 36, 38–40 are courtesy of Wiley; Figs 7, 28 are courtesy of Elsevier; Figs 8, 9, 18, 19, 27, 29, 32, 33, 42 are courtesy of the American Chemical Society; Figs 10, 11, 24–26, 41 are courtesy of Springer

Nature; Fig. 16 is a courtesy of the American Physical Society; Fig. 35 is a courtesy of Centre National de la Recherche Scientifique (CNRS) and the Royal Society of Chemistry; Fig. 37 is a courtesy of the International Society for Optical Engineering; Fig. 43 is a courtesy of American Association for the Advancement of Science.

References

1. G.M.Whitesides, B.Grzybowski. *Science*, **295**, 2418 (2002)
2. J.D.Halley, D.A.Winkler. *Complexity*, **14**, 10 (2008)
3. J.-M.Lehn. *Supramolecular Chemistry: Concepts and Perspectives*. (Weinheim: VCH Verlagsgesellschaft, 1995)
4. H.Kallmann, M.Pope. *Nature (London)*, **186**, 31 (1960)
5. H.Kallmann, M.Pope. *J. Chem. Phys.*, **32**, 300 (1960)
6. C.Tanase, E.J.Meijer, P.W.M.Blom, D.M.De Leeuw. *Org. Electron.*, **4**, 33 (2003)
7. F.Dinelli, M.Murgia, P.Levy, M.Cavallini, F.Biscarini, D.M.De Leeuw. *Phys. Rev. Lett.*, **92**, 116802 (2004)
8. O.V.Borshchev, S.A.Ponomarenko. *Polym. Sci., Ser. C*, **56**, 32 (2014)
9. C.R.Kagan. *Top. Curr. Chem.*, **312**, 213 (2011)
10. S.Casalini, C.A.Bortolotti, F.Leonardi, F.Biscarini. *Chem. Soc. Rev.*, **46**, 40 (2016)
11. F.Yang, S.Cheng, X.Zhang, X.Ren, R.Li, H.Dong, W.Hu. *Adv. Mater.*, **30**, 1801891 (2018)
12. P.K.Weimer. *Proc. IRE*, 1462 (1962)
13. G.Horowitz. *Adv. Mater.*, **10**, 365 (1998)
14. A.Dodabalapur, L.Torsi, H.E.Katz. *Science*, **268**, 270 (1995)
15. S.A.Ponomarenko. Doctoral Thrsis in Chemical Sciences, Institute of Synthetic Polymeric Materiasl, RAS, Moscow, 2010
16. V.Podzorov, V.M.Pudalov, M.E.Gershenson. *Appl. Phys. Lett.*, **82**, 1739 (2003)
17. G.Horowitz, X.Z.Peng, D.Fichou, F.Garnier. *J. Appl. Phys.*, **67**, 528 (1990)
18. G.Horowitz, R.Hajlaoui, H.Bouchriha, R.Bourguiga, M.Hajlaoui. *Adv. Mater.*, **10**, 923 (1998)
19. G.Horowitz, R.Hajlaoui, D.Fichou, A.El Kassmi. *J. Appl. Phys.*, **85**, 3202 (1999)
20. G.Horowitz, R.Hajlaoui, P.Delannoy. *J. Phys. III (France)*, **5**, 355 (1995)
21. A.R.Brown, C.P.Jarrett, D.M.De Leeuw, M.Matters. *Synth. Met.*, **88**, 37 (1997)
22. D.Natali, M.Caironi. *Adv. Mat.*, **24**, 1357 (2012)
23. G.Horowitz, P.Lang, M.Mottaghi, H.Aubin. *Adv. Funct. Mater.*, **14**, 1069 (2004)
24. S.G.J.Mathijssen, E.C.P.Smits, P.A.Van Hal, H.J.Wondergem, S.A.Ponomarenko, A.Moser, R.Resel, P.A.Bobbert, M.Kemerink, R.A.J.Janssen, D.M.De Leeuw. *Nat. Nanotechnol.*, **4**, 674 (2009)
25. H.H.Choi, K.Cho, C.D.Frisbie, H.Sirringhaus, V.Podzorov. *Nat. Mater.*, **17**, 2 (2017)
26. M.Halik, H.Klauk, U.Zschieschang, G.Schmid, W.Radlik, S.Ponomarenko, S.Kirchmeyer, W.Weber. *J. Appl. Phys.*, **93**, 2977 (2003)
27. M.Halik, H.Klauk, U.Zschieschang, G.Schmid, S.Ponomarenko, S.Kirchmeyer, W.Weber. *Adv. Mater.*, **15**, 917 (2003)
28. Q.Xia, M.Burkhardt, M.Halik. *Org. Electron.*, **9**, 1061 (2008)
29. H.Ebata, T.Izawa, E.Miyazaki, K.Takimiya, M.Ikeda, H.Kuwabara, T.Yui. *J. Am. Chem. Soc.*, **129**, 15732 (2007)
30. A.Pietrangelo, B.O.Patrick, M.J.Maclachlan, M.O.Wolf. *J. Org. Chem.*, **74**, 4918 (2009)
31. A.Y.Amin, K.Reuter, T.Meyer-Friedrichsen, M.Halik. *Langmuir*, **27**, 15340 (2011)
32. Y.Chung, E.Verploegen, A.Vailionis, Y.Sun, Y.Nishi, B.Murmann, Z.Bao. *Nano Lett.*, **11**, 1161 (2011)
33. A.Y.Amin, A.Khassanov, K.Reuter, T.Meyer-Friedrichsen, M.Halik. *J. Am. Chem. Soc.*, **134**, 16548 (2012)
34. H.Minemawari, T.Yamada, H.Matsui, J.Tsutsumi, S.Haas, R.Chiba, R.Kumai, T.Hasegawa. *Nature (London)*, **475**, 364 (2011)
35. M.Pope, C.E.Swenberg, M.Pope, in *Electronic Processes in Organic Crystals and Polymers*. (2nd Ed.). (New York: Oxford University Press, 1999). P. 39
36. D.Faltermeier, B.Gompf, M.Dressel, A.K.Tripathi, J.Pflaum. *Phys. Rev. B*, **74**, (2006)
37. C.Yumusak, M.Abbas, N. S.Sariciftci. *J. Lumin.*, **134**, 107 (2013)
38. J.Zaumseil, R.H.Friend, H.Sirringhaus. *Nat. Mater.*, **5**, 69 (2005)
39. R.Capelli, S.Toffanin, G.Generali, H.Usta, A.Facchetti, M.Muccini. *Nat. Mater.*, **9**, 496 (2010)
40. B.K.Yap, R.Xia, M.Campoy-Quiles, P.N. Stavrinou, D.D.Bradley. *Nat. Mater.*, **7**, 376 (2008)
41. F.Cicoira, C.Santato. *Adv. Funct. Mater.*, **17**, 3421 (2007)
42. S.Z.Bisri, T.Takenobu, Y.Yomogida, H.Shimotani, T.Yamao, S.Hotta, Y.Iwasa. *Adv. Funct. Mater.*, **19**, 1728 (2009)
43. J.Zaumseil, C.L.Donley, J.S.Kim, R.H.Friend, H.Sirringhaus. *Adv. Mater.*, **18**, 2708 (2006)
44. T.Takenobu, S.Z.Bisri, T.Takahashi, M.Yahiro, C.Adachi, Y.Iwasa. *Phys. Rev. Lett.*, **100**, 066601 (2008)
45. T.Yamao, Y.Shimizu, K.Terasaki, S.Hotta. *Adv. Mater.*, **20**, 4109 (2008)
46. A.Shehu, S.D.Quiroga, P.D'angelo, C.Albonetti, F.Borgatti, M.Murgia, A.Scorzoni, P.Stoliar, F.Biscarini. *Phys. Rev. Lett.*, **104**, 246602 (2010)
47. J.Huang, J.Sun, H.E.Katz. *Adv. Mater.*, **20**, 2567 (2008)
48. E.C.P.Smits, S.G.J.Mathijssen, P.A.Van Hal, S.Setayesh, T.C.T.Geuns, K.A.H.A.Mutsaers, E.Cantatore, H.J.Wondergem, O.Werzer, R.Resel, M.Kemerink, S.Kirchmeyer, A.M.Muzafarov, S.A.Ponomarenko, B.De Boer, P.W.M.Blom, D.M.De Leeuw. *Nature (London)*, **455**, 956 (2008)
49. M.Novak, A.Ebel, T.Meyer-Friedrichsen, A.Jedaa, B.F.Vieweg, G.A.Yang, K.Voitchovsky, F.Stellacci, E.Spiecker, A.Hitsch, M.Halik. *Nano Lett.*, **11**, 156 (2011)
50. A.Ringk, X.R.Li, F.Gholamrezaie, E.C.P.Smits, A.Neuhold, A.Moser, C.Van der Marel, G.H.Gelinck, R.Resel, D.M.De Leeuw, P.Strohriegl. *Adv. Funct. Mater.*, **23**, 2016 (2013)
51. W.C.Bigelow, D.L.Pickett, W.A.Zisman. *J. Colloid Interface Sci.*, **1**, 513 (1946)
52. E.E.Polymeropoulos, J.Sagiv. *J. Chem. Phys.*, **69**, 1836 (1978)
53. J.Sagiv. *J. Am. Chem. Soc.*, **102**, 92 (1980)
54. G.S.Tulevski, Q.Miao, M.Fukuto, R.Abram, B.Ocko, R.Pindak, M.L.Steigerwald, C.R.Kagan, C.Nuckolls. *J. Am. Chem. Soc.*, **126**, 15048 (2004)

55. M.Mottaghi, P.Lang, F.Rodriguez, A.Rumyantseva, A.Yassar, G.Horowitz, S.Lenfant, D.Tondelier, D.Vuillaume. *Adv. Funct. Mater.*, **17**, 597 (2007)
56. S.A.Ponomarenko, O.V.Borshchev, T.Meyer-Friedrichsen, A.P.Pleshkova, S.Setayesh, E.C.P.Smits, S.G.J.Mathijssen, D.M.De Leeuw, S.Kirchmeyer, A.M.Muzafarov. *Organometallics*, **29**, 4213 (2010)
57. G.Gelinck, P.Heremans, K.Nomoto, T.D.Anthopoulos. *Adv. Mater.*, **22**, 3778 (2010)
58. T.Schmaltz, A.Y.Amin, A.Khassanov, T.Meyer-Friedrichsen, H.G.Steinruck, A.Magerl, J.J.Segura, K.Voitchovsky, F.Stellacci, M.Halik. *Adv. Mater.*, **25**, 4511 (2013)
59. M.Melucci, M.Gazzano, G.Barbarella, M.Cavallini, F.Biscarini, P.Maccagnani, P.Ostoja. *J. Am. Chem. Soc.*, **125**, 10266 (2003)
60. H.G.Flesch, S.G.J.Mathijssen, F.Gholamrezaie, A.Moser, A.Neuhold, J.Novak, S.A.Ponomarenko, Q.Shen, C.Teichert, G.Hlawacek, P.Puschnig, C.Ambrosch-Draxl, R.Resel, D.M.De Leeuw. *J. Phys. Chem. C*, **115**, 22925 (2011)
61. F.Gholamrezaie, S.G.J.Mathijssen, E.C.P.Smits, T.C.T.Geuns, P.A.Van Hal, S.A.Ponomarenko, H.G.Flesch, R.Resel, E.Cantatore, P.W.M.Blom, D.M.De Leeuw. *Nano Lett.*, **10**, 1998 (2010)
62. A.M.Andringa, M.J.Spijkman, E.C.P.Smits, S.G.J.Mathijssen, P.A.Van Hal, S.Setayesh, N.P.Willard, O.V.Borshchev, S.A.Ponomarenko, P.W.M.Blom, D.M.De Leeuw. *Org. Electron.*, **11**, 895 (2010)
63. F.Marinelli, A.Dell'Aquila, L.Torsi, J.Tey, G.P.Suranna, P.Mastrorilli, G.Romanazzi, C.F.Nobile, S.G.Mhaisalkar, N.Cioffi, F.Palmisano. *Sens. Actuators, B*, **140**, 445 (2009)
64. E.V.Agina, I.A.Usov, O.V.Borshchev, J.Wang, A.Mourran, M.A.Shcherbina, A.V.Bakirov, S.Grigorian, M.Moller, S.N.Chvalun, S.A.Ponomarenko. *Langmuir*, **28**, 16186 (2012)
65. A.S.Sizov, E.V.Agina, F.Gholamrezaie, V.V.Bruevich, O.V.Borshchev, D.Y.Paraschuk, D.M.De Leeuw, S.A.Ponomarenko. *Appl. Phys. Lett.*, **103**, 043310 (2013)
66. Y.Cao, Z.M.Wei, S.Liu, L.Gan, X.F.Guo, W.Xu, M.L.Steigerwald, Z.F.Liu, D.B.Zhu. *Angew. Chem., Int. Ed.*, **49**, 6319 (2010)
67. Z.Wei, W.Xu, W.Hu, D.Zhu. *Langmuir*, **25**, 3349 (2009)
68. A.S.Sizov, D.S.Anisimov, E.V.Agina, O.V.Borshchev, A.V.Bakirov, M.A.Shcherbina, S.Grigorian, V.V.Bruevich, S.N.Chvalun, D.Y.Paraschuk, S.A.Ponomarenko. *Langmuir*, **30**, 15327 (2014)
69. E.J.Samuelsen, J.Mardalen, in *Handbook of Organic Conductive Molecules and Polymers: Conductive Polymers: Spectroscopy and Physical Properties*. Vol. 3. Ch. 2 (Ed. H.S.Nalwa). (Chichester: Wiley, 1997)
70. A.S.Komolov, E.F.Lazneva, Yu.M.Zhukov, S.A.Pshenichnyuk, E.V.Agina, D.I.Dominskii, D.S.Anisimov, D.Yu.Parashchuk. *Phys. Solid State*, **59**, 2491 (2017)
71. J.J.Brondijk, F.Torricelli, E.C.P.Smits, P.W.M.Blom, D.M.De Leeuw. *Org. Electron.*, **13**, 1526 (2012)
72. A.M.Andringa, C.Piliego, I.Katsouras, P.W.M.Blom, D.M.De Leeuw. *Chem. Mater.*, **26**, 773 (2014)
73. A.M.Andringa, E.C.P.Smits, J.H.Klootwijk, D.M.De Leeuw. *Sens. Actuators, B*, **181**, 668 (2013)
74. D.V.Anokhin, M.Defaux, A.Mourran, M.Moeller, Y.N.Luponosov, O.V.Borshchev, A.V.Bakirov, M.A.Shcherbina, S.N.Chvalun, T.Meyer-Friedrichsen, A.Elschner, S.Kirchmeyer, S.A.Ponomarenko, D.A.Ivanov. *J. Phys. Chem. C*, **116**, 22727 (2012)
75. A.Kreyes, S.Ellinger, K.Landfester, M.Defaux, D.A.Ivanov, A.Elschner, T.Meyer-Friedrichsen, U.Ziener. *Chem. Mater.*, **22**, 2079 (2010)
76. V.A.Trukhanov, D.S.Anisimov, V.V.Bruevich, E.V.Agina, O.V.Borshchev, S.Ponomarenko, J.Zhang, A.A.Bakulin, D.Y.Paraschuk, in *Organic Photovoltaics XVIII. Ser. Proceedings of SPIE*. Vol. 9942. (Bellingham, WA: Society of Photo-Optical Instrumentation Engineers, 2016). No. 994210
77. E.V.Agina, A.A.Mannanov, A.S.Sizov, O.Vechter, O.V.Borshchev, A.V.Bakirov, M.A.Shcherbina, S.N.Chvalun, V.G.Konstantinov, V.V.Bruevich, O.V.Kozlov, M.S.Pshenichnikov, D.Y.Paraschuk, S.A.Ponomarenko. *ACS Appl. Mater. Interfaces*, **9**, 18078 (2017)
78. K.Maruyama, K.Sawabe, T.Sakanoue, J.P.Li, W.Takahashi, S.Hotta, Y.Iwasa, T.Takenobu. *Sci. Rep.*, **5**, No. 10221 (2015)
79. S.Hotta, T.Yamao. *J. Mater. Chem.*, **21**, 1295 (2011)
80. O.V.Borshchev, A.S.Sizov, E.V.Agina, A.A.Bessonov, S.A.Ponomarenko. *Chem. Commun.*, **53**, 885 (2017)
81. C.S.Smithson, D.Ljubic, Y.Wu, S.Zhu. *Org. Electron.*, **37**, 42 (2016)
82. A.A.Trul, A.Sizov, V.Chekusova, O.Borshchev, E.Agina, M.A.Shcherbina, A.V.Bakirov, S.N.Chvalun, S.Ponomarenko. *J. Mater. Chem. C*, **6**, 9649 (2018)
83. E.V.Agina, M.S.Polinskaya, A.A.Trul, V.P.Chekusova, A.S.Sizov, O.V.Borshchev, S.A.Ponomarenko, in *Organic Field-Effect Transistors XVI. (Ser. Proceedings of SPIE. Vol. 10365)*. (Bellingham, WA: Society of Photo-Optical Instrumentation Engineers, 2017). No. 1036500
84. L.Torsi, M.Magliulo, K.Manoli, G.Palazzo. *Chem. Soc. Rev.*, **42**, 8612 (2013)
85. C.Zhang, P.Chen, W.Hu. *Chem. Soc. Rev.*, **44**, 2087 (2015)
86. A.Lv, Y.Pan, L.Chi. *Sensors (Basel)*, **17**, 213 (2017)
87. F.Gholamrezaie, A.M.Andringa, W.S.C.Roelofs, A.Neuhold, M.Kemerink, P.W.M.Blom, D.M.De Leeuw. *Small*, **8**, 241 (2012)
88. P.A.Bobbert, A.Sharma, S.G.J.Mathijssen, M.Kemerink, D.M.De Leeuw. *Adv. Mater.*, **24**, 1146 (2012)
89. S.G.Mathijssen, M.J.Spijkman, A.M.Andringa, P.A.Van Hal, I.Mcculloch, M.Kemerink, R.A.Janssen, D.M.De Leeuw. *Adv. Mater.*, **22**, 5105 (2010)
90. M.Defaux, F.Gholamrezaie, J.B.Wang, A.Kreyes, U.Ziener, D.V.Anokhin, D.A.Ivanov, A.Moser, A.Neuhold, I.Salzmann, R.Resel, D.M.De Leeuw, S.C.J.Meskers, M.Moeller, A.Mourran. *Adv. Mater.*, **24**, 973 (2012)
91. A.V.Glushkova, E.Y.Poimanova, V.V.Bruevich, Y.N.Luponosov, S.A.Ponomarenko, D.Y.Paraschuk, in *Organic Field-Effect Transistors XVI. Ser. Proceedings of SPIE*. Vol. 10365. (Bellingham, WA: Society of Photo-Optical Instrumentation Engineers, 2017). No.1036504
92. B.Peng, S.Huang, Z.Zhou, P.K.L.Chan. *Adv. Funct. Mater.*, **27**, 1700999 (2017)
93. Q.Wang, J.Qian, Y.Li, Y.Zhang, D.He, S.Jiang, Y.Wang, X.Wang, L.Pan, J.Wang, X.Wang, Z.Hu, H.Nan, Z.Ni, Y.Zheng, Y.Shi. *Adv. Funct. Mater.*, **26**, 3191 (2016)

94. G.H.Roche, D.Thuau, P.Valvin, S.Clevers, T.Tjoutis, S.Chambon, D.Flot, Y.H.Geerts, J.J.E.Moreau, G.Wantz, O.J.Dautel. *Adv. Electron. Mater.*, **3**, 1700218 (2017)
95. J.-H.Lee, S.Kim, H.Kim, J.Lee. *Org. Electron.*, **52**, 184 (2018)
96. Q.Wang, E.J.Juarez-Perez, S.Jiang, L.Qiu, L.K.Ono, T.Sasaki, X.Wang, Y.Shi, Y.Zheng, Y.Qi, Y.Li. *J. Phys. Chem. Lett.*, **9**, 1318 (2018)
97. D.He, J.Qiao, L.Zhang, J.Wang, T.Lan, J.Qian, Y.Li, Y.Shi, Y.Chai, W.Lan, L.K.Ono, Y.Qi, J.B.Xu, W.Ji, X.Wang. *Sci. Adv.*, **3**, e1701186 (2017)
98. L.Jiang, H.Dong, Q.Meng, H.Li, M.He, Z.Wei, Y.He, W.Hu. *Adv. Mater.*, **23**, 2059 (2011)
99. H.Chen, S.Dong, M.Bai, N.Cheng, H.Wang, M.Li, H.Du, S.Hu, Y.Yang, T.Yang, F.Zhang, L.Gu, S.Meng, S.Hou, X.Guo. *Adv. Mater.*, **27**, 2113 (2015)
100. M.Li, D.K.Mangalore, J.Zhao, J.H.Carpenter, H.Yan, H.Ade, H.Yan, K.Mullen, P.W.M.Blom, W.Pisula, D.M.De Leeuw, K.Asadi. *Nat. Commun.*, **9**, 451 (2018)
101. I.Vladimirov, M.Kellermeier, T.Gessner, Z.Molla, S.Grigorian, U.Pietsch, L.S.Schaffroth, M.Kuhn, F.May, R.T.Weitz. *Nano Lett.*, **18**, 9 (2018)
102. A.Yamamura, S.Watanabe, M.Uno, M.Mitani, C.Mitsui, J.Tsurumi, N.Isahaya, Y.Kanaoka, T.Okamoto, J.Takeya. *Sci. Adv.*, **4**, eaao5758 (2018)